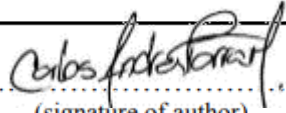




Universitetet
i Stavanger

FACULTY OF SCIENCE AND TECHNOLOGY

MASTER'S THESIS

Study programme/specialisation: MSc in Offshore Technology / Marine and Subsea Technology	Spring / Autumn semester, 2018.. Open/ Confidential
Author: Carlos Andres Parra	 (signature of author)
Programme coordinator: Supervisor(s):	Prof. Muk Chen Ong Prof. Muk Chen Ong / Dr. Lin Li / Dr. Xinying Zhu
Title of master's thesis: Numerical Study on Offshore Lifting Operations of a Subsea Spool	
Credits: 30 ECTS	
Keywords: Offshore lifting operations; subsea spool; lift-off; lowering through wave zone; time-domain simulations; operability analysis; weather window analysis.	Number of pages: 114 + supplemental material/other: Stavanger, June 29 / 2018 date/year

Abstract

Within the scope of marine operations, offshore lifting operations present significant challenges due to the instability and harshness of environmental conditions. Therefore, lifting operations become expensive and risky. Lifting operations call for an early planning in order to assess operative procedures, carry out logistical tasks and to determine workable weather windows. In order to contribute to the solution, accurate numerical models and methods have become essential tools for predicting the response of the lifting systems.

This thesis addresses a numerical study on offshore lifting operations of a subsea spool. The two operations studied within the subsea lift process are: the lift-off of the spool from the deck of a transportation barge (the lift-off phase), and the lowering of the spool through the wave zone (the lowering phase). Moreover, accurate numerical models of the lifting systems were developed. The process also included the hydrodynamic analysis of the construction vessel and the transportation barge supporting the operations.

The use of numerical models and methods, along with the conduction of time-domain analyses, bring relevant benefits and advantages to the assessment of allowable sea states. In this thesis work, a systematic methodology was followed for the assessment of the allowable sea states governing the lifting operations. Firstly, the corresponding critical events and limiting parameters were defined. The calculation of the characteristic responses was then carried out by means of time-domain simulations. Finally, the allowable sea states were obtained by comparing the characteristic responses and the corresponding allowable limits.

Particularly, the assessment of the allowable sea states was a comprehensive task in this thesis. The process in itself required the statistical uncertainty to be reduced, which demanded numerous time-domain simulations. In addition, a methodology was suggested to filter seeds that present a suitable scenario for the lift-off phase. The assessment delivered that the allowable sea states obtained for the lift-off phase are lower than those for the lowering phase.

Since the operability of marine operations plays an important role during the planning phase, an operability analysis was also conducted in this thesis. The methodology principally considered weather window analysis and two methods devised for the installation of a given number of spools. One of the differences between the methods resides in the allowable sea states that govern the lift-off of the spool. In the first installation method, the entire subsea lift process is governed by the allowable sea states obtained for the lowering through the wave zone. In the second method, the lift-off occurs from the deck of a transportation barge and thus the respective allowable sea states apply.

The main objective of the operability analysis was to determine which of the methods, in terms of time, provides the most efficient option for the installation of a given number of spools. It was observed that low allowable sea states governing even one single activity may virtually make a marine operation unfeasible.

Lastly, a sensitivity study to the navigation time of the construction vessel was conducted. The outcome suggests that this parameter may become decisive in determining whether transportation barges should be integrated in order to reduce the overall installation time.

Acknowledgement

This master's thesis was conducted under supervision of Prof. Muk Chen Ong, Dr. Lin Li and Dr. Xinying Zhu. I would like to express my sincere gratitude for their professional support and guidance in terms of time, expertise and resources. Regarding Prof. Ong, I found his enthusiasm and feedback of great assistance. I am very grateful for Dr. Li's patience and continuous advice on every detail in the thesis. I want to thank Dr. Zhu for the technical data provided, constructive comments and her time allocated to the meetings. It was a great experience to work with all of them.

I would also like to thank my classmates and friends who created a joyful and pleasant atmosphere. By sharing day-to-day activities with them at school, I found the process of completing this thesis less stressful.

Lastly, my warmest appreciation goes to my family in Colombia for their continuous encouragement and endless love, and also to my girlfriend Mari Elvira, for her unconditional support and being the best companion throughout almost my whole master's.

Carlos Andres Parra
June 2018
Stavanger, Norway

Acronyms and abbreviations

AHC	Active Heave Compensated
CAT	Connector Actuation Tool
CoF	Centre of Force
CoG	Centre of Gravity
DAF	Dynamic Amplification Factor
DLC	Dynamic Load Capacity
FEM	Finite Element Method
FFT	Fast Fourier transform
IM	Installation Method
MBL	Minimum Breaking Load
NCS	Norwegian Continental Shelf
OD	Outside Diameter
OIT	Overall Installation Time
PLEM	Pipeline End Manifold
PLET	Pipeline End Termination
RAO	Response Amplitude Operator
ROV	Remote Operated Vehicle
SF	Safety Factor
SPS	Subsea Production System
STAAD	Structural Analysis and Design computer program

SURF	Subsea Umbilicals, Risers and Flowlines
SWL	Safe Working Load
WOWW	Workable Weather Window
WT	Wall Thickness

Contents

1	Introduction	12
1.1	Motivation and background	12
1.2	Subsea Tie-in systems and jumper spools	13
1.2.1	Load-out, transportation and installation of subsea structures	14
1.2.2	Deployment and installation procedure for a horizontal tie-in system	16
1.2.3	Challenges during the installation of subsea structures	17
1.3	Modelling and analysis of marine operations	19
1.4	Aim and scope	21
1.5	Thesis outline	23
2	Theoretical basis and recommended practices for offshore lifting operations	25
2.1	General	25
2.2	Potential flow theory	25
2.2.1	Boundary conditions	26
2.3	Wave-induced motions and loads on floating structures	28
2.3.1	Response in regular waves	28
2.3.2	Response of floating structures in irregular waves	30
2.3.3	Wave spectrum	31
2.4	Wave loading on slender structures	33
2.4.1	Morison's formula for slender structures	33
2.4.2	Hydrodynamic coefficients of slender cylinders	35
2.4.3	Slamming loads crossing the wave zone	36
2.5	Recommended practices for offshore lifting operations	38
2.5.1	General	38
2.5.2	Lift-off of an object	40
3	Lifting systems and numerical models	41
3.1	General	41
3.2	Systems	42
3.2.1	Subsea spool	42
3.2.2	Construction vessel	42
3.2.3	Transportation barge	43
3.2.4	Configuration for the lift-off of the spool from the deck of the barge	44
3.2.5	Configuration for the lowering of the spool through the wave zone	46
3.3	Hydrodynamic analysis of the floating vessels	48
3.3.1	Hydrodynamics of the construction vessel	48
3.3.2	Hydrodynamics of the construction vessel and the transportation barge	50

3.4	Numerical models of the lifting systems	55
3.4.1	General	55
3.4.2	Modelling of the wire couplings	55
3.4.3	Modelling of the positioning system for the floating vessels	59
3.4.4	Modelling of the fender couplings for the lift-off phase	59
3.4.5	Modelling for hydrodynamic loads on the spool	60
4	Assessment of allowable sea states	65
4.1	General	65
4.2	Time-domain analysis and setting of simulation parameters	67
4.2.1	Main analysis parameters	67
4.2.2	Simulation settings for the lift-off of the spool from the deck of the barge	68
4.2.3	Simulation settings for the lowering of the spool through the wave zone	68
4.3	Methodology to select seeds with suitable scenario for the lift-off of the spool from the barge deck	69
4.4	Criteria to assess allowable sea states	72
4.4.1	Potential snap load in slings	72
4.4.2	Slack-wire condition of slings	73
4.4.3	Re-hit of the spool	73
4.4.4	Minimum clearance between the spool and the construction vessel	74
4.5	Presentation of results and discussion	75
4.5.1	Static condition analysis	75
4.5.2	Allowable sea states for the lift-off of the spool from the deck of the barge	76
4.5.3	Allowable sea states for the lowering of the spool through the wave zone	83
5	Operability analysis	89
5.1	General	89
5.1.1	Planning of marine operations	90
5.1.2	Metocean condition	91
5.2	Methodology to conduct the operability analysis	92
5.2.1	Methods for installation of the spool	92
5.2.2	Comparative study on the operability between installation methods	96
5.2.3	Sensitivity of the installation methods to the navigation time of the construction vessel	99
5.3	Results and discussion	99
5.3.1	Base case	99
5.3.2	Sensitivity of the installation methods to the navigation time of the construction vessel	105
6	Conclusions and recommendations for future work	107
6.1	Conclusions	107
6.2	Recommendations for future work	110
	Appendices	114
A	Hindcast wave data	114

List of Figures

1.1	Subsea architecture of the spool	14
1.2	Subsea lift process	17
1.3	Stages in the installation of a horizontal tie-in system	18
1.4	Relation between modelling and analysis of marine operations, the design of structures and the planning of operations	20
1.5	General scope of the thesis work	22
2.1	Boundary conditions for solving the Laplace equation	26
2.2	Superposition of wave excitation, added mass, damping and restoring loads	28
2.3	Definition of the rigid-body motion modes	29
2.4	Torsethaugen wave spectrum	33
2.5	Normal, tangential and lift forces on a slender element	34
2.6	High frequency limit of vertical added mass coefficient and its derivative	37
2.7	Definition of the centres of gravity, buoyancy and force of a body	38
3.1	General sketch of the spool	43
3.2	Configuration layout for the lift-off of the spool from the deck of the barge	45
3.3	Configuration layout for the lowering of the spool through the wave zone	47
3.4	Flowchart for the hydrodynamic analysis of the floating vessels	48
3.5	First order motion transfer functions of the construction vessel: single-body condition	49
3.6	First order motion transfer functions of the barge: single-body condition	51
3.7	WADAM multi-body hydromodel of the vessel and the barge	52
3.8	First order motion transfer functions of the construction vessel and the barge: multi-body condition	53
3.9	First order motion transfer functions of the construction vessel: single- and multi-body conditions	54
3.10	General arrangement of the slings	56
3.11	Definition of the strip coordinate system for tubular members of the spool	60
3.12	Wake amplification factor	62
3.13	Variation of C_{Dt} with angle of attack α	62
3.14	Variables in the depth-dependent scaling of hydrodynamic coefficients	63
3.15	Depth-dependent hydrodynamic coefficients	64
4.1	General methodology to establish allowable sea states	65
4.2	Comparison of scenarios for the lift-off of the spool from a barge	70
4.3	Allowable sea states for the lift-off of the spool from the deck of a barge based on Δt_{check}	77

4.4	Allowable sea states for the lift-off of the spool from the deck of a barge . . .	78
4.5	Allowable sea states for the lift-off of the spool from the deck of a barge based on the different criteria for assessment	78
4.6	Convergence study on extremes responses during the lift-off of the spool from the deck of a barge	80
4.7	Responses and limiting parameters of interest during the lift-off of the spool from the deck of a barge	81
4.8	Allowable sea states for the lowering of the spool through the wave zone . . .	84
4.9	Allowable sea states for the lowering of the spool through the wave zone based on the different criteria for assessment	84
4.10	Convergence study on extremes responses during the lowering of the spool through the wave zone	85
4.11	Responses and limiting parameters of interest during the lowering of the spool through the wave zone	86
4.12	Comparison between sway motion of the spool and variation of clearance between the spool and the vessel	88
5.1	Operation periods	90
5.2	Methodology for weather window analysis during the planning of marine operations	92
5.3	Allowable sea states governing the activities established by IM1	94
5.4	Allowable sea states governing the activities established by IM2	96
5.5	Methodology for estimating the OIT and WOWWs	97
5.6	Comparison of OIT_{mean} between IM1 and IM2 along the operating season . .	100
5.7	Comparison of OIT_{mean} : by month	101
5.8	Comparison of OIT_{mean} : by method of installation	102
5.9	Empirical distribution function of OIT when installing 2 spools	103
5.10	Comparison of the estimate P50 between IM1 and IM2: by month	104
5.11	Feasibility of the installation methods based on the estimate P50	104
5.12	Comparison of the estimate P50 for sensitivity cases no. 1 and no. 2	106
6.1	Comparison of allowable sea states: lift-off phase vs. lowering phase	108

List of Tables

- 2.1 Dependence parameters between C_{Dt} and C_{Dn} 36
- 3.1 Dimensions and mass of members of the spool 42
- 3.2 Main features of the construction vessel 43
- 3.3 Main features of the barge 44
- 3.4 Features of slings attached to the spool 57
- 3.5 Tension in slings obtained from STAAD and SIMO analyses (static condition) 57
- 3.6 Main features of the lift-wire 58
- 3.7 Parameters of the fixed force-elongation elements for the positioning system . 59
- 3.8 Features of the coupling elements (fenders) 59
- 3.9 Estimate wave length for the offshore field 60
- 3.10 Hydrodynamic coefficients of tubular members of the spool 61
- 3.11 Depth-dependent hydrodynamic coefficients 64
- 4.1 Sequence of actions and events during the lift-off of the spool from the deck of a barge 68
- 4.2 Combinations of T_P and H_S for the time-domain simulations of the lift-off phase 68
- 4.3 Sequence of actions and events during the lowering of the spool through the wave zone 69
- 4.4 Combinations of T_P and H_S for the time-domain simulations of the lowering phase 69
- 4.5 Filtered seeds suitable for the lift-off from a barge 72
- 4.6 Tilt of the spool under static condition 75
- 4.7 Pitch and roll motions of the spool under static condition 75
- 4.8 Forces on fenders under static condition 76
- 4.9 Allowable sea states for the lift-off of the spool from the deck of a barge based on Δt_{check} 77
- 4.10 Allowable sea states for the lift-off of the spool from the deck of a barge . . . 78
- 4.11 Filtered seeds suitable for lift-off from a barge (analysis of sea states with T_P 12s and results) 83
- 4.12 Allowable sea states for the lowering of the spool through the wave zone . . . 83
- 4.13 Minimum and maximum tensions in slings during the lowering of the spool through wave zone 87
- 5.1 General information and statistics of the offshore site chosen for metocean condition 91
- 5.2 Activities established by IM1 93
- 5.3 Activities established by IM2 95

5.4	Sensitivity cases to the navigation time of the construction vessel	99
A.1	10-year scatter diagram of H_S and T_P of the offshore site chosen for metocean condition	114

Chapter 1

Introduction

1.1 Motivation and background

Offshore lifting operations are essential within the scope of the installation of subsea assets. This type of operations are categorised as marine operations, and thus are subjected to the hazards of the marine environment [1].

The instability and harshness of environmental conditions are in essence factors that make marine operations expensive and risky. To cite an instance, in the case of offshore wind farms that may require the installation of a large number of wind turbine units, the operating season is generally limited to a certain span of the year in order to reduce operative risks and costs due to weather down time [2].

In general terms, lifting operations affect the installation costs for a subsea field development, and these, in turn, impact directly the overall capital expenditure. The installation of offshore assets calls for an early planning in order to assess operative procedures and carry out logistical tasks, as well as to determine workable weather windows, among others [3].

It was found that offshore crane operations account for the longest down time due to environmental loads. In order to broaden their workable weather windows, numerical modelling for predicting the response of the lifting system has become an essential tool [2].

Based on behavior of the system, critical events and operational limits for the operation can be identified during the planning phase. Consequently, by comparing wave forecasted data, the allowable sea states for executing the operation can also be assessed, as well as the operability of the marine operation [4]. The latter can be linked to the likelihood of having acceptable weather conditions, whose evaluation is considered of usefulness for weather-sensitive marine operations [5].

The use of numerical models in the analysis of lifting operations can be extended to different configurations and purposes. For instance, when lifting massive loads from the deck of another vessel, or during the lowering of a load through the wave zone [2].

This thesis work addresses a numerical study on offshore lifting operations of a subsea spool. Generally, the present study consists of the development of numerical models that allowed for the assessment of allowable sea states of the following operations: the lift-off of the spool from the deck of a transportation barge, as well as its lowering through the wave zone. Furthermore, an operability analysis was conducted based on two installation methods including the lifting operations aforementioned.

1.2 Subsea Tie-in systems and jumper spools

According to ISO 13628-1 [6], a subsea production system (SPS) is the arrangement of components and structures whose purpose is to develop reservoirs offshore. Furthermore, the injection of water or gas either for disposal or to maintain the pressure of the reservoir can be also carried out by means of subsea equipment.

Among the subsea equipment placed on the seabed, manifold pipeline systems allow for the conduction of fluid streams from multiple individual wells into multiple production flowline headers [7]. By means of piping and valves installed to combine, distribute and control fluid flow, the number of flowlines and risers is minimised as well as the fluid flow is optimised [3].

The tie-in of subsea systems (e.g., pipeline systems and export systems) is carried out by pipeline end manifolds at both pipeline ends. A pipeline end manifold (PLEM) is a subsea structure that provides the connection between rigid pipeline and subsea components such as manifolds or well trees. A pipeline end termination (PLET) also contributes to that purpose by supporting one pipeline valve and one vertical connector [3].

In a SPS, jumpers are installed to provide the connection of PLEM/PLETs, riser bases or other subsea components [7]. Moreover, jumpers naturally allow for the conduction in itself of wells streams and for the injection of water or chemicals into a well if desired [3].

Tie-in systems

Tie-in systems are used in the development of a subsea fields by providing the connection means between flowlines, subsea wells, manifolds and offshore processing facilities, among others [7].

Tie-in systems are classified into vertical and horizontal systems, and are also provided with related connection devices [3]. Vertical tie-in systems are provided with two vertically oriented downward connectors and a pipe spool. The connectors are directly mounted onto the receiving hubs during tie-in [3]. Horizontal tie-in systems are usually installed in shallow water fields. However, they can also be found in deep water fields where their installation includes rigid jumpers. The installation is completed with the assistance of remote operated vehicles (ROVs) and connector actuation tools (CATs). By means of a subsea winch, the termination heads are conveyed into the connection hub where the tie-in is completed by clamp connectors. The horizontal connection is mounted in a straight line (i.e. horizontal jumpers are used) [3].

Subsea rigid jumper or spool

The general configuration of a typical jumper consists of two end connectors (termination heads) and a pipe between them. The type of the pipe can be either flexible or rigid. Generally, rigid jumpers are also called jumper pipe spools, or simply spools. Spools are usually resting horizontally on the seabed, and their common configuration is M-shaped, inverted U-shaped or horizontal Z-shaped, among others [3]. Spools are typically manufactured in sizes from 4 to 18 inches diameter and lengths no shorter than 50m [7].

Fig. 1.1 shows the subsea architecture of the spool addressed in this thesis work. In the horizontal tie-in system, the spool is connecting a platform riser at one end, and a production PLET at the other.

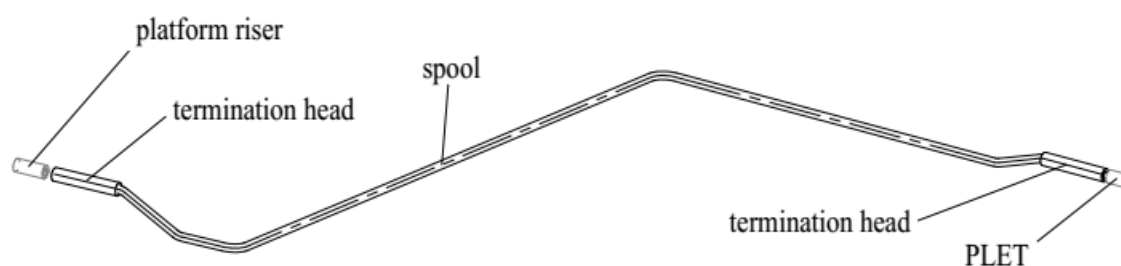


Fig. 1.1. Subsea architecture of the spool (horizontal tie-in)

Subsea spools shall be designed and manufactured in a way that ensures sufficient flexibility to fit measurement and fabrication tolerances (e.g., minimum 3D pipe bends). Spools should also accommodate the end displacements caused by pipeline expansions and withstand the bending and torsional permissible limits of the connection devices [3].

According to Bai and Bai [3], the design concept must be supported through the analysis of the following loading conditions:

- *Transportation*: Loads that might exist during the load-out and transportation of the spool from the fabrication place to the offshore site.
- *Offshore lifting*: Load factors considering the dynamics of the installation vessel should be included. The design parameters normally include: keelhauling and cross hauling, lowering to seabed and landing, wave current and forces.
- *Installation*: assembly (ROV impact, subsidence, operation-induced) and testing loads should be analysed along with vibration fatigue.
- *Load stress analyses*: Analyses that are conducted for all joints, lifting points and highly stressed welds.

1.2.1 Load-out, transportation and installation of subsea structures

The installation of a subsea structure is composed of the stages listed below [3]. A separate section is dedicated to the deployment and the installation of a horizontal tie-in system.

- Load-out and sea-fastening
- Transportation
- Site survey
- Deployment
- As-built survey

Load-out and sea-fastening DNVGL-ST-N001 [1] defines a load-out as the marine operation where a load is transferred onto a vessel or barge, for instance, by lifting. Tide is of great relevance for a load-out operation, therefore, extreme tide levels and rates of change should be taken into account [1]. Furthermore, the following aspects should be considered during the planing of load-out operations:

- Transport vessel dimensions and strength
- Assessment of clearances and obstructions (route survey)
- Object position and support height on transport vessel
- Water depths
- Local environmental events due to waves and swell, currents, squalls and thunderstorms
- Others related to the yard and quay

Sea-fastening is defined as the devices (generally welded steels) retaining the transported structure on the vessel. The effects of hydrodynamic loads and wave slamming on sea-fastening should be considered, as well as those of impact loads [1]. Moreover, sea-fastening should,

- prevent slender elements and structures from swinging and vibrating during their transportation,
- provide easy release for offshore lifting operations and,
- allow for the sufficient support and horizontal restraint until the object can be lifted clear of the vessel.

Transportation According to DNVGL-ST-N001 [1], the transportation (sea voyages) of objects includes the dry towages on transportation barges, the transport on self-propelled vessels, wet towages and location moves of jack-ups. The most important aspects that should be taken into account are:

- Motion response
- Design and strength
- Floating stability
- Transport and tug selection
- Voyage planning

The structure should be provided with the adequate and sufficient shipping stands. Shipping stands should support the structure as in the condition to be installed or while en route to the offshore location. Welding down shall be possible and stands should allow for quick-easy release of the spool tie-downs during the installation. The latter should be completed at the deck level [3].

In this work, the transportation of the subsea spool may be carried-out by a construction vessel (i.e. self-propelled), transportation barge(s) or a combination of both depending on the installation methods defined in Section 5.2.1.

Site survey and as-built survey Site survey is a regular activity carried out before the start of marine operations such as drilling and the installation of subsea structures. The aim of the survey is to acquire the precise bathymetry of the seabed and assess the quality of its properties for offshore installation foundation. The result is a detailed mapping of the seabed that is generally completed by a ROV and other technologies (e.g., sub-bottom profiler, multi-beam echo sounder, side-scan sonar) [3].

Once the deployment is finished and the lifting gear has been recovered, an as-built (or as-left) survey is performed. This is normally carried out by a ROV and includes visual survey, video recording, mapping of coordinates, among others [8].

1.2.2 Deployment and installation procedure for a horizontal tie-in system

As stated in DNVGL-RP-N201 [8], the deployment stage is comprised by the following phases:

- *Pre-lift*: this is the very last stage before the lift-off occurs. The installation vessel is in its final position.
- *Lift-off*: the object is lifted off from the deck.
- *Overboard*: the object is manoeuvred clear of the transportation vessel, outboard over the sea.
- *splash zone*: the object is lowered through the wave zone (air-wave interface). Here the effects of waves in terms of motions and loads are considerable.
- *Lowering*: the object is lowered through the wave column down to the seabed.
- *Move or positioning*: the vessel adjusts its position so as the object gets closer to the landing position.
- *Landing*: the object is landed on the seabed

In a similar way, DNVGL-RP-N103 [9] specifies that a typical subsea lift process consists of all the phases above with the exception of pre-lift (see Fig. 1.2). General operational aspects of the two phases of interest in this thesis are presented next.

During the pre-lift, lift-off and overboard stages, control over the horizontal motion of the object, re-hit of the object, snap loads in the wire couplings and contingency measures in case of the failure of control devices (e.g., tugger lines, bumpers) are operational aspects of great relevance [8].

In the case of the lowering of the object through the wave zone, several aspects are addressed during the planning and execution. In general terms, the aspects are slamming loads in the splash zone, potential damage of the object, potential snap load in wire couplings, slack slings, and shift or tilt of the lifted object, among others [8].

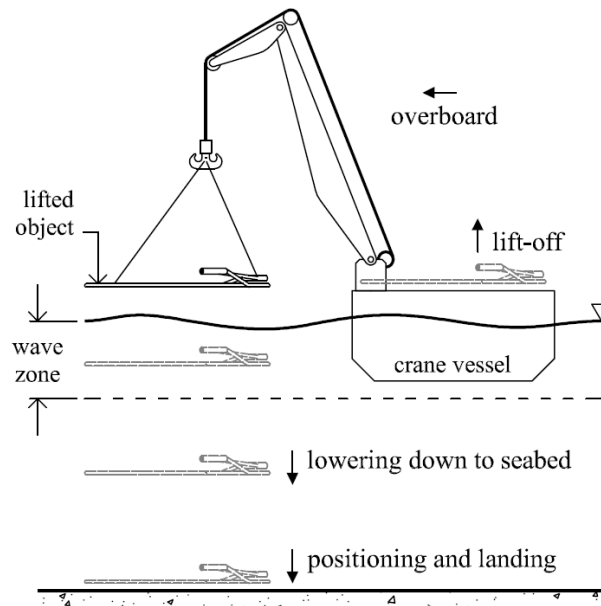


Fig. 1.2. Subsea lift process

Installation procedure for a horizontal tie-in system

Bai and Bai [3] suggest that the regular installation of a horizontal tie-in system is carried out as follows:

- Deployment and lowering of the spool close and above the subsea structures.
- Sequentially, the stab on each termination head is inserted into the stab receptacle on the respective tie-in porch (Fig. 1.3(a)). The second termination head always remains horizontally aligned.
- The ROV conveys and fastens the CAT on the first termination head (Fig. 1.3(b)).
- Horizontal levelling and fastening of the first termination. Caps are disconnected from the connector and the inboard hub (Fig. 1.3(c)).
- The first termination head is coupled to the inboard hub and the connector is closed (Fig. 1.3(d)). Consequently, integrity of the seals is checked by a pressure test.
- The CAT is unlocked and conveyed to the second termination head and then complete the connection. The CAT remains close to the seabed afterwards.

1.2.3 Challenges during the installation of subsea structures

With regard to the installation of subsea structures, several challenges have to be addressed during the planning and execution phases. For instance, as the installation of subsea structures is taken to deeper water developments, the installation capability of a system is affected by the limitations of the lifting and lowering sub-system. If a steel lift-wire is used, the payload capability of a system is reduced by the weight of the wire as depth increases. In addition, further decrease may occur due to significant hydrodynamic loads provoked by resonance in the system [3].

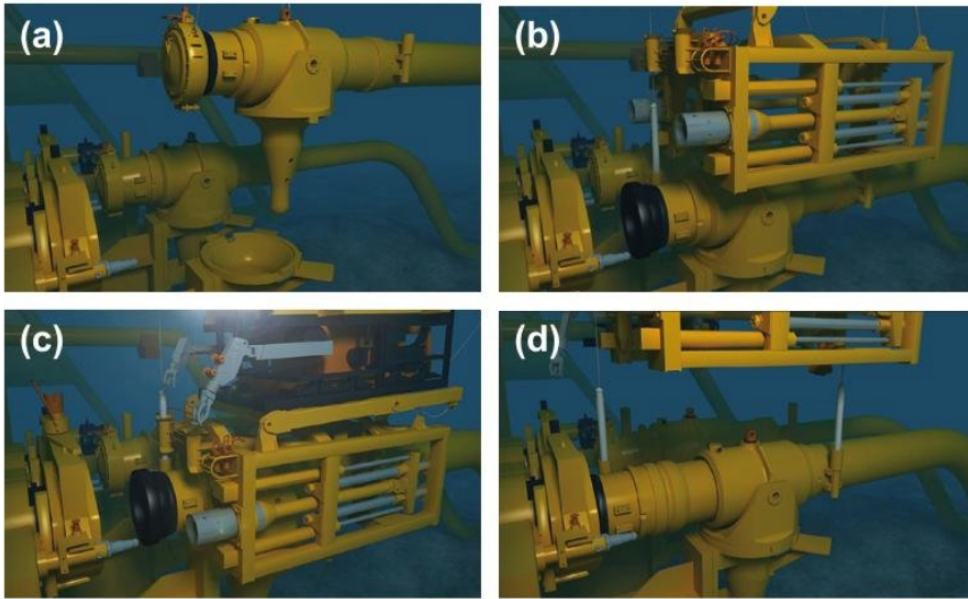


Fig. 1.3. Stages in the installation of a horizontal tie-in system [3]

For the Wheatstone Project in Western Australia, a campaign was carried out for the installation of 68 spools. The following challenges presented by Cosson et al. [10] were addressed:

- Slack-wire condition of slings during the lowering of spools of small diameter (4 inches to 8 inches) through the wave zone: based on a preliminary analysis, the lowering phase was found very restricted (in terms of allowable sea states) due to the slack-wire condition of slings. This resulted from the high hydrodynamic loading on those particular spools. Time-domain simulations were conducted to assess in a more accurate way the slam loading. Consequently, this allowed for an optimized design of slings and an increase of the allowable sea states from 1.0m to 2.0m in terms the significant wave height.
- Re-hit, excessive snap loading in slings, and collision between the spools and other structures on the transportation barge: these critical events may occur when the lift-off of the spool is carried out from the deck of a transportation barge. Both vessels move independently and therefore the relative motion between them was required to be evaluated for reducing the risk of the critical events.

Similar challenges were addressed during the execution of lifting operations for the Skarv Project in the North Sea during 2009 and 2010. A total of 24 subsea structures of massive weight and large outer dimensions were installed by using a construction vessel. The operations had to be carried out close to the vessel capacity limit. Due to the large size of the structures, a long lift radius was required for their safe deployment [11].

Another challenge was the large hydrodynamic loading obtained for closed structures and suction anchors by using hydrodynamic coefficients that did not account for the effects of perforations and the high frequency limit of vertical added mass when crossing the free surface. Moreover, drag coefficients recommended for regular shaped objects under steady flow should not be considered when crossing the wave zone. The nature of the flow in this zone is unsteady and thus higher drag coefficients should apply [11].

A sensitivity study was conducted on hydrodynamic coefficients followed by numerical analyses in software packages such as SIMO and MACSI [11]. The numerical analyses included the following aspects:

- modelling of the geometry of the structure and setting of its hydrodynamic as much as practicable,
- several sensitivity studies on the depth of submergence, the wind sea and swell heading angles, the weight of the structure and the winch speed and,
- the use of 10 random seeds with the purpose of evaluating extreme values

Conservatism in the analysis was reduced by including the high frequency limit of vertical added mass in proximity to free surface. However, the allowable sea states were optimized as a result of the numerical analyses and sensitivity studies aforementioned [11].

Finally, the cases aforementioned demonstrate that higher allowable sea states for lifting operations of subsea structures, design optimization and cost-effectiveness of processes can be reachable by conducting simulations of the corresponding numerical models. Safe installation criteria are fulfilled while delineating those models in a more accurate way.

Challenges are continuously increasing since offshore field developments call for heavier and larger structures to be installed [11]. Therefore, the analyses and methods adopted shall keep up with the upcoming challenges.

1.3 Modelling and analysis of marine operations

According to DNVGL-RP-N101 [12], marine operations involve the handling of objects at sea during temporary phases. These activities normally take place from the construction site until the installation site offshore prior to operation. The planning requires that the activities are designed to be practicable and carried out in a safe way.

The design of structures and structural components should also include the conditions that may occur during the temporary phases. These design conditions are denoted by DNVGL-OS-C101 [13] as temporary conditions (e.g., fabrication, transportation and installation, among others). Naturally, this contributes to the achievement of recognized safety levels during the planning and execution of marine operations [1].

The flowchart shown in Fig. 1.4 is a modified version of that suggested by Lin [14]. The flowchart depicts the relation between modelling and analysis of marine operations (i.e. lifting operations of a subsea spool), the design of structures and the planning of operations.

For a subsea structure, the design process normally includes a complete analysis to ensure that no damage occurs during its installation. This analysis aims at establishing the limiting weather criteria for the installation. Generally, a preliminary dynamic analysis is conducted in early stages with the goal of doing an appraisal of structural design criteria and operational requirements [3].

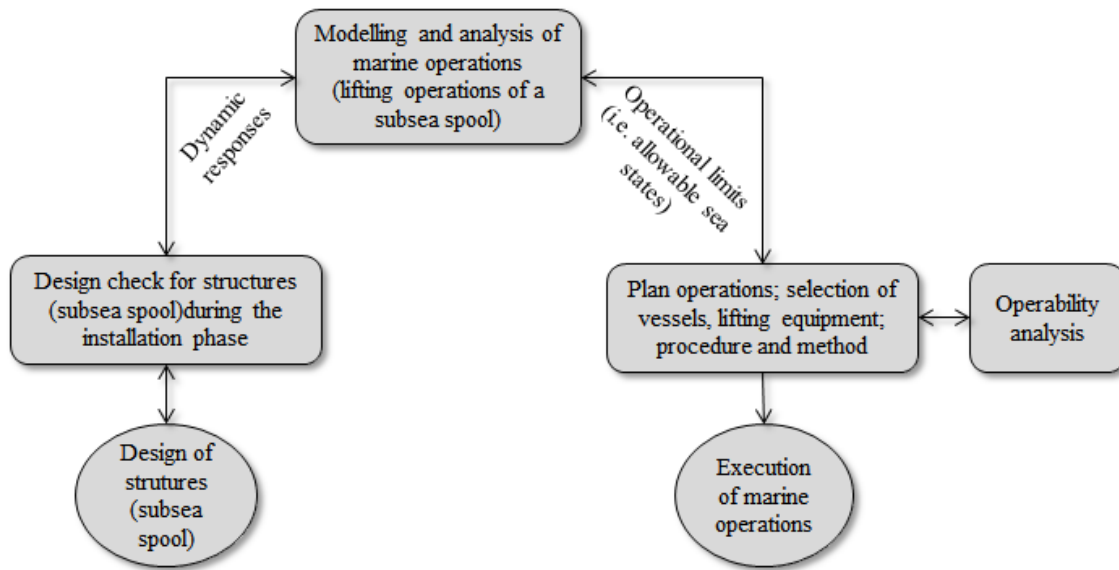


Fig. 1.4. Relation between modelling and analysis of marine operations, the design of structures and the planning of operations [14]

In the case of lifting operations, dynamic forces can be quantified by conducting a lifting analysis. As a result, critical phases can be identified. The lifting analysis generally follows the phases of the subsea lift process presented in Section 1.2.2. Moreover, if the lifting analysis involves the assessment of allowable sea states, further analyses can be conducted for the estimation of operational weather windows [3].

Lin [14] suggests that the selection of vessels and installation appliances depends to a large extent on the analysis of operations. For instance, factors such as extreme dynamic load amplification and instability during landing of the load influence the capability of an installation system. In this case, active and passive compensation systems are used to counteract vertical heave motions [3].

An additional challenge found during the Wheatstone Project (see Section 1.2.3) was the selection of a fit-for-purpose installation vessel and lifting appliances to complete the installation. This challenge dealt with the wide variation in geometry, configuration, slenderness and weight of the spools. Hence, requirements in terms of station keeping, crane and ROV capability, and deck space were considered in complex assessments during the planning phase [10].

As presented in Section 1.2.3, the use of numerical studies took a significant role in overcoming the challenges found during the installation of subsea structures. DNVGL-ST-N001 [1] also recommends either frequency- or time-domain analyses based on numerical models. The scope includes jacket mooring analysis, launch operations, on-bottom stability and piling, float-over and lifting operations, among others. Numerical models are also of great relevance when evaluating hydrodynamic interaction between floating bodies, for instance, when studying the lift-off of an object from or to a transportation barge in close proximity [9].

During the analysis of marine operations, installation procedures and methods can be optimized by integrating operational limits to the analysis process [14]. In fact, the operability of a marine operation can be estimated by considering operational limits (i.e. sea state parameters) and scatter diagrams of the offshore site [4]. Wu [15] presented a numerical analysis of docking operation between service vessels and offshore wind turbines. The study was conducted based on the calculation of limiting parameters (e.g., significant wave height, wave peak period and wave heading). Moreover, a frequency-domain approach was proposed.

One can say that operability analyses play an important role in the optimization of planning of marine operations. Yang et al. [16] studied the probabilistic operability for a drilling riser system. The analysis delivered that reduction in drilling operation costs can be achieved by extending the operability envelope in ultra-deep water. Further reliability methods were proposed to predict operability window.

In this vein, a step accounting for operability analyses can be added to the flowchart in Fig. 1.4. The interaction between this step and that of the planning of operations is considered reciprocal since they both depend as much from one as from the other.

1.4 Aim and scope

Based on the challenges presented in Section 1.2.3, the use of accurate numerical models, along with the conduction of time-domain analyses, bring relevant benefits and advantages to the assessment of allowable sea states of lifting operations. The prime challenges addressed within the scope of this study are described as follows:

- To build accurate numerical models of the systems involved in the following lifting operations:
 - lift-off of a subsea spool from the deck of a transportation barge
 - lowering of the subsea spool through the wave zone
- To assess the corresponding allowable sea states to the lifting operations outlined above
- To conduct an operability analysis using two methods for the installation of the subsea spool

The following stages were defined to overcome the challenges aforementioned:

- To conduct hydrodynamic analyses of the floating vessels supporting the lifting operations.
- To build specific models of the spool, the rigging assembly and the floating vessels.
- To suggest a methodology to select suitable scenarios for the lift-off of the subsea spool from the deck of a transportation barge.
- To assess the characteristic responses of the systems obtained during the time-domain simulations of the lifting operations.
- To define the criteria to assess the corresponding allowable sea states.
- To suggest a methodology for comparison of the two installation methods based on the results obtained from weather window analyses.

Fig. 1.5 depicts the general scope of this thesis work along with some of the stages outlined above.

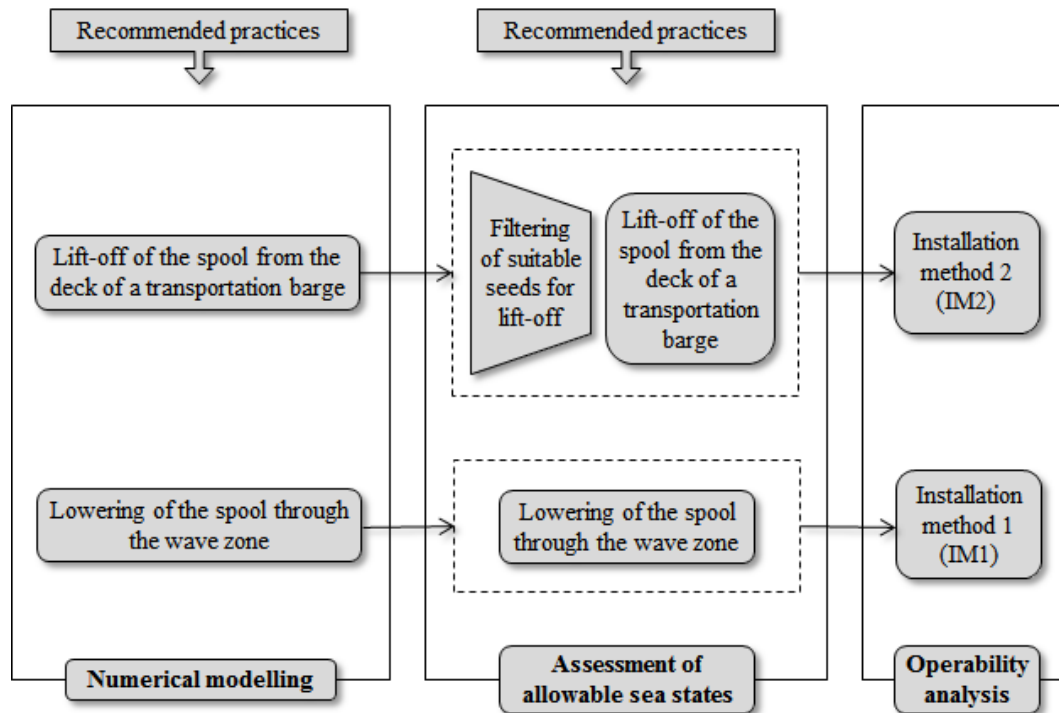


Fig. 1.5. General scope of the thesis work

The first installation method includes one single construction vessel. The second installation method includes one construction vessel and at least one transportation barge. With regard to the subsea lift process of the spool, the prime difference between the installation methods resides in how the lift-off is carried out. In the former case, the lift-off occurs from the deck of the same construction vessel, whereas for the latter case, it occurs from the deck of the transportation barge in close proximity.

The reason why only the two lifting operations aforementioned are studied in this thesis is because of the way their allowable sea states govern the lift-off of the spool in the two installation methods, respectively. In one installation method, the entire subsea lift process is governed by the allowable sea states obtained for the lowering through the wave zone. In the other method, the lift-off occurs from the deck of the transportation barge and thus the respective allowable sea states apply. Further explanation is given in Section 5.2.1.

The purpose of defining one method using transportation barge(s) was to reduce costs by avoiding trips of the construction vessel going back and forth between the harbour and the offshore site when various spools are required to be installed. The rate of a construction vessel is normally more expensive than that of a transportation barge. That being said, the main objective of the operability analysis is to determine which of the methods, for the installation of a given number of spools, offers the most efficient option in terms of overall installation time. This option may become the most cost-effective, however, further cost estimation is required to evaluate so. Cost estimation is not addressed in this work.

The aim during the operability analysis was to determine which of the two methods offers a better outlook in reference to the estimated overall installation time. A new term is introduced here. The *feasibility* of a method accounts for the chance, in terms of time, of successfully completing the installation of a certain number of spools.

Lastly, it should be underlined that specific nouns were adopted in this thesis work with the intention of simplifying some terms. For instance, the construction vessel supporting the lifting operations is denoted as ‘vessel’, whereas the transportation barge is denoted as ‘barge’. The subsea spool is often denoted as ‘spool’. Unless noted otherwise, the operation ‘lift-off of the spool from the deck of a transportation barge’ is simply called ‘the lift-off phase’ and should not be mistaken with that happening from the deck of the same construction vessel. In a similar manner, the operation ‘lowering of the spool through the wave zone’ is denoted as ‘the lowering phase’.

1.5 Thesis outline

This thesis is composed of six chapters, and structured in such a way that it follows the diagram shown in Fig. 1.5. A brief description of each chapter is described next:

Chapter 1 This chapter introduces the motivation and background related to subsea tie-in systems, the installation of subsea structures and the modelling and analysis of marine operations. In addition, the aim and scope, as well as the outline of the thesis are presented here.

Chapter 2 This chapter presents the theoretical background and the recommended practices for offshore lifting operations. The former includes potential theory, wave-induced motions and wave loading. The latter covers design and operational aspects that to a large extent demarcated the numerical modelling and the time-domain analyses in this work.

Chapter 3 This chapter describes the lifting systems (i.e. the subsea spool, the construction vessel and the transportation barge) and also covers the numerical models involved in the lift-off and lowering phases. The hydrodynamic analysis of the vessel and the barge is also included in this Chapter.

Chapter 4 This chapter deals with the assessment of the allowable sea states for the lift-off and lowering phases. Chapter 4, in turn, is divided into four main sections: addressing the time-domain analyses, the suggested methodology to filter seeds with suitable scenario for the lift-off from a barge deck, the criteria defined to assess the allowable sea states for both lifting phases, as well as the presentation and discussion of results.

Chapter 5 This chapter mainly addresses the methodology for conducting the operability analysis. The operability analysis is based on the allowable sea states obtained in Chapter 4, as well as on provided hindcast wave data. The methodology discusses the two methods for the installation of a given number of spools, and the outlines defining their comparative study. Moreover, a sensitivity study on the navigation time of the construction vessel is included. Lastly, the results obtained are presented and discussed.

Chapter 6 Conclusions and recommendations for future work are presented in this Chapter.

Chapter 2

Theoretical basis and recommended practices for offshore lifting operations

2.1 General

The theoretical basis presented along this chapter is linked to the simulation processes conducted in this thesis work, and thus, to the software packages used. Potential flow theory is related to wave induced motions and loads acting on floating vessels (i.e. the construction vessel and the barge) [17]. Another section addresses the wave loading on slender structures since such is the nature of the spool (due to the reasons expounded in Section 3.4.5). Finally, the recommended practices presented here amply demarcated the numerical modelling of the lifting systems and the time-domain analysis of the lifting operations.

2.2 Potential flow theory

Potential flow theory derives from relevant assumptions regarding the type of fluid. In the case of flowing water far from the seabed, it is assumed that particles deform, but do not rotate. This makes the flow non-rotational given that no shear forces exist between the particles (i.e. frictionless flow) [18]. The following expression is fulfilled for a non-rotational flow:

$$\nabla \times \vec{U} = \vec{0} \quad (2.1)$$

where \vec{U} is the velocity of particles. Another assumption establishes that the fluid is incompressible (i.e. constant mass density) and whose mass flow reads Eq. (2.2) where u , v and w account for the components of the particle velocity vector in x -, y - and z -direction, respectively [18].

$$\nabla \cdot \vec{U} = \frac{\partial u}{\partial x} + \frac{\partial v}{\partial y} + \frac{\partial w}{\partial z} = 0 \quad (2.2)$$

In order to obtain the Laplace differential equation, the velocity potential function $\varphi = \varphi(x, y, z, t)$ is introduced in a way that its partial derivatives with respect to the directions are equal to the velocities in these directions [18], that is,

$$\nabla\varphi = \frac{\partial\varphi}{\partial x}\vec{i} + \frac{\partial\varphi}{\partial y}\vec{j} + \frac{\partial\varphi}{\partial z}\vec{k} = \vec{U} \quad (2.3)$$

From developing this expression further, and based on the assumption that the fluid is incompressible, the Laplace differential equation of second order follows:

$$\nabla^2\varphi = 0 \quad (2.4)$$

From the derivation of the potential function φ with respect to a given direction, the velocity and acceleration of particles can be found, which will allow for the calculation of forces later [18].

2.2.1 Boundary conditions

Boundary conditions are needed in order to solve the Laplace equation in Eq. (2.4) given that partial differential equations have several solutions [18]. Note that the fluid flow is still assumed incompressible and non-rotational. The boundary conditions shown in Fig. 2.1 are explained next.

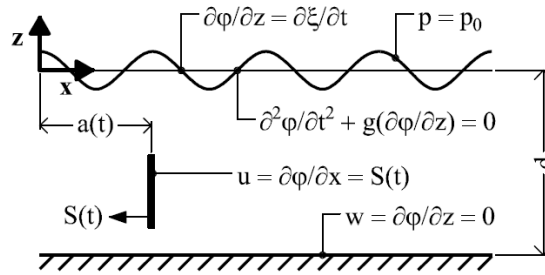


Fig. 2.1. Boundary conditions for solving the Laplace equation

The bottom boundary condition

The bottom boundary condition establishes that it is not allowed for water to flow through the seabed [18]. The seabed is considered flat and located at $z = -d$. Thus, the bottom boundary condition is expressed as:

$$w|_{z=-d} = 0 \quad \therefore \quad \left. \frac{\partial\varphi}{\partial z} \right|_{z=-d} = 0 \quad (2.5)$$

The wall boundary condition

The wall boundary condition establishes that it is impossible for water to flow through a wall located at $x=a$ [18]. If the wall moves with velocity $S(t)$ at time t , the wall boundary condition is defined by:

$$u|_{x=a(t)} = \frac{\partial \varphi}{\partial x} \Big|_{x=a(t)} = S(t) \quad (2.6)$$

In the case of a floating vessel, the velocity component referred to a coordinate system moving with the vessel, and that is normal to its hull, is equal to zero [18]. Hence,

$$\frac{\partial \varphi}{\partial n} \Big|_{(x_i, y_i, z_i)} = 0 \quad (2.7)$$

The surface boundary conditions

The surface boundary conditions determine that water cannot flow through the surface [18].

The kinematic free surface boundary condition establishes a no-leak condition where the vertical velocity of a water particle at the free surface equates to that of the same free surface [19]. Thus, the water particle "will always remain at the free surface" [18, p. 11]. The kinematic free surface boundary condition establishes the following linearised condition:

$$\frac{\partial \varphi}{\partial z} \Big|_{z=\xi(x,t)} = \frac{\partial \varphi}{\partial z} \Big|_{z=0} = \frac{\partial \xi}{\partial t} \quad (2.8)$$

where the wave elevation surface is denoted as $\xi=\xi(x, t)$. The first term refers to the velocity at the wave surface. Hence, the velocity at still surface is specified by setting $z=0$.

The dynamic free surface boundary condition establishes that the pressure, p , at the free surface, $z=\xi(x, t)$, is constant and equal to the atmospheric pressure, p_0 [18][19]. Based on the general form of Bernoulli equation, and after disregarding its second order terms, the dynamic free surface boundary condition expresses that,

$$\xi = -\frac{1}{g} \frac{\partial \varphi}{\partial t} \Big|_{z=0} \quad (2.9)$$

where g is the acceleration of gravity. The following expression is obtained from the combination of the two free surface boundary conditions (i.e. Eqs. (2.8) and (2.9)):

$$\frac{\partial^2 \varphi}{\partial t^2} + g \frac{\partial \varphi}{\partial z} = 0 \quad \text{for } z = 0 \quad (2.10)$$

In this way, the Laplace differential equation (Eq. (2.4)) can be solved so as to obtain the potential function φ . In effect, velocity \vec{U} of the water particle can also be found [18].

2.3 Wave-induced motions and loads on floating structures

2.3.1 Response in regular waves

Wave-induced motions and loads in floating structures can be described by linear wave theory, so-called because the velocity potential is proportional to the wave amplitude [17]. Hydrodynamics of a floating structure can be studied by considering incident regular sinusoidal waves. In addition, no transient effects occur on account of initial conditions (i.e. steady state condition). Therefore, the frequency of linear motions and loads on the structure matches that of the wave loads exciting the structure [17].

Hydrodynamics in regular waves addressed two type of forces and moments acting on a structure; the wave excitation loads and the added mass, damping and restoring loads. By superposing these loads, the total hydrodynamic loads are obtained (see Fig. 2.2) [17].

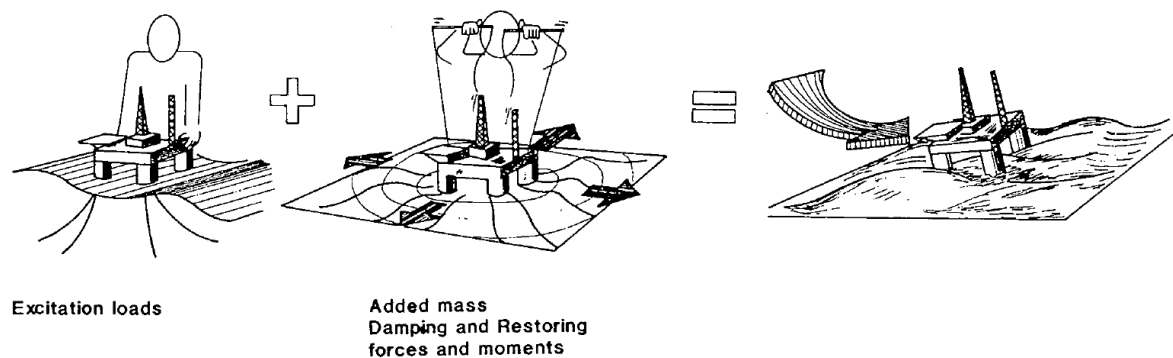


Fig. 2.2. Superposition of wave excitation, added mass, damping and restoring loads [17]

Wave excitation loads

The wave excitation loads derive from the incident waves on the structure as this was restrained from oscillating. These loads comprise the so-called Froude-Kriloff and diffraction forces and moments. The former result from the undisturbed pressure field respective to the unsteady pressure, whereas the latter are due to the variation of the pressure field on the structure [17].

The prime difference between these loads resides in the boundary conditions that have to be established to solve the velocity potential. Their normal velocity components have to be opposite to each other and of identical magnitude. In this way there is a counteraction of their normal velocity components [17].

Added mass, damping and restoring terms

With regard to the added mass, damping and restoring loads, no waves are coming in on the structure, which in turn oscillates with their excitation frequency in any rigid-body motion

mode (i.e. harmonic motions). Forces and moments acting on the structure are obtained by integrating the fluid pressure forces on its surface [17].

The following expression allows for obtaining the hydrodynamic added mass and damping loads as a consequence of the harmonic motion mode η_j :

$$F_k = -A_{kj} \frac{d^2 \eta_j}{dt^2} - B_{kj} \frac{d\eta_j}{dt} \quad (2.11)$$

where F_k denotes the force components in x -, y and z -direction (i.e. F_1 , F_2 and F_3). In a similar way, F_4 , F_5 and F_6 are the moment components along the same axes in that order. A_{kj} and B_{kj} are the added mass and damping coefficients, respectively, which are function of the form of the body and its forward speed, as well as of the oscillation frequency [17].

The expression for F_k in Eq. (2.11) is referred to the right-handed coordinate system (x, y, z) shown in Figure 2.3 where,

- the origin is in the plane of the (undisturbed) free surface,
- z -direction is vertically positive upwards through the centre of gravity of the body and,
- the body is symmetric with respect to the x - y plane.
- η_1 , η_2 and η_3 are translational motions in the x -, y and z -directions, respectively. In the same order, the displacements are called surge, sway and heave.
- η_4 , η_5 and η_6 are rotational motions about the x -, y and z -axes, respectively, so that η_4 is the roll, η_5 is the pitch and η_6 is the yaw angle.

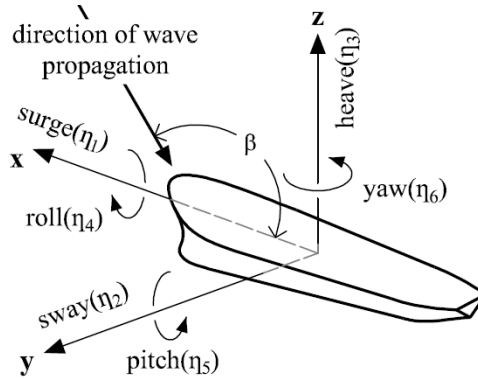


Fig. 2.3. Definition of the rigid-body motion modes [17]

The restoring forces and moments involve hydrostatic mass considerations [17]. These are given by:

$$F_k = -C_{kj} \eta_j \quad (2.12)$$

where C_{kj} are the restoring coefficients.

The equations of motion

The equations of rigid-body motions (Eq. (2.13)) can be obtained from the equations of linear and angular momentum. The process requires the substitution of η_k for $\bar{\eta}_k \exp(-i\omega_0 t)$, where $\bar{\eta}_k$ are the complex amplitudes of the motion modes [17].

$$\sum_{k=1}^6 [(M_{jk} + A_{jk})\ddot{\eta}_k + B_{jk}\dot{\eta}_k + C_{jk}\eta_k] = F_j \exp(-i\omega_0 t) \quad \text{where } j = 1, 2, \dots, 6 \quad (2.13)$$

M_{jk} are the components of the mass matrix of the structure, F_j are the complex amplitudes of the exciting loads and moment-components, and ω_0 is the frequency of waves.

The following equation of motion allows for obtaining the complex 6 by 1 motion vector $X(\omega, \beta)$ and is used by the computer program WADAM [20].

$$[-\omega^2(M + A(\omega))i\omega(B(\omega)_p + B_v) + C + C_e]X(\omega, \beta) = F(\omega, \beta) \quad (2.14)$$

where:

- M is the body inertia matrix
- $A(\omega)$ is the frequency dependent added mass matrix
- $B(\omega)_p$ is the frequency dependent potential damping matrix
- B_v is the linearised viscous damping matrix
- C is the hydrostatic restoring matrix
- C_e is the external restoring matrix
- $F(\omega, \beta)$ is the 6 by 1 complex exciting force vector

The matrices listed above are sized 6 by 6. Note that both $X(\omega, \beta)$ and $F(\omega, \beta)$ are dependent on frequency ω and the wave propagation direction angle β .

By reorganizing Eq. (2.14), the following expression is obtained for the motion vector $X(\omega, \beta)$:

$$X(\omega, \beta) = \frac{F(\omega, \beta)}{[-\omega^2(M + A(\omega))i\omega(B(\omega)_p + B_v) + C + C_e]}$$

2.3.2 Response of floating structures in irregular waves

Vessel responses may limit the feasibility of marine operations [18]. For instance, for lifting operations involving a crane vessel, roll and pitch motions largely influence the displacement of the crane tip due to its long distance to the centre of gravity (CoG) of the vessel [21]. For a monohull vessel, roll motion is a relevant factor that strongly depends on H_S and T_P . Furthermore, roll motion is highly sensitive to the direction of wave propagation [18].

The response of a linear response system, which is exposed to a harmonic wave component $\xi_n(t)$, will also be a harmonic function of time [22]. The shift in time (or delay) of the response with respect to the wave process is considered by the inclusion of a phase angle θ as follows:

$$x_n(t) = x_{0,n} \cos(\omega_n t - \phi_n + \theta_n) = RAO(\omega_n) \xi_{0,n} \cos(\omega_n t - \phi_n + \theta_n)$$

where ϕ_n is the phase shift of the non-transient vibration response [22]. Hence,

$$x_{0,n} = RAO(\omega_n) \xi_{0,n} \quad (2.15)$$

The function will therefore be a function of frequency, $RAO(\omega_n)$. The response amplitude operator (RAO) of a floating structure is defined as the ratio of response amplitude, x_0 , to wave amplitude ξ_0 . The difference between the RAO and the complex valued transfer function, $h_{\Xi X}(\omega_n)$, resides in that the former only provides information about amplitude scaling, whereas the latter deals with phases for the various frequency components [22]. Their relation reads:

$$h_{\Xi X}(\omega_n) = RAO(\omega_n) \exp(i\theta_n) \quad , \quad \text{where} \quad |h_{\Xi X}(\omega_n)| = RAO(\omega_n) \quad (2.16)$$

That being said, by affecting the motion vector $X(\omega, \beta)$ in Eq. (2.14) with a complex valued function $H(\omega, \beta)$, the function of frequency $RAO(\omega, \beta)$ can be obtained as follows:

$$RAO(\omega, \beta) = \frac{X(\omega, \beta)}{H(\omega, \beta)} \quad (2.17)$$

The function $H(\omega, \beta)$ is defined as,

$$H(\omega, \beta) = |H(\omega, \beta)| \exp(-i\phi) \quad (2.18)$$

where $|H(\omega, \beta)|$ is the amplification amplitude of the non-transient vibration response [23].

2.3.3 Wave spectrum

Wave spectrum is defined as "the power spectral density function of the vertical sea surface displacement" [24, p. 60]. A sea state is normally characterised by a wave spectrum (i.e. a sea surface elevation process) [18], [24].

According to Haver [22], the relation between wave spectrum, $S_{\Xi \Xi}(\omega)$, and wave amplitude, ξ_0 , follows:

$$S_{\Xi \Xi}(\omega_n) = \frac{\xi_{0,n}^2}{2\Delta\omega} \quad (2.19)$$

In a similar manner, the response spectrum can be defined as,

$$S_{XX}(\omega_n) = \frac{x_{0,n}^2}{2\Delta\omega} \quad (2.20)$$

By introducing Eq. (2.15), the relation between response and wave spectra is given by:

$$S_{XX}(\omega_n) = [RAO(\omega_n)]^2 S_{\Xi\Xi}(\omega_n) \quad (2.21)$$

In this way, the response spectrum can be obtained directly from the RAO and the wave spectrum [22].

The most preferred spectral models for applications within the NCS are the Pierson-Moskowitz wave spectrum, the JONSWAP wave spectrum and the Torsethaugen wave spectrum. Wave spectrum are often defined by the significant wave height, H_S , and the spectral peak period, T_P [22].

The significant wave height, H_S was formerly defined as the average of a third of the highest waves in a particular pool of waves or within a fixed span. However, it has latterly been determined as four times the standard deviation of surface elevation [18]. DNVGL-RP-C205 [24] defines the spectral peak period, T_P , as the inverse of the frequency value at which the wave spectrum reaches the highest peak.

The Pierson-Moskowitz spectral model depicts the wave spectrum of a sea state whose nature is fully developed. A fully developed (wind) sea signifies that the wave spectrum will remotely change since evenness exists during the wave growth process [22]. On top of fully developed seas, the JONSWAP spectral model deals with growing wind seas [18],[24]. Growing seas are those that undergo a progressive development and thus their wave spectrum changes (e.g., wave period increases) [22].

The Torsethaugen wave spectrum

The Torsethaugen two-peak spectrum, so-called since it gathers the combination of two JONSWAP spectra; one accounting for the wind sea and the other representing the swell system, where not necessarily their direction of propagation coincide. Thus, this spectral model may represent well short term sea states for applications that require independence of the two systems [22].

The period $T_F = a_f H_S^{1/3}$ discriminates the wind dominated and swell dominated regions, where a_f is specified as 6.6 or 5.3 $\text{sm}^{1/3}$ for fetch length 370 or 100km, respectively. In other words, T_F accounts for the fully developed sea condition. For wave spectral period $T_P < T_F$, wind sea predominates, whereas for $T_P > T_F$, swell system does [24]. Eq. (2.22) specifies the Torsethaugen wave spectrum.

$$S(f) = \sum_{j=1}^2 E_j S_{n_j}(f_{n_j}) \quad (2.22)$$

where f is the wave frequency, and the primary and secondary sea systems are characterised by $j=1$ and $j=2$, respectively. Moreover,

$$f_{n_j} = f \cdot T_{Pj}, \quad E_j = \frac{1}{16} H_{Sj}^2 T_{Pj}, \quad \text{and} \quad S_{n_j}(f) = G_0 A_{\gamma_j} \Gamma_{Sj} \gamma_{Fj}$$

The parameters G_0 , A_{γ_j} , Γ_{Sj} , and γ_{Fj} depend on other parameters that are function of H_S and T_P .

For the lifting operations studied in this thesis, the Torsethaugen wave spectrum was adopted so accounting for the characteristic sea states in the offshore area. This spectrum was specified by $T_P=6\text{s}$, $H_S=2.5\text{m}$ and a cosine squared directional distribution of wave energy expressed by 11 wave directions, where 165° is the direction of wave propagation.

Fig. 2.4 shows the Torsethaugen wave spectrum aforementioned. The boundary between the wind dominated and swell dominated areas can be considered from roughly $T_F=7\text{s}$ to 9s . Hence, given that $T_P < T_F$, the sea system associated with $T_P=6\text{s}$ is a growing wind sea (i.e. wind sea predominates). Note that the peak period for the swell system is approximately 11s .

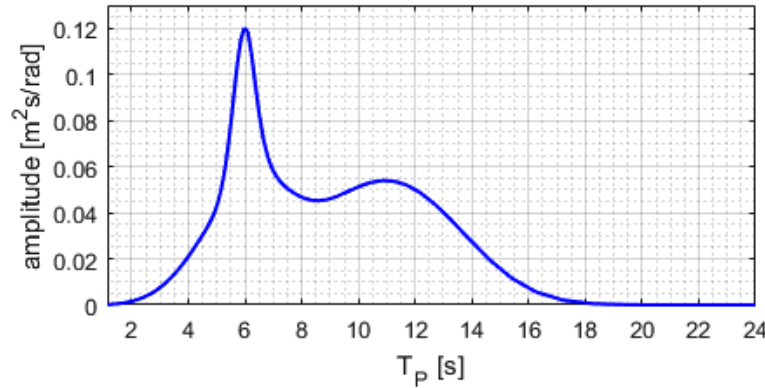


Fig. 2.4. Torsethaugen wave spectrum; T_P 6s, H_S 2.5m, direction of wave propagation 165°

2.4 Wave loading on slender structures

2.4.1 Morison's formula for slender structures

Hydrodynamic forces acting on a slender structure can be estimated by using Morison's formula, which adopts the summation of the inertia force and the drag force [25][24]. The nature of the inertia force (i.e. the former term in Eq. (2.23)) is linear and it comes from potential theory and oscillating flows, whereas the quadratic drag force (the latter term in Eq. (2.23)) deals with real flows and constant currents [19].

$$F(t) = F_{inertia}(t) + F_{drag}(t) \quad (2.23)$$

The resultant hydrodynamic force on a slender structure can be obtained from the summation of sectional forces met by each member (strip) of the structure [24]. For a given structure to be classified as slender, its members shall be small enough to the extent that,

$$\frac{D}{\lambda} = \frac{1}{5} \quad (2.24)$$

where λ is the wave length and D , in the case of a cylindrical member, is its outer diameter [24]. The wave length can be estimated by using the following expression based on airy wave theory (general water depth):

$$\lambda = T \sqrt{\frac{g}{k} \tanh(kd)} \quad (2.25)$$

where g is the acceleration of gravity (9.81m/s^2), d is the water depth, T is the wave period and k is the wave number defined as $2\pi\lambda^{-1}$ [24].

Fig. 2.5 shows the arrangement of the forces acting on a slender element. These are the tangential force f_T , the normal force f_N and the lift force f_L . For an inclined element, α is the angle between the velocity vector \vec{v} and the axis of the slender element. v_N is the normal component of the water particle velocity vector (i.e. $v_N = v \cdot \sin \alpha$).

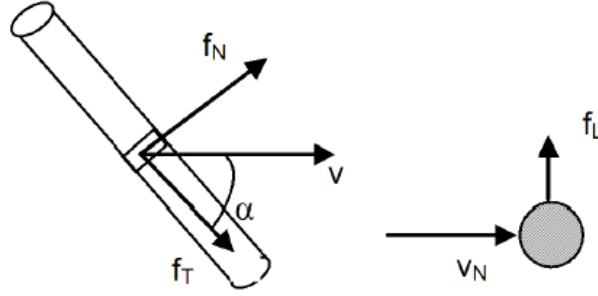


Fig. 2.5. Normal, tangential and lift forces on a slender element [9]

Normal force

For a slender structure crossing the wave zone, the normal force acting on their slender elements can be estimated by means of the following expression [9]:

$$f_N = -\rho C_A A \ddot{x}_N + \rho(1 + C_A) A \dot{v}_N + \frac{1}{2} \rho C_D D v_{rN} |v_{rN}| \quad (2.26)$$

where:

- ρ is the mass density of water
- A is the cross-sectional area
- C_A is the added mass coefficient
- C_D is the drag coefficient
- D is the diameter of the slender element
- \ddot{x}_N is the acceleration of the slender element normal to its axis
- v_{rN} is the relative velocity normal to the element
- \dot{v}_N is the water particle acceleration in normal direction

The first couple of terms in Eq. (2.26) represents the inertia force. The last term accounts for the normal drag force, which for an inclined cylinder can be expressed as:

$$f_{dN} = \frac{1}{2} \rho C_{Dn} D v_N |v_N| \quad (2.27)$$

where C_{Dn} is the normal drag coefficient [24].

Tangential force on an inclined cylinder

The tangential drag force acting on a bare slender cylinder is small in comparison with the normal drag force and normally results from skin friction [24]. The tangential force on a slender element can be obtained from the following expression:

$$f_T = \frac{1}{2} \rho C_{Dt} D v^2 \quad (2.28)$$

where C_{Dt} is the tangential drag coefficient [24]. Note that f_T is considered proportional to the square of the (total) fluid particle velocity.

2.4.2 Hydrodynamic coefficients of slender cylinders

Drag coefficients

Drag coefficients for cylinders with a certain roughness are dependent on Reynolds number in a steady uniform flow [24]. For a Reynolds number larger than 10^6 and large Keulegan-Carpenter number K_C , the drag coefficient for steady flow C_{DS} (dependent on roughness Δ) can be estimated from the following:

$$C_{DS} = \begin{cases} 0.65 & ; \Delta < 10^{-4} (\text{smooth}) \\ (29 + 4 \log_{10}(\Delta))/20 & ; 10^{-4} < \Delta < 10^{-2} \\ 1.05 & ; \Delta > 10^{-2} (\text{rough}) \end{cases}$$

For smooth and rough cylinders subjected to a flow with supercritical Reynolds number, the drag coefficient C_D as a function of K_C can be approximately estimated by,

$$C_D = C_{DS} \cdot \psi(K_C) \quad (2.29)$$

where $\psi(K_C)$ is the amplification factor (see Fig. 3.12) [24].

The normal drag coefficient C_{Dn} in Eq. (2.27) can be taken as independent of the angle α for sub-critical and super-critical flow. However, this may vary considerably with flow direction for critical flow [24].

The tangential drag coefficient C_{Dt} can be obtained by the following formula suggested by Eames [26][24]:

$$C_{Dt} = C_{Dn}(m + n \sin \alpha) \cos \alpha \quad (2.30)$$

where the parameters m and n depend on the type of element as listed in Table 2.1.

Type of element	m	n
Bare cables, smooth cylinders	0.02 - 0.03	0.04 - 0.05
Faired cables	0.25 - 0.50	0.50 - 0.25
6-stranded wire	0.03	0.06

Table 2.1. Dependence parameters between C_{Dt} and C_{Dn} [26][24]

Added mass coefficient

The non-dimensional added mass coefficient for a cylindrical slender element is given by,

$$C_A = \frac{m_a}{\rho A} = \frac{m_a}{\rho} \frac{4}{\pi D^2} \quad (2.31)$$

where m_a is the added mass per unit length, A is the cross-sectional area and D is the diameter [24].

2.4.3 Slamming loads crossing the wave zone

The term slamming refers to the impulse loads caused by the impact between a body and water [17]. When crossing the wave zone, these loads on the body are considered transient loads [1].

The slamming force of an object that is lowered through the free surface is defined as the rate of change of fluid momentum and can be estimated by using Eq. (2.32), where v_s is

the slamming velocity (assumed positive) and $a_{33}^{\infty}(t)$ is the instantaneous high-frequency limit heave added mass [9], [24].

$$f_s(t) = \frac{d}{dt}(a_{33}^{\infty}v_s) = a_{33}^{\infty}\dot{v}_s + v_s^2 \frac{d}{dh}(a_{33}^{\infty}) \quad (2.32)$$

In the case of a horizontal cylinder, the sectional slamming force in terms of a slamming coefficient C_s follows,

$$f_s(t) = \frac{1}{2}\rho C_s D v_s^2 \quad (2.33)$$

where ρ is the mass density of water, D is the diameter of the cylinder and C_s is specified by,

$$C_s = \frac{2}{\rho D} \frac{d}{dh}(a_{33}^{\infty}) \quad (2.34)$$

where the term $\frac{d}{dh}(a_{33}^{\infty})$ is the rate of change of sectional added mass with submergence h (see Fig. 2.6) [9]. The relative position of the cylinder to the free surface (i.e. h/r) refers to the term 'depth-dependent'.

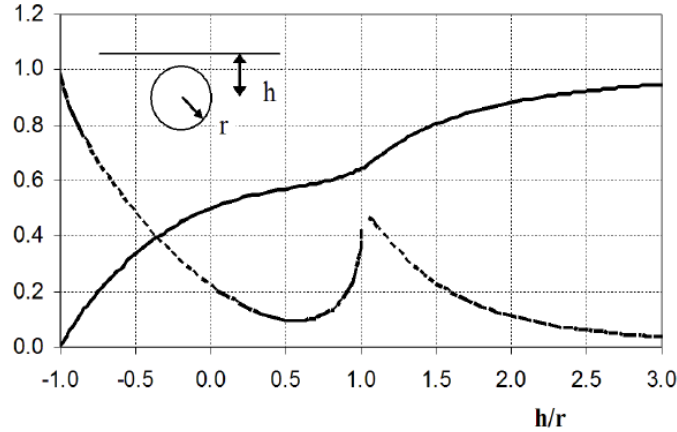


Fig. 2.6. High frequency limit of vertical added mass coefficient and its derivative [9]

The solid line in Fig. 2.6 denotes the non-dimensional added mass coefficient defined as,

$$C_A = \frac{a_{33}^{\infty}}{\rho\pi r^2} \quad (2.35)$$

The dotted line denotes the derivative of C_A as a function of the submergence (i.e. $\frac{d}{dh}(a_{33}^{\infty})\frac{1}{\rho\pi r}$).

For a cylinder crossing the free surface at high speed, the vertical added mass can be taken as its high frequency limit [24]. Therefore, from Eq. (2.32), the sectional slamming force is reduced to the following expression:

$$f_s(t) = \frac{d}{dt}(m_a v_s) = m_a \dot{v}_s + v_s^2 \frac{d}{dh}(m_a) \quad (2.36)$$

where m_a is the vertical added mass and \dot{v}_s is the slamming acceleration.

2.5 Recommended practices for offshore lifting operations

The recommended practices presented in this section demarcate to a large extent the numerical modelling and time-domain analyses in the thesis work. These guidelines are related to offshore lifting operations that are thoroughly planned, designed and executed, as well as are endorsed by reliable documentation. Specific guidance was taken from the following standards:

- DNVGL-RP-N103 [9],
- DNVGL-ST-N001 [1] and,
- DNVGL-RP-N201 [8].

Relevant design and operational aspects that are associated with offshore lifting operations involving floating vessels with cranes of moderate capacity are presented next.

2.5.1 General

Stability of lifted objects

During the lowering of a partly air-filled object, its buoyancy is distributed differently from its mass [9]. This may cause tilt of the object, which affects the sling load distribution of the rigging configuration [1]. Therefore, attention should be directed to the stability during the lifting operations [9].

Fig. 2.7 shows a submerged body whose centre of gravity (CoG), C_G , and centre of buoyancy (CoB), C_B , are vertically misaligned. The centre of force (CoF), C_F , can be obtained from using the following expression:

$$C_F = \frac{Mg \cdot C_G - \rho g V \cdot C_B}{Mg - \rho g V} \quad (2.37)$$

where M is the mass of the body, V is the displaced volume of water and g is the acceleration of gravity. Once the body is submerged, it will not tilt provided that the lift-wire is attached vertically above its CoF [9].

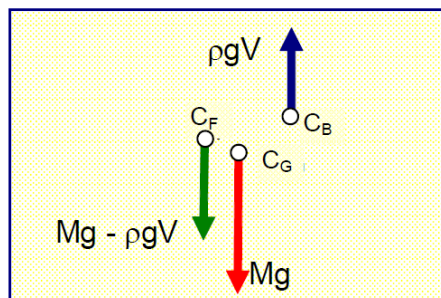


Fig. 2.7. Definition of the centres of gravity, buoyancy and force of a body [9]

When the expected maximum tilt of the object is larger than 2° , related effects should be considered in the sling load calculations [1]. Stability (i.e. tilt) of the spool under static condition was verified during the numerical modelling process in this work.

Clearances

For all phases of a lifting operation, all the minimum required clearances (including those under water) should be properly defined, assessed and considered [8], [1]. According to DNVGL-RP-N103 [9], the following are considered operational aspects during a lifting operation, among others:

- clearance between the lifted object and crane boom
- clearance between the lifted object and any other object or structure
- clearance between the underside of the lifted object and the seafastening structure for its transport

For instance, one relevant aspect during the lift-off and over-boarding of an object is to control its horizontal motion or swinging [8]. During the lift-off and lowering of the object through the wave zone, tugger lines are commonly used to control and restrain horizontal and rotational motions of the object [8], [1].

According to DNVGL-ST-N001 [1], the following clearances should be kept when using a crane on a floating vessel:

- 3m between any part of the lifted object and the crane boom
- 5m between the lifted object and other objects on the same transport vessel, unless bumpers or tugger lines are fitted
- 3m between the lifted object and any other structures (horizontally), such as the installation vessel, unless guides or bumpers are used.

Some of the criteria above were adopted as the allowable limits for the assessment of allowable sea states for the lowering phase.

Effects of short-crested sea

DNVGL-ST-N001 [1] recommends that for motion analysis, short-crested sea shall be considered when allowable sea states (in terms of wave height) are to be found for operating in different vessel headings. Roll motion is likely to be more influenced in short-crested sea than in long-crested sea. Thus, larger vertical crane tip motions may be expected [9], [5]. The effects of short-crested sea were taken into consideration for the lifting operations studied in this thesis work.

2.5.2 Lift-off of an object

The lift-off of an object from the deck of the same crane vessel is a simple operation. This is due to the relative motion between the crane tip and the vessel is virtually negligible [9]. Particularly, the lifting operations of the spool are categorised as light lifts since its weight is less than 2% of the displacement of the construction (crane) vessel. In this case, the crane boom is considered a stiff structure and the crane tip motion follows the wave-induced rigid body motion of the construction vessel.

When the object has been transported onto a barge and the lift-off involves the crane vessel to be positioned side by side, the relative motion between the crane hook and the barge becomes a critical parameter [9].

According to DNVGL-RP-N103 [9], the feasibility of a lift-off operation depends on the following parameters:

- The hosting speed of the crane, which is normally higher than 0.1 m/s
- The combined motion responses of the two floating vessels
- Combination of the weather condition and the orientation of the floating vessels

Chapter 3

Lifting systems and numerical models

3.1 General

Transportation barges and heavy lift vessels assist the installation of subsea structures. Normally, these structures are transported by means of a barge to the offshore location, where a heavy lift vessel is already positioned to accomplish their installation [3].

The selection of a barge is based on different aspects that depend on the subsea structure in itself, the offshore location, weather conditions and cost, among others. In the case of spool components or rigid jumpers, a barge is a practical option for their transportation [3].

Regarding heavy lift vessels, these are equipped with a crane whose lift capacity may reach thousands of tonnes. Heavy lift vessels are required for lifting heavy structures with large dimensions. When a subsea structure is transported by a barge, its lift-off and transfer is carried out by means of one of the cranes the heavy lift vessel is provided with [3].

Within the scope of this work, the installation or deployment of a spool is carried out by a construction vessel. The construction vessel meets with the requirements in terms of space and load capacities, sea behaviours and positioning.

Both the construction vessel and barge(s) may participate in the transportation activity depending on the amount of spools intended to be installed. This aspect is in detail presented in Section 5.2.1.

The subsea lift process of the spool can be summarized into the following main phases:

- Lifting the spool off from the deck by means of the main crane of the construction vessel and manoeuvring it to the planned position for its lowering.
- Lowering the spool through the wave (splash) zone.
- Further lowering of the spool down to the seabed.
- Positioning the spool onto the corresponding mating hubs.

This chapter presents the numerical models for the lifting systems involved in the lift-off and lowering phases this work deals with. The main components of the systems are:

- Subsea spool
- Construction vessel
- Transportation barge

The hydrodynamic analysis of the construction vessel and the barge is also presented in this chapter. This analysis was required in order to predict (linear) wave-induced motions and loads on both vessels [17]. In the case of the lift-off of the spool from the deck of the barge, RAOs of the construction vessel may be affected by the barge due to proximity (hydrodynamic interaction). RAOs for both vessels should be computed by means of multi-body analysis [9].

The lift-off phase addressed in this thesis work is that where the lift-off of the spool occurs from the deck of the barge (i.e. the spool has been transported on the same barge). Therefore, the term *lift-off phase* throughout this work, exclusively refers to such event rather than the lift-off from the deck of the construction vessel (see Section 5.2.1 for further explanation).

3.2 Systems

3.2.1 Subsea spool

Dimensions and mass of the tubular elements (members) comprising the spool are listed in Table 3.1.

Member	OD [mm]	WT [mm]	Mass [kg]
Reinforcement pipe(s)	406.4	25.4	14110
Steel pipe(s) with coating	461.6	19.05	25826
Termination head(s)	358.8	19.05	4697
Secondary member(s)	358.8	19.05	458
Reinforcement pipe(s)	457.2	25.4	107
Total	-	-	45178

Table 3.1. Dimensions and mass of members of the spool

A general sketch of the spool is shown in Fig. 3.1. Its centre of gravity (CoG) was taken from a STAAD input file provided and also validated during the numerical modelling. STAAD is a structural analysis and design computer program, and its file included technical information (e.g., dimensions, material) of the members comprising the spool and others such as slings.

3.2.2 Construction vessel

The construction vessel used in this work is a floating installation vessel suitable for subsea umbilicals, risers and flowlines (SURF) operations and also provided with an efficient dynamic positioning system. The main features of the vessel are shown in Table 3.2.

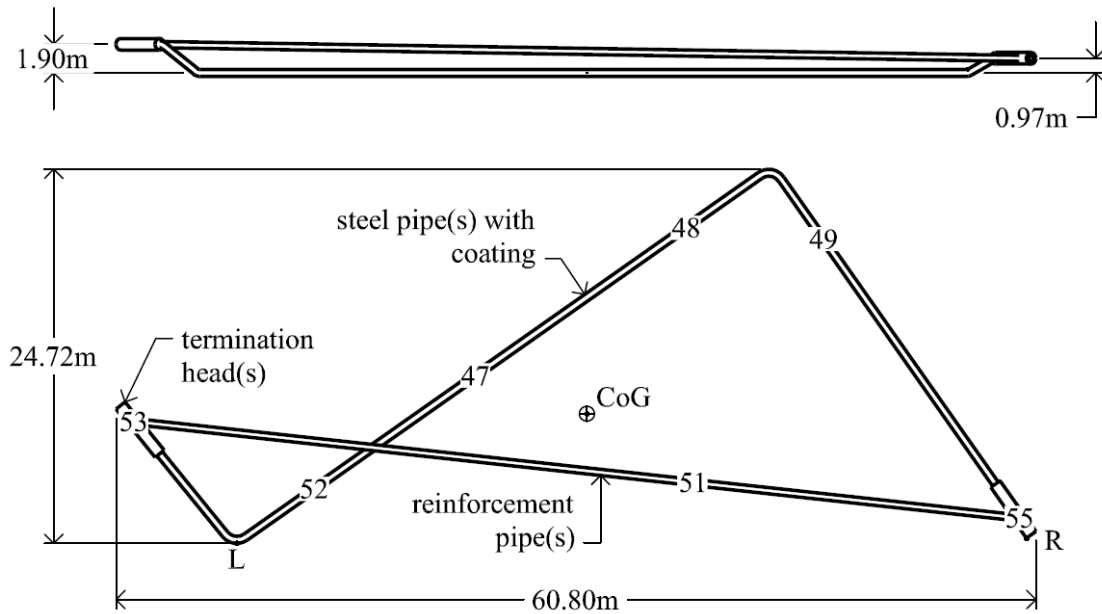


Fig. 3.1. General sketch of the spool

Length overall	[m]	156.7
Breadth	[m]	27
Max. draught	[m]	8.5

Table 3.2. Main features of the construction vessel

By choosing an operational draught 8.0m, the main deck (free-board) of the vessel is located at 4.0m above the sea water line.

Main crane

The vessel has an active heave compensated (AHC) crane with a maximum lift capacity of 400t in normal speed mode. The minimum and maximum lift radius of this crane are 10m and 40m, respectively. The crane is provided with a crane block whose theoretical mass is 12t. These components and their features were relevant in the numerical modelling of the lifting operations in this work, basically, when locating the crane tip height, estimating the length of the lift-wire and calculating the total weight of the lifting assembly.

3.2.3 Transportation barge

The transportation barge is a conventional barge for operations in the Norwegian continental shelf (NCS) and also suitable to transport the spool on its deck. The main features of the barge are presented in Table 3.3.

The operational draught of the barge was taken as 4.0m, hence, its deck (free-board) is located 4.5m above the sea water line.

Length overall	[m]	100
Breadth	[m]	25.6
Draught	[m]	4.0
Depth	[m]	8.5
Displacement	[T]	10417

Table 3.3. Main features of the barge

3.2.4 Configuration for the lift-off of the spool from the deck of the barge

The configuration for the lift-off of the spool from the deck of the barge consists of the following:

- The construction vessel
- The subsea spool
- The transportation barge
- Hoisting elements (slings, lift-wire and winch)

Fig. 3.2 depicts the general arrangement of these elements during the lift-off phase.

The relative location on the x - y plane of the barge with respect to the vessel is fully dependent on the position of the spool on board and the crane tip location. This is located in such a way that the CoG of the spool matches the crane tip position in the x - y plane. In this manner, a 10m-clearance was sought to maintain between the starboard of the barge and the portside of the vessel during the lifting operations.

Regarding the crane tip, its location on the x - y plane coincides with that during the lowering phase (see Section 3.2.4 for further detail). However, this is located 4.6m higher in comparison with that for the lowering phase since additional length of lift-wire is required to be retrieved.

The hoisting elements are mainly the slings coupling the spool to the hook of the crane block, the lift-wire between the crane block and the crane tip, and the winch. The wire couplings are in detail presented in Section 3.4.2.

Location of the crane tip

The location of the crane tip considered the following aspects:

- orientation of the crane boom
- load chart of the main crane (lift radius and capacity)
- size of the crane block and length of coupling elements (slings, lift-wire)
- initial position of the spool in z -direction to be lowered (as modelled)
- orientation of the spool on the x - y plane

The spool was positioned on the x - y plane in such a way that its points L and R (see Fig. 3.1) were oriented towards the portside of the vessel and also keeping a distance to its portside not less than 9m, approximately.

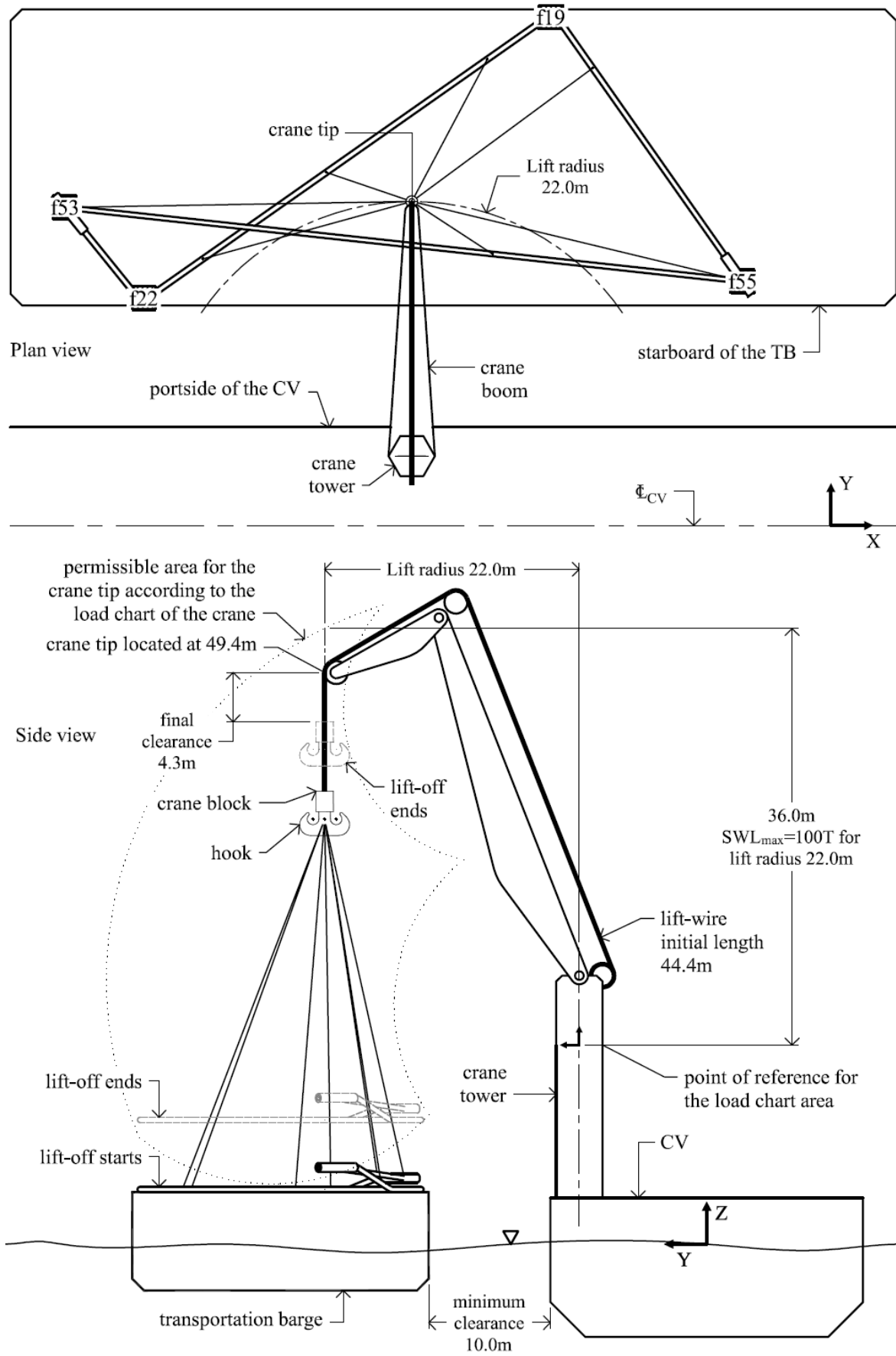


Fig. 3.2. Configuration layout for the lift-off of the spool from the deck of the barge

The crane boom was perpendicularly oriented to the portside of the vessel in order to optimise the lift capacity for any given lift radius. In this way, the crane tip would be located in y -direction the closest possible to the vessel so as to reduce its roll motions during lifting operations of the spool.

Taking as a starting point the constraints above, the potential lift radius was defined as 22m. According to the load chart of the main crane, a 22m-lift radius allows for lifting a combined safe working load (SWL) no larger than 100t, approximately.

The crane tip height was finally located at 44.8m. Its definition was based on the initial position the spool was intended to be lowered from, the size of the crane block and the length of wire couplings.

3.2.5 Configuration for the lowering of the spool through the wave zone

Excepting the barge, the configuration for the lowering of the spool through the wave zone is the same as in the lift-off phase. A general layout of the lowering phase is shown in Fig. 3.3. Note that the orientation of the spool being lowered through the wave zone is the same as when it is transported on the deck of the barge for the lift-off phase.

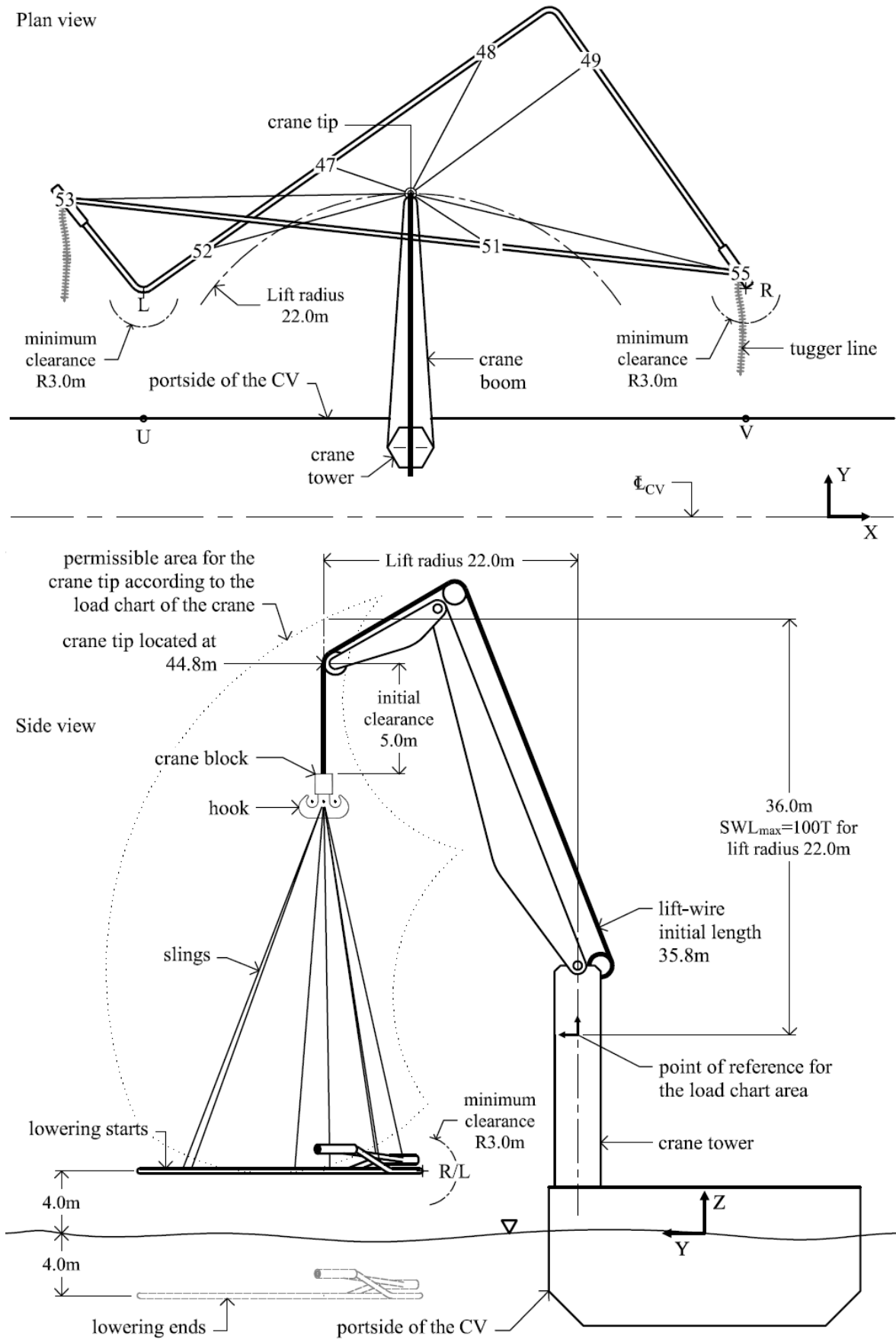


Fig. 3.3. Configuration layout for the lowering of the spool through the wave zone

3.3 Hydrodynamic analysis of the floating vessels

The hydrodynamic analysis of floating vessels was conducted by means of the program WADAM (version 9.3.7), which allows for calculating wave-structure interaction of structures of arbitrary shape [27]. WADAM was executed from HydroD (version 4.9.2), which is an analysis tool pertaining to the software suite Sesam.

Panel models were used for hydrodynamic analysis. Hydrodynamic forces on large-volume bodies are obtained from using potential theory [17]. Frequency-domain analyses of the stationary floating vessels involved in the lifting operations were conducted. Consequently, the corresponding results were input for subsequent time-domain analyses.

The analysis of two cases (hydromodels) was necessary: the first hydromodel only included the construction vessel for the analysis of its linear steady state response during the lowering phase (Section 3.3.1). The second hydromodel included the barge on top of the vessel for analysis of responses during the lift-off phase (Section 3.3.2).

3.3.1 Hydrodynamics of the construction vessel

The lowering phase required the hydrodynamic analysis of the vessel alone since the barge does not participate in it. Therefore, this analysis required a single-body hydromodel which was built upon the panel model of the vessel provided.

Fig. 3.4 shows the steps carried-out for the hydrodynamic analysis. An appropriate resolution of the frequency was set in order to check the range of interest the vessel is likely to work within. In this way, the guideline suggested by DNVGL-RP-C205 [24] regarding the computation of at least 30 frequencies when analysing motions of a floater in frequency domain was followed. Given that roll motion of a vessel close to the roll resonance period cannot be estimated from using panel models [17], an additional damping matrix was also specified in order to achieve realistic responses in roll motion by considering viscous effects on the vessel. Roll damping of a vessel is importantly influenced by viscous effects, primarily, if the vessel is provided with bilge keels [28].

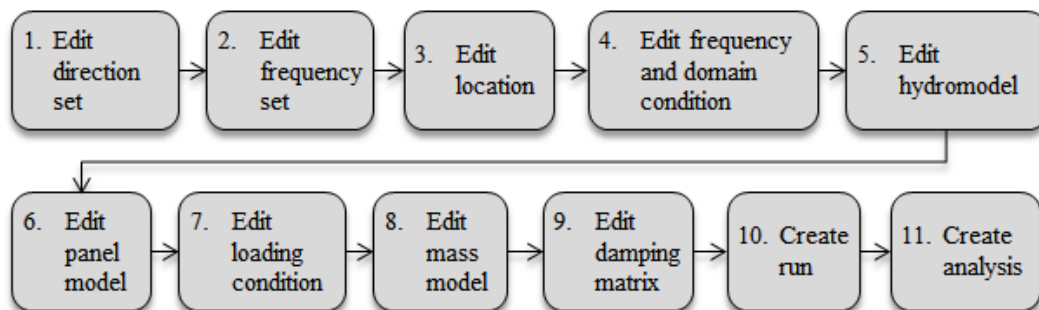


Fig. 3.4. Flowchart for the hydrodynamic analysis of the floating vessels

Fig. 3.5 shows the first order motion transfer function, or RAO, of the vessel across the different ship motions obtained from the single-body hydrodynamic analysis.

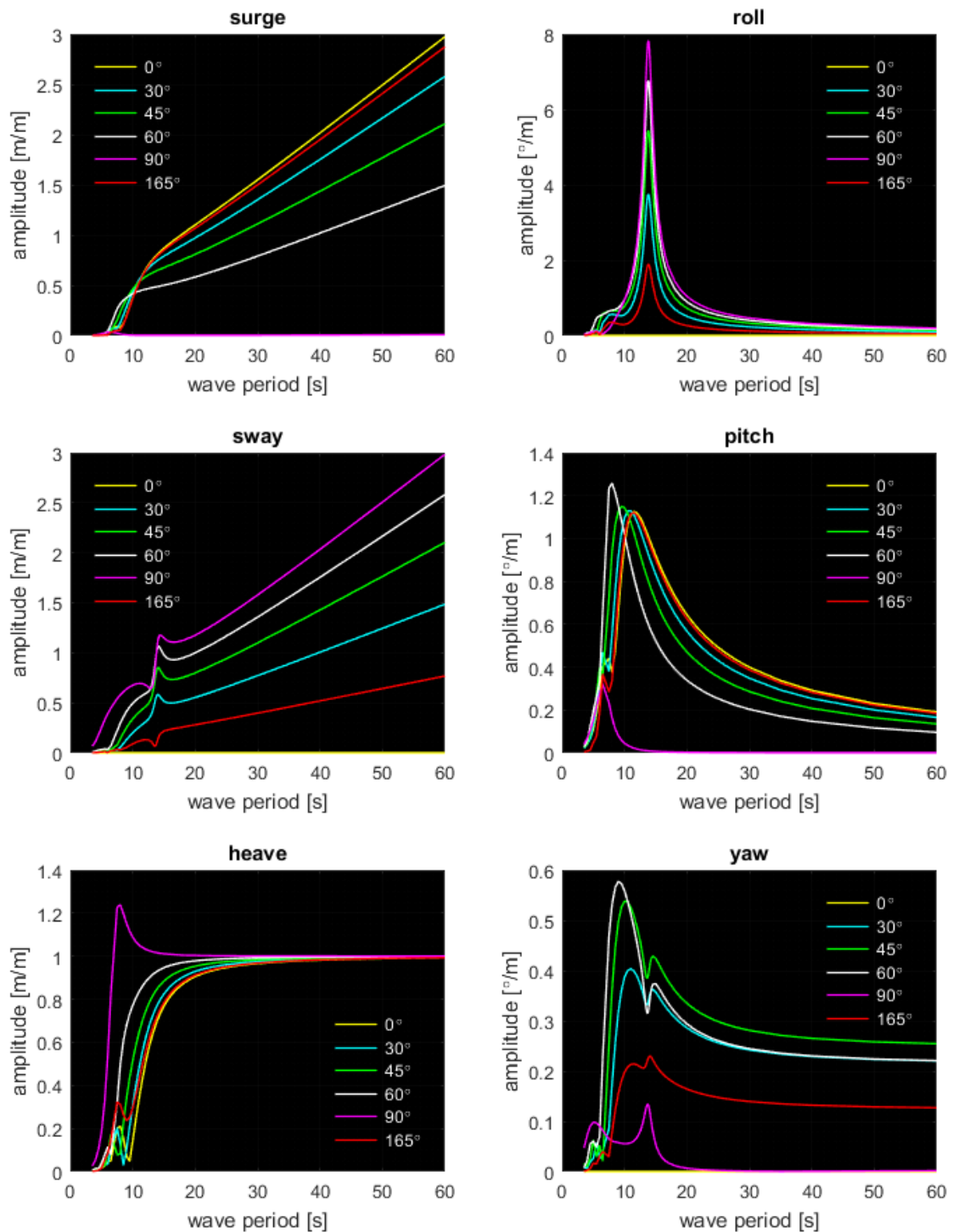


Fig. 3.5. First order motion transfer functions of the construction vessel: single-body condition

Roll, pitch and heave motions are of interest in this work due to their effects on the crane tip motion. Moreover, one can say that surge, sway and yaw motions are to some extent counteracted by the numerical modelling for the positioning (mooring) system of the vessel(s).

Responses in Fig. 3.5 present a typical behaviour for vessels with similar features (e.g., dimensions, mass). Additional validation was carried out by comparing these responses with the real ones provided of the same vessel. As a result, no deviation was found between them.

The roll motion presents the characteristic peaked response with the highest amplitudes at 14s, approximately. Amplitude decreases on both sides of the peak period. This decrease is more pronounced when the direction of wave propagation is perpendicular to the vessel (i.e. 90°), since at this direction roll motion reaches its maximum amplitude at roughly $8^\circ/\text{m}$. Naturally, the roll is marginal at direction 0° .

Pitch motion follows a similar trend to that of pitch, however the downward trend of amplitudes after wave peak period is not that sudden. The peak of the responses occurs between wave periods 7s to 12s, being $1.3^\circ/\text{m}$ the largest amplitude for a direction of wave propagation 60° .

Heave motion shows the typical response where the amplitude converges to the unit after an upward trend. Amplitudes present an intermediate peak around the wave period zone 6 to 8s, where the highest (i.e. approximately $1.3\text{m}/\text{m}$) is reached at 8s with direction 90° .

Responses of surge and sway motions present an opposite behaviour between them in terms of amplitude for perpendicular directions of wave propagation. That is to say, in the former the highest amplitudes are reached with direction 0° , whereas in the former these are reached with direction 90° . The response of both motions show an upward trend as wave period increases due to the relatively small water depth (104m) at the offshore location. In sway motion, peaks are mostly aligned when wave period is roughly 14s.

3.3.2 Hydrodynamics of the construction vessel and the transportation barge

An hydrodynamic analysis including both the construction vessel and the barge was required for the lift-off phase. An uncoupled multi-body hydromodel was built upon independent hydromodels of the vessel and the barge.

Regarding the barge, whose panel model was also provided, the input matrix for its mass model was calculated based on its features (see Table 3.3) and complementary data such as CoG and radii of gyration. A damping matrix was also added in order to obtain realistic motion responses by considering viscous effects in roll damping. The steps shown in Fig. 3.4 were also followed during the hydrodynamic analysis of the barge.

Fig. 3.6 shows the first order motion transfer function of the barge standing alone across the different motions (i.e. hydromodel of the vessel is not included). These responses present a typical behaviour of a barge of its kind.

In broad terms, the behaviour of the RAOs of the barge are rather similar to those of the vessel. However, amplitudes are different mainly for roll and pitch motions. The largest amplitude for roll motion (also at direction of wave propagation 90°) is $4.5^\circ/\text{m}$ when wave period is 9s, approximately. The largest amplitudes for pitch motion occur in the wave period zone from 7s to 10s. In the case of heave motion, the largest amplitude when the direction of wave propagation is 90° meets almost $1.2\text{m}/\text{m}$ at wave period 7s, approximately.

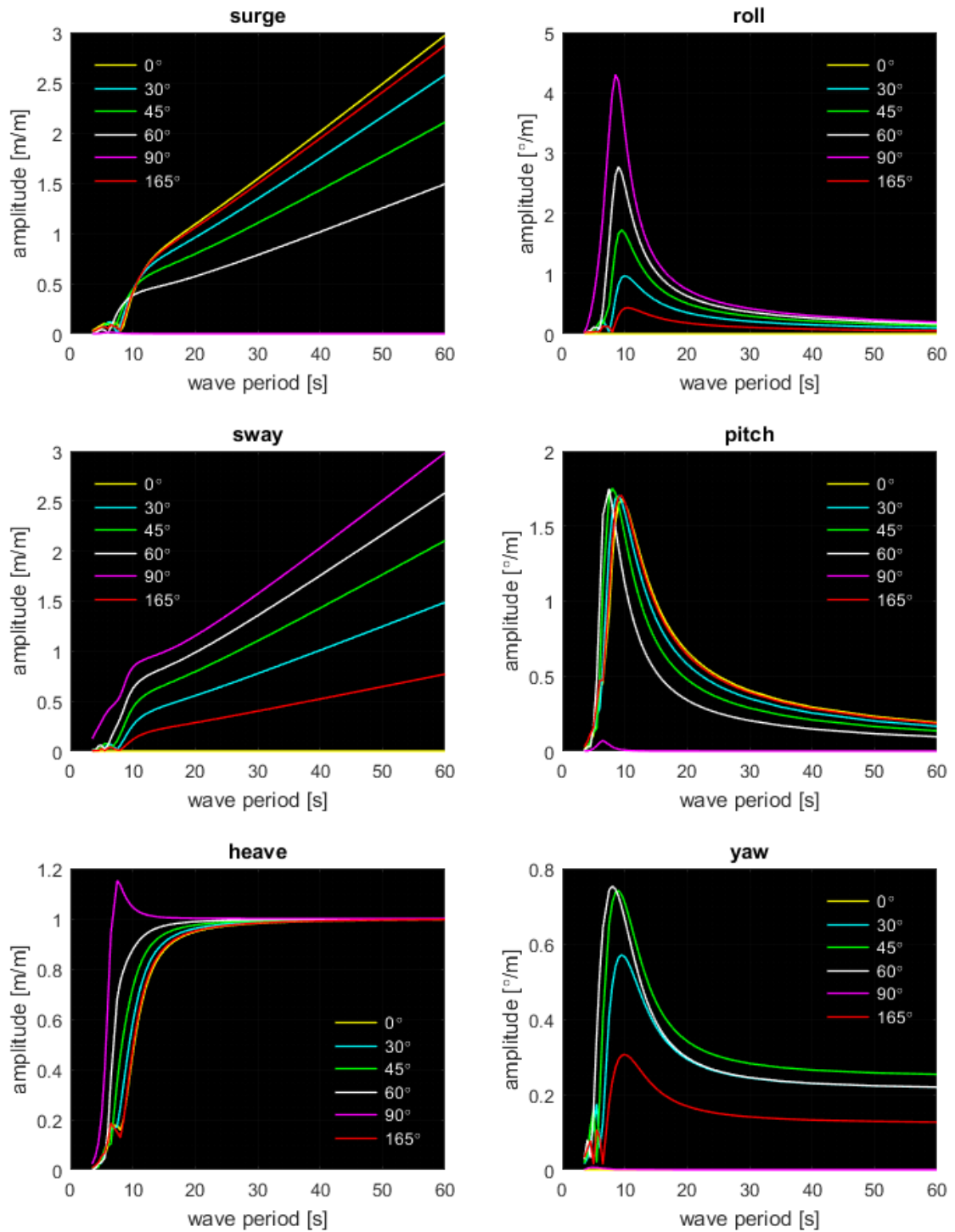


Fig. 3.6. First order motion transfer functions of the barge: single-body condition

Following the arrangement presented in Section 3.2.4, the multi-body hydromodel comprising the vessel and the barge was generated (see Fig. 3.7). The gap between the two bodies as modelled is 10.51m. The global response obtained was therefore the input for the modelling of the lift-off phase in SIMA-SIMO. Fig. 3.8 shows the first order motion transfer function of both bodies interacting in the lift-off phase, in which case the average wave propagation direction is 165°.

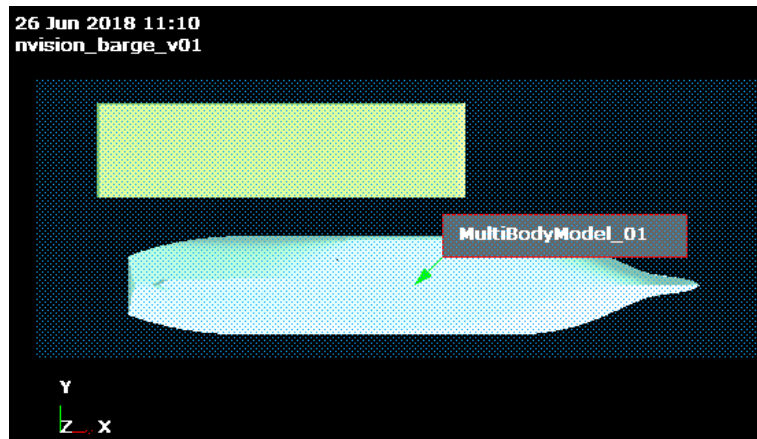


Fig. 3.7. WADAM multi-body hydromodel of the vessel and the barge (plane view)

Surge, sway and heave motions in Fig. 3.8 show a similar behaviour of RAOs for both bodies. However, amplitudes and peak wave periods differ across roll, pitch and yaw motions. The largest difference occurs for roll motion. The highest peak reached by the vessel is roughly $1.9^\circ/\text{m}$ at wave period 14s, whereas for the barge it is $0.6^\circ/\text{m}$ at 9s. In the case of pitch motion, the amplitude difference is approximately $0.5^\circ/\text{m}$ where the barge meets the largest (i.e. roughly $1.6^\circ/\text{m}$). One can say that peak wave periods for the vessel and the barge are 11s and 10s, respectively. The plotting of the RAOs shows some punctual irregularities across some of the motions. These irregularities result from mesh properties in the hydromodel, however, these did not influence subsequent processes.

Finally, Fig. 3.9 shows the comparison of the RAOs of the construction vessel between single- and multi-body conditions. One can say that the responses virtually show the same trends and amplitudes, mainly in peak zones. The vessel directly meets waves coming from the dominating direction of propagation (i.e. there is no an intermediate body as in the case of the barge). However, for wave periods from 5s to 9s, the responses for multi-body condition present additional peaks in sway and yaw motion. This also happens to the roll motion where the difference in amplitude is marginal in comparison to that of the peak.

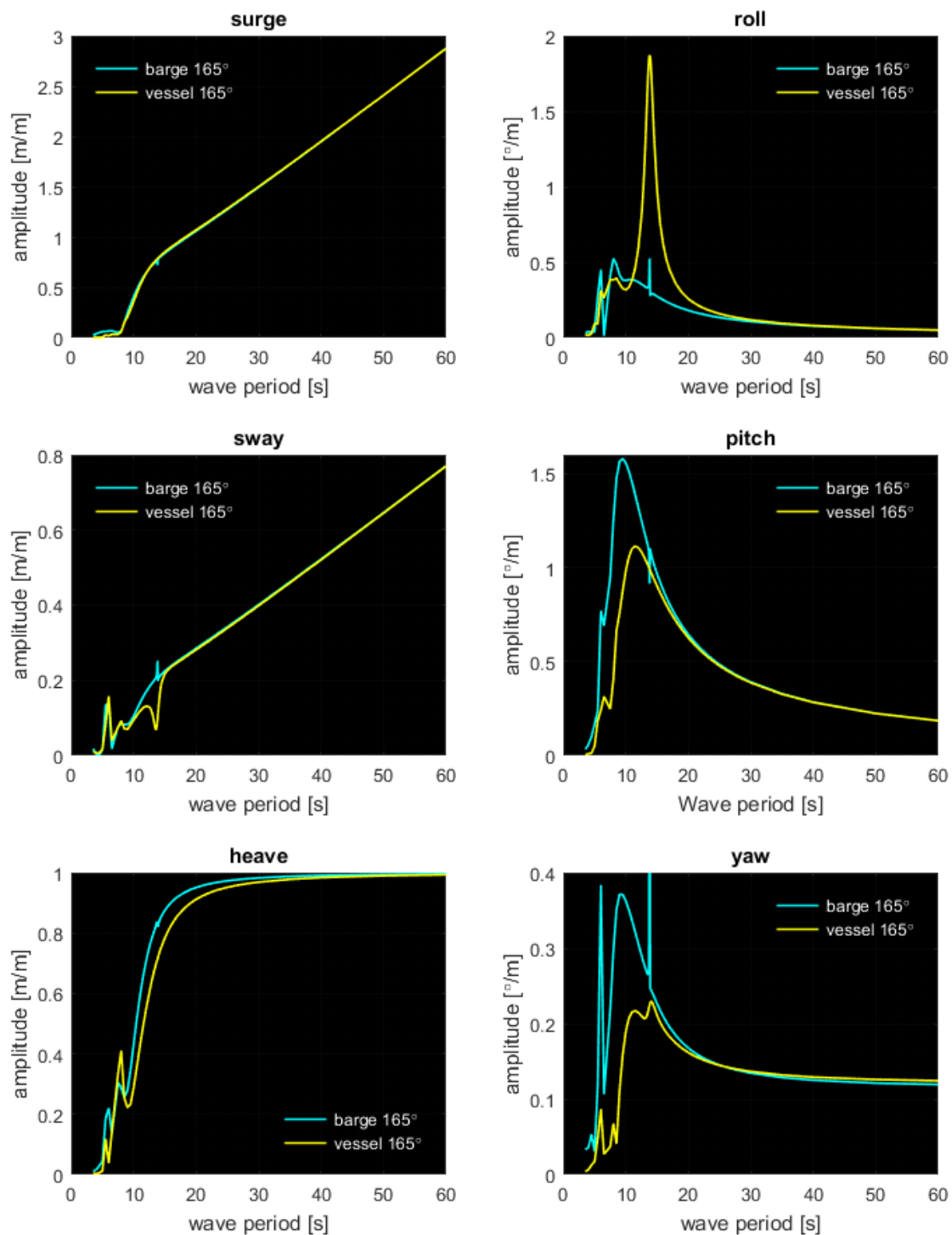


Fig. 3.8. First order motion transfer functions of the construction vessel and the barge: multi-body condition

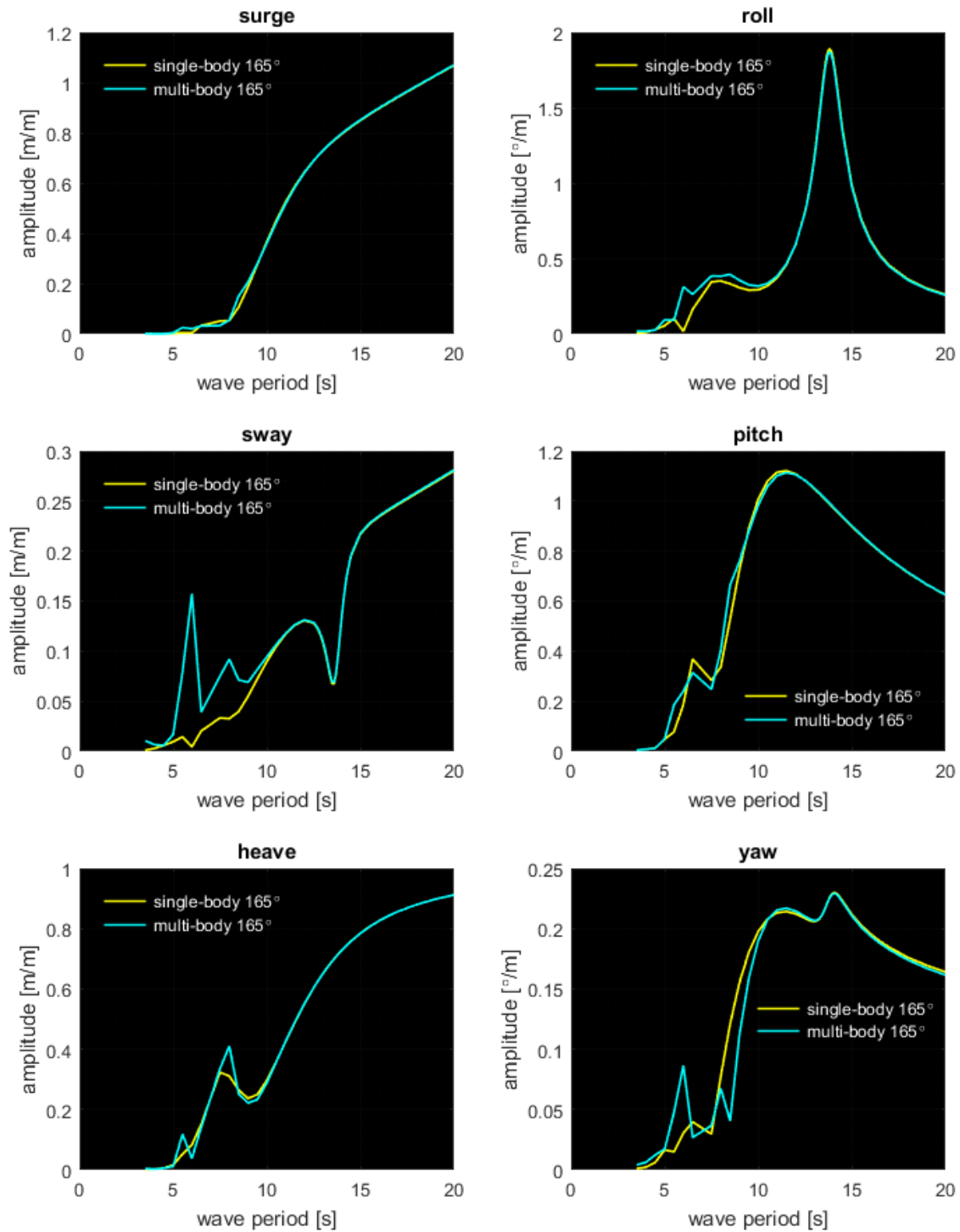


Fig. 3.9. First order motion transfer functions of the construction vessel: single- and multi-body conditions

3.4 Numerical models of the lifting systems

3.4.1 General

The numerical modelling of the lifting systems was carried out by using SIMA workbench (version 3.3.3), which is a simulation and analysis tool for marine operations and floating systems (e.g., lifting and installation of subsea equipment). SIMA is built on a software for dynamic analysis. SIMA also belongs to the software suite Sesam, which is used for hydrodynamic and structural analysis of ships and offshore structures [27].

SIMA, in turn, supports the analysis program SIMO, which focuses on complex multi-body calculations and also deals with the simulation of motions and station-keeping behaviour of comprehensive systems (e.g., floating vessels and suspended loads) [27]. In this work, SIMO was used for the modelling of the slender elements of the spool and couplings (e.g., slings, the lift-wire, contact points between the spool and the deck of the barge), as well as for the specification of hydrodynamic coefficients (including those depth-dependent), among others.

Both lifting scenarios (lift-off of the spool from the deck of the barge and its lowering through the wave zone) share the same numerical model for the following systems:

- Arrangement of slings coupling the spool to the hook of the crane block
- The lift-wire linking the crane block to the main crane (however, its initial modelled length is different)
- Positioning system for the floating vessels

Particular numerical modelling of other systems was also carried out for each lifting phase. For instance, the lift-off phase required the modelling of coupling elements between the spool and the deck of the barge, whereas the lowering phase required the definition of hydrodynamic coefficients for the spool. The simplification of tugger lines can be included within the scope of the wire couplings.

3.4.2 Modelling of the wire couplings

In this work, wire couplings refer to:

- The seven slings attached to the spool and connected to the hook of the crane block
- The single lift-wire linking the crane block to the main crane

The slings have their length fixed during the complete lifting operation, whereas the length of the lift-wire varies as a function of time for the purpose intended, i.e. either for the lift-off or lowering of the spool.

The wire couplings were individually modelled as a linear spring whose coupling force reads the following expression:

$$T = k \cdot \Delta l \tag{3.1}$$

In Eq. (3.1), T is the wire tension, Δl is the wire elongation and k is the effective axial stiffness [14].

Once the connecting points of the corresponding bodies were defined, the numerical modelling of the wire couplings was carried out by means of simple wire coupling elements.

Slings between the spool and the hook

The points on the spool the slings are attached to, as well as their connecting point to the hook of the crane block, were provided by the STAAD input file. The connecting point to the hook is aligned in z -direction with the CoG of the spool. Hence, the lift-wire is attached right above the CoG of the spool instead of its centre of force (CoF). This particular aspect is discussed in Section 4.5.1.

In this work, the notation for a given sling is defined by the point on the spool the sling is attached to (e.g., sling $s48$ is that attached to point 48 on the spool). Fig. 3.10 shows the general arrangement of the slings.

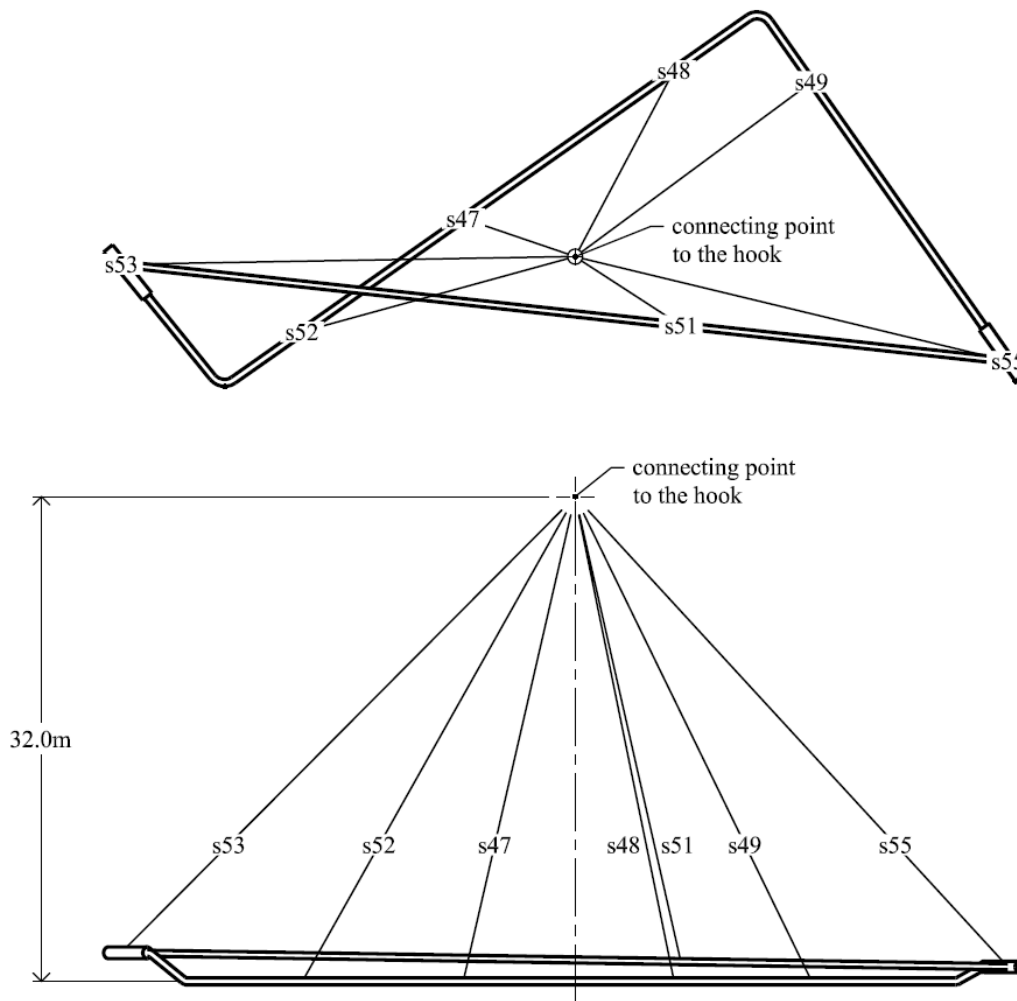


Fig. 3.10. General arrangement of the slings

The spool is not a completely-stiff body. In order to achieve reliable outcomes, the model has to include the variation of tension in the slings as a result of the deformation of the spool while being lifted.

This was accomplished by including a flexibility constant, $1/k_0$, whose value is independent for each sling. The total stiffness of the sling, including the deflection of the spool, is given by the following expression:

$$\frac{1}{k} = \frac{l}{EA} + \frac{1}{k_0} \quad (3.2)$$

where k is the effective axial stiffness of the series connection considering the deflection of the spool, E is the modulus of elasticity, A is the cross-sectional area of the sling and l is the non-stretched length of the sling [14].

The constant $1/k_0$ for each sling was found by modifying its value to the point of matching the tension value of the sling under static condition in SIMO, with that obtained from the STAAD outcome.

The main features of the slings are listed in Table 3.4.

Sling	EA [N]	Flexibility, $1/k_0$ [m/N]	Length, l [m]
s47	2.0361×10^8	4.35×10^{-7}	32.40
s48	2.0361×10^8	5.25×10^{-7}	34.90
s49	2.0361×10^8	2.30×10^{-7}	37.43
s51	2.0361×10^8	7.30×10^{-7}	32.13
s52	2.0361×10^8	2.95×10^{-7}	37.06
s53	2.0361×10^8	1.20×10^{-7}	42.26
s55	2.0361×10^8	2.50×10^{-7}	42.51

Table 3.4. Features of slings attached to the spool

Table 3.5 shows the comparison of tension values in slings between those obtained from the STAAD outcome and those obtained from the analysis under static analysis in SIMO.

Sling	STAAD [N]	SIMO [N]	Deviation
s47	68820	69253	0.63%
s48	39533	39755	0.56%
s49	69527	70011	0.70%
s51	63552	63659	0.17%
s52	94627	94446	-0.19%
s53	88127	87597	-0.60%
s55	109092	108280	-0.74%

Table 3.5. Tension in slings obtained from STAAD and SIMO analyses (static condition)

Given that comparison in Table 3.5 shows a good agreement, the deformation of the spool is somehow considered even the spool is modelled as a stiff body in SIMA-SIMO.

Lift-wire linking the crane block to the main crane

Features such as the modulus of elasticity E , and the cross-sectional area A of the lift-wire are expected to remain constant during the lifting operation. However, the length l does not remain constant as it varies as a function of time for the purpose intended. This means that the term l/EA also varies in time.

With regard to the initial length of the lift-wire, this is different between the lift-off and the lowering phases given that the crane tip height and the initial position of the spool in z -direction are also different.

In SIMO, a guide-point is a fixed point where a coupling element may slide through [29]. This point was modelled at the crane tip to simulate a sheave. In addition, this would minimise the variation of the crane tip motion. The length of the lift-wire is measured starting from the winch-point until the connecting point at the crane block, going along the crane boom and also passing through the guide-point as shown in Figs. 3.2 and 3.3. The winch point is therefore located on the crane tower. Winch parameters influencing the lifting operations are in detail listed in Sections 4.2.2 and 4.2.3.

The flexibility constant $1/k_0$ and other features of the lift-wire are listed in Table 3.6.

EA	Flexibility, $1/k_0$	Material damping
[N]	[m/N]	[Ns]
1.2038×10^9	1.30×10^{-7}	1.0×10^7

Table 3.6. Main features of the lift-wire

Simplification of tugger lines

According to DNVGL-ST-N001 [1], tugger lines can be used in order to restrain pendulum motions of the lifted object. DNVGL-RP-N103 [9] also recommends that in the case the horizontal motion of the lifted object is controlled by guide wires, these shall be modelled as constraints or horizontal springs in the equations of motion for the object.

Yaw stiffness was added to the spool for simplicity, only to represent the restoring forces from tugger lines. Assuming an auxiliary winch (for each tugger line) with a pulling capacity of 19.6kN (2000kgF), the yaw stiffness can be estimated. In practice, two tugger lines may be used and attached to points L and R of the spool, respectively.

3.4.3 Modelling of the positioning system for the floating vessels

With the aim of modelling the positioning (mooring) system, a set of four fixed force-elongation elements was included in the numerical model of the positioning system of each floating vessel (i.e. the construction vessel and the barge). Such elements are governed by a force-elongation relationship, which may be designated as a station-keeping force. In addition, their purpose is to describe axial and shear forces (e.g., when using a hawser or anchor line) [30]. These (mooring) elements were given pretension and their force-elongation parameters are shown in Table 3.7.

Distance	Force
[m]	[kN]
80	-600
100	600
120	1800

Table 3.7. Parameters of the fixed force-elongation elements for the positioning system

Since the analysis of tensions in mooring elements is not within the scope of this work, these are not presented here. However, the actual model allowed for maintaining the 10m-clearance between the vessel and the barge during the lift-off of the spool as mentioned in Section 3.2.4.

3.4.4 Modelling of the fender couplings for the lift-off phase

During its transportation for the lift-off phase, the spool is lying down directly on the deck of the barge. Four points underneath the spool were defined as the most likely to collide with the deck during its lift-off; points *f19*, *f22*, *f53* and *f55* (see Fig. 3.2). Therefore, four couplings elements were modelled as fenders at these contact points between the spool and the barge. These points indicate if re-hit occurs during the corresponding time-domain simulations.

A fender comprises one single sliding plane defined by a point and its normal vector. As a consequence, there will exist a friction force along the sliding plane (i.e. along the deck) as well as a compressive force perpendicular to the sliding plane [30]. The compressive perpendicular force is obtained by linear interpolation, from a specific relation between distance and force, and also from the particular internal damping [30][31].

Table 3.8 shows some features of the coupling elements (fenders). Friction coefficients were adopted on the basis that the physical contact was hard-steel on hard-steel [32][31]. Shear stiffness associated with friction was assumed from typical values.

Friction coefficient		Shear stiffness
Static	Dynamic	[N/m]
0.42	0.78	4.68×10^7

Table 3.8. Features of the coupling elements (fenders) [32][31]

3.4.5 Modelling for hydrodynamic loads on the spool

The numerical model primarily addressed the calculation of hydrodynamic coefficients of the spool by following the theoretical basis presented in Sections 2.4.1 and 2.4.2.

Among the tubular elements of the spool, the largest ratio D/λ is as follows:

$$\frac{D}{\lambda} = \frac{0.462\text{m}}{25\text{m}} = 0.0185 < \frac{1}{5}$$

where D is the largest diameter among the tubular elements of the spool and λ is the lowest possible wave length across the range of wave periods T (see Table 3.9). The values of λ were obtained by using Eq. (2.25) as follows:

$$\lambda = T \sqrt{\frac{9.81\text{m/s}^2}{k} \tanh(k \cdot 104\text{m})}$$

T [s]	4	5	6	7	8	9	10	11	12	13	14
λ [m]	25	39	56	76	100	126	156	188	223	260	298

Table 3.9. Estimate wave length for the offshore field

Therefore, according to the theoretical basis presented in Section 2.4.1, the spool is considered as a structure composed of slender cylinders and its hydrodynamics can be calculated using the Morison's load formula [9].

Hydrodynamic coefficients

The hydrodynamic coefficients of the tubular members of the spool were defined with reference to the coordinate system of the element shown in Fig. 3.11. These coefficients are listed in Table 3.10 and their explanation in detail is presented next.

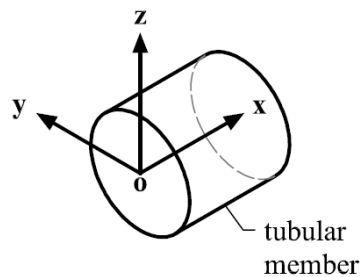


Fig. 3.11. Definition of the strip coordinate system for tubular members of the spool

Member	D [mm]	$C2Y, C2Z$ [Ns ² /m ³]	$C2X$ [Ns ² /m ³]	AMY, AMZ [kg/m]	AMX [kg]	open ends
Reinforcement pipe(s)	406.4	437.4	46.4	234.8	36.0	yes
Steel pipe(s) with coating	461.6	496.8	52.7	171.5	52.8	no
Termination head(s)	358.8	386.2	41.0	103.6	24.8	no
Secondary member(s)	358.8	386.2	41.0	103.6	24.8	no
Reinforcement pipe(s)	457.2	492.1	52.2	301.2	51.3	yes

Table 3.10. Hydrodynamic coefficients of tubular members of the spool

Quadratic transverse drag coefficients $C2Y$ and $C2Z$ These coefficient were obtained from using Eq. (2.27) as follows:

$$C2Y, C2Z = \frac{f_{dN}}{v_N |v_N|} = \frac{1}{2} \rho C_{Dn} D$$

Since there is no explicit relation between the the normal drag force coefficient C_{Dn} and the drag coefficient C_D in Eq. (2.27), it was assumed that $C_{Dn} \approx C_D$. Therefore, the normal drag force coefficient C_{Dn} was estimated from using a steady drag coefficient C_{DS} for cylinders with roughness $\Delta > 10^{-2}$ (i.e $C_{DS} = 1.05$) and a wake amplification factor $\psi(K_C)$ (see Eq. (2.29)).

From Fig. 3.12, and also by assuming flows with Keulegan-Carpenter number K_C close to 12, the wake amplification factor $\psi(K_C)$ was taken as 2.0. That being said, the normal drag force coefficient C_{Dn} reads:

$$C_{Dn} \approx C_D = C_{DS} \cdot \psi(K_C) = (1.05)(2.0) = 2.10$$

therefore,

$$C2Y, C2Z = \frac{1}{2} \left(1025 \frac{kg}{m^3} \right) (2.10) D \quad \left[\frac{Ns^2}{m^3} \right]$$

This approach for estimating C_{Dn} is to some extent similar to that suggested by Aarset et al. [11], where drag coefficients may be taken as twice the steady state values in the event that no experimental data is available.

Quadratic longitudinal drag coefficient $C2X$ This coefficient was calculated from using Eqs. (2.28) and (2.30). The maximum value for such coefficient is reached when the largest ratio C_{Dt}/C_{Dn} occurs. Hence,

$$\text{for } \frac{d}{d\alpha} \left(\frac{C_{Dt}}{C_{Dn}} \right) = 0, \quad \alpha = \arcsin \frac{-m \pm \sqrt{m^2 + 8n^2}}{4n}$$

Since parameters m and n were assumed 0.02 and 0.05, respectively (see Table 2.1), it was found that the ratio C_{Dt}/C_{Dn} was equal to 0.04 for an angle α approximately equal to 37.9° (see Fig. 3.13). Therefore,

$$C2X = \frac{f_T}{v_n^2} = \frac{1}{2} \rho C_{Dt} \frac{D}{\sin^2 \alpha} = \frac{1}{2} \left(1025 \frac{kg}{m^3} \right) (0.04 \cdot 2.10) \frac{D}{\sin^2 (37.9^\circ)} \quad \left[\frac{Ns^2}{m^3} \right]$$

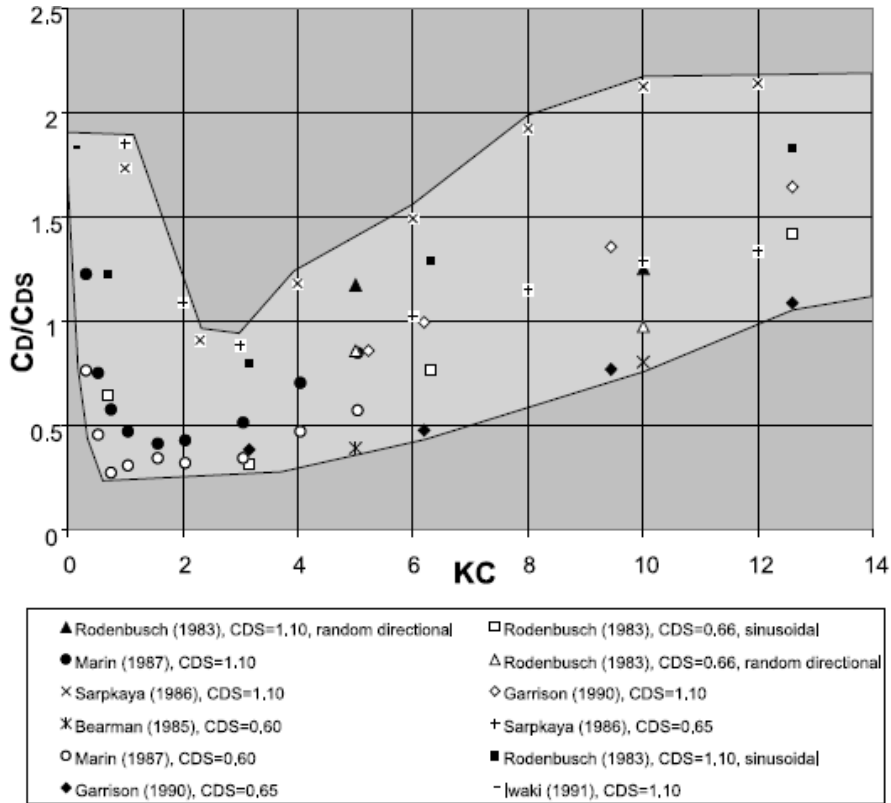
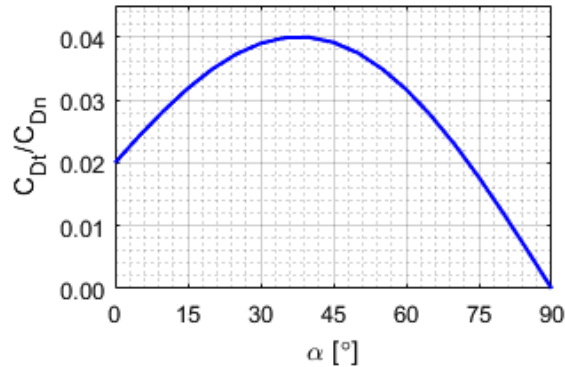


Fig. 3.12. Wake amplification factor [9]


 Fig. 3.13. Variation of C_{Dt} with angle of attack α

Transpose added mass coefficients AMY and AMZ These coefficients were calculated from using Eq. (2.31) and by following the standard DNVGL-RP-N103 [9]. According to the latter, the non-dimensional added mass coefficient C_A is taken as 1.00 for a right circular cylinder (no open ends) when $b/2a \rightarrow \infty$, therefore,

$$AMY, AMZ = m_a = \rho C_A \frac{\pi}{4} D^2 = \left(1025 \frac{kg}{m^3}\right) (1.00) \frac{\pi}{4} D^2 \quad \left[\frac{kg}{m}\right]$$

For tubular elements lowered with open ends, their transpose added mass coefficient becomes roughly double of its value in case of close-ends (see Table 3.10) since the actual mass of water inside the tubular element is added.

Longitudinal added mass coefficient AMX This added mass coefficient was estimated as that for a circular disc in accordance with DNVGL-RP-N103 [9]. However, since the spool comprises long tubular elements, this coefficient was only applied to elements forming the ends and bends. This coefficient was also affected by the number of strips modelled, N_i , and their length l_i :

$$AMX = \frac{m_a}{N_i l_i} = \frac{\rho C_{AVR}}{N_i l_i} = \frac{\rho}{N_i l_i} \frac{2}{\pi} \left[\frac{4}{3} \pi \left(\frac{D}{2} \right)^3 \right] = \frac{1025 \frac{kg}{m^3}}{N_i l_i} \frac{D^3}{3} \quad \left[\frac{kg}{m} \right]$$

Depth-dependent scaling of hydrodynamic coefficients

SIMO gives the option of specifying depth dependent scaling of hydrodynamic coefficients and also calculates the slamming force only if these data are given. This force is met by slender elements with nearly horizontal angle when crossing the water surface (wave zone) [29]. The slamming force was calculated by choosing the option given by SIMO, which is linked to the corresponding theoretical basis presented in Section 2.4.3.

Likewise the traverse and longitudinal coefficients previously presented, the depth-dependent coefficients (ratios) were also defined based on the coordinate system of the element shown in Fig. 3.11. Their estimation was carried out based on the following expressions (see Fig. 3.14 for a better understanding):

$$RVOL = \frac{A_{sub}}{\pi r^2} \quad RCQX = \frac{arc_{sub}}{2\pi r} \quad RCQY = \frac{h_{sub}}{2r} \quad RCQZ = \frac{l_{sub}}{2r} \quad (3.3)$$

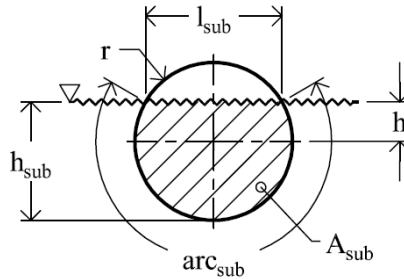


Fig. 3.14. Variables in the depth-dependent scaling of hydrodynamic coefficients

Furthermore, the following considerations were taken:

- Relative linear drag coefficients are equal to quadratic drag coefficients in the corresponding x -, y -, and z -direction.
- Since skin friction is the driver for forces in x -direction, it is assumed that $RAMX$ has the same value as $RCQX$
- Given that the projected area is the driver for forces in y -direction, it is assumed that $RAMY$ has the same value as $RVOL$
- The relative added mass in z -direction $RAMZ$ is calculated by using Eq. (2.35).

The coefficients above follow the same notation as in SIMA-SIMO [29] where,

- $ROVL$ is the volume relative to fully submerged volume
- $RAMX$ is the relative added mass in longitudinal, local element x -direction
- $RAMY$ and $RAMZ$ are the relative added mass in local element y - and z -directions, respectively
- $RCQX$ is the relative quadratic drag in longitudinal, local element x -direction
- $RCQY$ and $RCQZ$ are the relative quadratic drag in local element y - and z -directions, respectively

Table 3.11 lists the depth-dependent hydrodynamic coefficients as a function of h/r for a cylinder with radius r . These coefficients are also plotted in Fig. 3.15.

h/r	$RVOL, RAMY$	$RCQX, RAMX$	$RCQY$	$RCQZ$	$RAMZ$
-1.00	0.00	0.00	0.00	0.00	0.00
-0.75	0.07	0.23	0.13	0.66	0.20
-0.50	0.20	0.33	0.25	0.87	0.34
-0.25	0.34	0.42	0.38	0.97	0.43
0.00	0.50	0.50	0.50	1.00	0.50
0.50	0.80	0.67	0.75	1.00	0.57
1.00	1.00	1.00	1.00	1.00	0.67
2.00	1.00	1.00	1.00	1.00	0.88
3.00	1.00	1.00	1.00	1.00	0.94

Table 3.11. Depth-dependent hydrodynamic coefficients

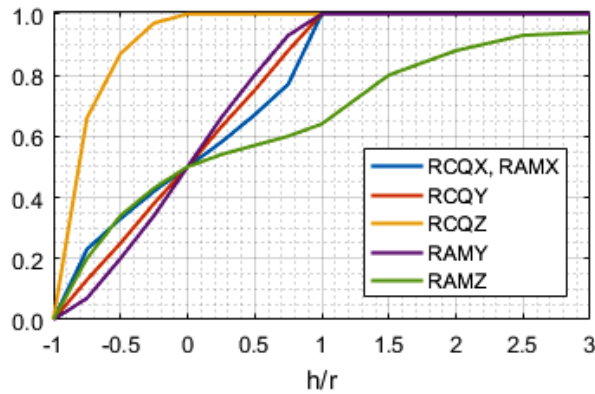


Fig. 3.15. Depth-dependent hydrodynamic coefficients

By using the depth-dependent coefficients (ratios) outlined above, loads on the slender elements of at different positions relative to the instantaneous free surface can be adequately calculated.

Chapter 4

Assessment of allowable sea states

4.1 General

Allowable sea states play an important role in the planning phase of a marine operation. Their comparison against history records of hindcast wave data of the offshore site can be used for analysing the operability of a system in a marine operation [4].

Fig. 4.1 depicts the general methodology to establish allowable sea states suggested by Li [14, pp. 56–58] and Guachamin Acero et al. [4]. The general terms and steps included in this methodology are explained below.

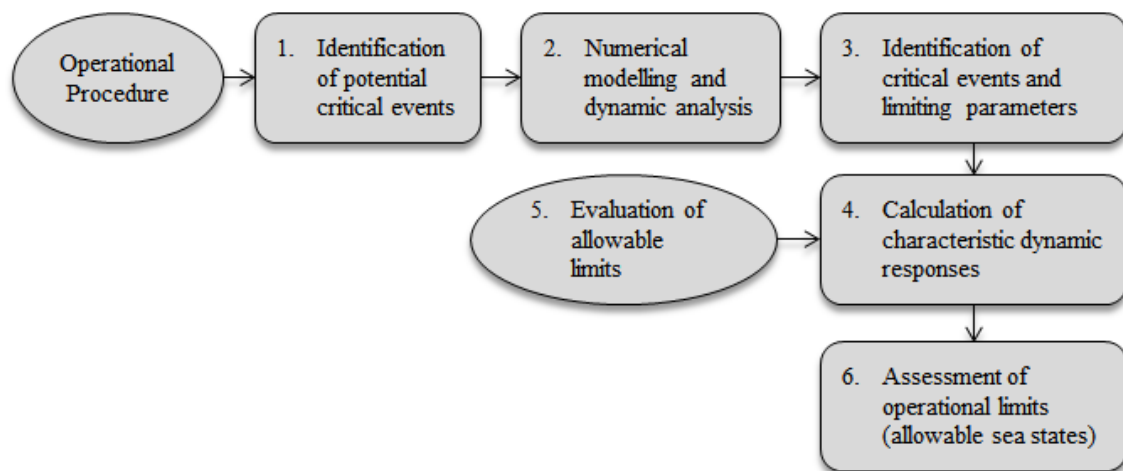


Fig. 4.1. General methodology to establish allowable sea states [14, p. 57]

- Critical events: the events that occur if the operational limits are exceeded and that may endanger the operation (e.g., collision of objects).
- Limiting parameters: the parameters that limit the operation and define the critical events (e.g., the characteristic total force in sling can be used as a limiting parameter for sling breakage).
- Allowable limits: the limits that portray the threshold values for the corresponding limiting parameters.

- Operational limits: the necessary limits for decision-making processes in marine operations [1] , [14] , [4]. In this work, these limits are specified in reference to allowable sea states.

The steps involved in the methodology in [14, pp. 56–58] and [4] are:

- Step 1 "*Identification of potential critical events*": critical events that might exist during activities established by an operational procedure are identified by means of qualitative reliability methods. Specialists on the subject often conduct the selection of such activities.
- Step 2 "*Numerical modelling and dynamic analysis*": numerical analyses of the activities are conducted based on coupled dynamic models of the system. Next, under environmental conditions expected to be found in-site, global dynamic analyses are also conducted. The latter will reveal which parameters are likely to reach extreme responses in comparison with their allowable limits and will consequentially limit the operation (quantitative assessment of dynamic responses).
- Step 3 "*Identification of critical events and limiting parameters*": for every activity and their respective failure events, the governing limiting parameters (dynamic responses) are detected.
- Step 4 "*Calculation of characteristic dynamic responses*": the dynamic coupled models involved in the corresponding activities are selected. Subsequently, computation of characteristic values of responses for the limiting parameters is carried out. Here, the simulation process is conducted for every seed of the pool of possible sea states.
- Step 5 "*Evaluation of allowable limits*": these limits are used to reduce, to the extent possible, the likelihood of having a failure during the marine operation(s). The failure might occur on account of exceeding normal operating criteria or structural overloading. Allowable limits consider safety criteria and regularly demand structural analyses or FEM.
- Step 6 "*Assessment of operational limits*": allowable sea states are found by correlating the allowable limits and the characteristic values found in step 4.

As it was stated in Section 1.4, the two lifting operations studied are the lift-off of the spool from the deck of a transportation barge and its lowering through the wave zone. Based on the two installation methods devised for conducting the operability analysis in Chapter 5, their allowable sea states are critical during the deployment of the spool (see Section 5.2.1 for further explanation).

The assessment of the allowable sea states for the lifting operations studied in this work was conducted by following the methodology above. The different aspects in steps 4, 5 and 6, the results obtained and their discussion are presented in this chapter.

4.2 Time-domain analysis and setting of simulation parameters

Where extreme load effects are to be predicted, time-domain analysis methods are of great usefulness since non-linear higher load effects can be captured [24]. This is particularly the case of the lifting operations studied in this work, which are time-varying non-stationary processes and the assessment of allowable sea states are submitted to the criteria presented in Section 4.4. Time-domain analyses are also suggested when non-linear effects need to be considered [24]. Furthermore, time-domain analyses are recommended by DNVGL-RP-N103 [9] in cases involving objects with large horizontal extent such as long slender structures.

As it was mentioned in Section 3.4.1, the numerical modelling of the lifting phases was carried out by using SIMA workbench. However, since the scope of this work demanded a large number of simulations to be undertaken, batch mode was the most appropriate option when conducting the assessment of allowable sea states for both lifting phases. This is mainly due to the way batch mode responds to detected error during the program execution [29].

The detailed setting of the time-domain simulations are explained next.

4.2.1 Main analysis parameters

Wave generation method The combined method was selected for the generation of waves. Here, the pre-generation series by the Fast Fourier transform (FFT) and cosine series are combined in the time domain [29]. Waves responses for vessels such as first order wave force and motion, wave drift forces and damping forces followed the calculation by FFT. However, for the spool, wave particle motions and those with distributed hydrodynamic forces followed the calculation by cosine series.

Random seeds for waves Different time series of waves were generated based on the number of seeds specified for each lifting phase. Such seeds introduced the randomness of phase angles to the process [29]. 50 seeds were defined for the lowering of the spool through the wave zone, whereas for the lift-off from a barge 100 seeds were considered.

Time increment and time step The FFT demands equal frequency spacing and a number of frequencies $N = 2^r$, where r is an integer number [30]. The relation between the frequency increment, $\Delta\omega$, the number of time steps, N_t , and the time increment, Δt , is given by:

$$\Delta\omega = \frac{2\pi}{N_t\Delta t} \quad (4.1)$$

For both lifting phases, and after checking the resolution and deviation of results from preliminary analyses (e.g., tension in slings), the value for the time step and time increment was set equal to 0.02s. The duration of simulation for both lifting phases was set equal to 120s.

In addition, the selected integration method was the third order Runge-Kutta-like and the load ramp duration was set equal to 10s.

Range of wave periods T_P Integer wave periods T_P between 4s and 14s were established to delimit the assessment of allowable sea states. Hence, all possible combinations of H_S and T_P for further assessment are found in such range.

4.2.2 Simulation settings for the lift-off of the spool from the deck of the barge

The sequence of actions and events occurring during the lift-off of the spool from the deck of the barge is presented in Table 4.1.

Action		Winch speed	Instant	Event
No.	Description	[m/s]	[s]	
1	Start of the simulation	0	0	The spool rests on the deck
2	Winch activation	-0.2	35	Hoist (trip) of the spool
3	Winch activation	-0.5	40	
4	Winch deactivation	0	50	
5	End of the simulation	0	120	The spool is suspended in the air

Table 4.1. Sequence of actions and events during the lift-off of the spool from the deck of a barge

The hoist of the spool in this phase consisted of two winch intervals, each of which has a different winch speed. The reason why the winch speed is lower during first interval is mainly because snap load in slings was intended to be reduced. Since re-hit of the spool against the deck is very likely to occur, the absolute value of the winch speeds is higher than that in the lowering phase. Negative values for the winch speed denotes the retrieval of the lift-wire.

The lift-wire was modelled approximately 1.5m longer than the minimum length required to have zero tension under static condition. The total length of the lift-wire retrieved during the hoist of the spool is 6.0m.

A total of 9700 simulations were run in order to conduct the assessment of allowable sea states for the lift-off phase based on 100 seeds for each possible combination of T_P and H_S . Table 4.2 lists the pool of combinations considered in the process.

		T_P [s]										
		4	5	6	7	8	9	10	11	12	13	14
H_S [m]	from	1.3	1.2	0.8	0.7	0.7	0.8	0.6	0.5	0.6	0.7	0.4
	to	2.0	2.1	1.8	1.5	1.3	1.4	1.4	1.2	1.6	1.3	1.3

Table 4.2. Combinations of T_P and H_S for the time-domain simulations of the lift-off phase

4.2.3 Simulation settings for the lowering of the spool through the wave zone

In a similar manner, the sequence of actions and events occurring during the lowering of the spool through the wave zone is presented in Table 4.3.

Action		Winch speed	Instant	Event
No.	Description	[m/s]	[s]	
1	Start of the simulation	0	0	The spool is suspended in the air
2	Winch activation	0.1	30	The spool crosses the splash zone
3	Winch deactivation	0	110	
4	End of the simulation	0	120	The spool is fully submerged

Table 4.3. Sequence of actions and events during the lowering of the spool through the wave zone

Unlike the lift-off phase, the lowering phase considered one single winch interval. The total length of the lift-wire during the payout is 8.0m. The winch speed 0.1m/s is recommended by DNVGL-RP-N103 [9] as the lower limit. Its positive value denotes payout of the lift-wire.

Given the corresponding number of seeds (i.e. 50), a total of 4100 simulations were run in order to conduct the assessment of allowable sea states for the lowering phase based on the possible combinations of T_P and H_S . Table 4.4 lists the pool of combinations considered in this process.

		T_P [s]										
		4	5	6	7	8	9	10	11	12	13	14
H_S [m]	from	2.4	2.3	2.0	1.8	1.8	1.7	1.6	1.4	1.5	1.1	1.1
	to	3.1	2.6	2.7	2.5	2.5	2.4	2.3	1.7	2.2	2.0	1.8

Table 4.4. Combinations of T_P and H_S for the time-domain simulations of the lowering phase

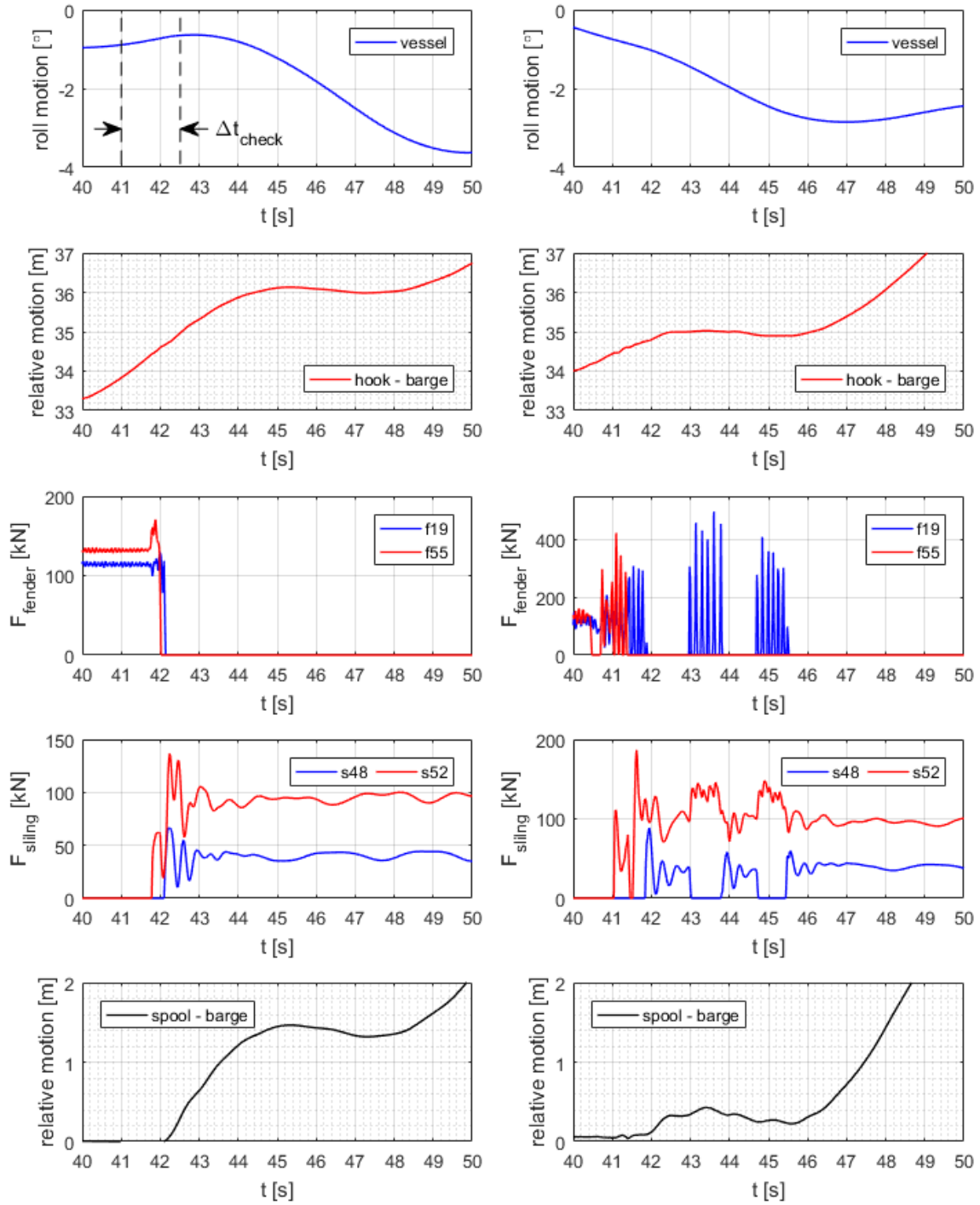
4.3 Methodology to select seeds with suitable scenario for the lift-off of the spool from the barge deck

In practice, given the appropriate environmental conditions, the instant at which the winch is activated for the lift-off of an object is usually determined by the expertise of the operations personnel based on the reading of motions in real time. In this particular case, if an object is transported on a barge and the lift-off is carried out by using the crane of a vessel positioned beside the barge, the relative motion between the crane hook and the deck of the barge is a crucial parameter [9].

For all seeds of the possible combinations of T_P and H_S allocated to the lift phase, the activation instant of the winch was fixed. For some of the seeds, due to the randomness of the wave process, relative motions (e.g. that between the crane hook and the deck of the barge) may not present a favourable condition for the lift-off to occur. Therefore, those seeds should not be considered for further assessment of allowable sea states.

For instance, for two random sea states, Fig. 4.2 shows responses of interest to evaluate whether a lift-off is feasible or not. Fig. 4.2(a) presents a suitable scenario for lift-off of the spool, whereas Fig. 4.2(b) does not. The responses shown are: roll motion of the vessel, relative motion between the hook and the deck of the barge, force on fenders $f19$ and $f55$, tension in slings $s48$ and $s52$, as well as clearance between the spool and the deck of the barge

(measured to the origin the spool was modelled from). Only the four coupling elements were chosen randomly for a clear visualization of the analysis below.



(a) Suitable scenario for the lift-off

(b) Non-suitable scenario for the lift-off

Fig. 4.2. Comparison of scenarios for the lift-off of the spool from a barge

On the one hand, from Fig. 4.2(a) the following can be observed:

- Based on the time-history of the force on fenders F_{fender} , no re-hit is registered after the lift-off occurs at approximately $t = 42$ s.

- The lift-off at the two fender points may be considered simultaneous since the difference is negligible (around 0.3s).
- The relative motion between the hook and the deck of the barge has a favourable upward trend until shortly after $t = 44$ s.
- The relative motion between the spool and the deck of the barge shows a beneficial increase after the lift-off occurs. The spool reaches approximately 1.5m after 3s.
- No slack-wire condition of slings is registered after these meet positive tension for the first time.

On the second hand, from Fig. 4.2(b) the following can be said:

- Based on the time-history of the force on fenders, the lift-off occurs between $t = 41$ s and $t = 42$ s, approximately.
- Once the lift-off occurs, the increase of the relative motion between the hook and the deck of the barge is marginal.
- Regarding the relative motion between the spool and the deck of the barge, the spool scarcely reaches 0.4m within the first 5s after the lift-off occurs.
- Re-hit occurs three times after the first attempt of lift-off. This is noticed from the response of the slings and fenders at around $t = 41.5$ s, $t = 43$ s and $t = 44.8$ s.
- Slack in the slings occurs as a consequence of the re-hit of the spool.

For all of the above reasons, it is necessary to select (filter) seeds that present a suitable lift-off scenario for further assessment of allowable sea states. The suggested methodology considered that the feasibility of a given seed, in terms of lift-off, is dominated by the the roll motion of the vessel. This was suggested given the fact that roll motion of the vessel importantly influences the relative motion between the crane hook and the deck of the barge.

With reference to Fig. 4.2(a), the methodology considered the following aspects:

- For every seed, the roll response of the vessel was evaluated by introducing a period Δt_{check} . During this period, the variation of roll motion every 0.02s (same as the time step) should be positive with respect to the coordinate system.
- The instant $t=41$ s was defined as the starting point of the period Δt_{check} . At this instant, the lift-off of the spool is likely to occur based on time-simulations parameters (e.g., winch speed and length of the lift-wire).

The critical events and responses happening in Fig. 4.2(b) should be avoided during the execution of a lift-off. Note that this seed does not meet with the aspects defined in the methodology suggested.

Primarily, the methodology aimed at the selection of seeds where, for at least a period Δt_{check} , the vessel rolls away from the barge right before the lift-off occurs. Naturally, the longer Δt_{check} was, the less number of resulting seeds was obtained for a given H_S . This reasoning can be observed in Table 4.5, which lists the number of filtered seeds for different Δt_{check} when analysing sea states with T_P 12s. Note that a total of 100 seeds for each combination of T_P and H_S was the sample size to conduct the filtering.

H_S [m]	Δt_{check} [s]		
	1.0	1.5	2.0
0.6	15	4	0
0.7	17	7	2
0.8	19	10	5
0.9	20	10	5
1.0	20	12	7
1.1	22	17	9
1.2	22	17	11
1.3	22	17	11

Table 4.5. Filtered seeds suitable for the lift-off from a barge (analysis of sea states with T_P 12s)

During the conception of this methodology, it was observed that relative (vertical) motion between the hook and the barge do not always show the characteristic sinusoidal response the roll of the vessel does. Hence, if such relative motion is considered for the filtering, this would result in far fewer seeds with a favourable lift-off scenario for each combination of T_P and H_S . Due to all of the above, the methodology adopted the roll motion of the vessel in order to find the suitable lift-off seeds.

4.4 Criteria to assess allowable sea states

The criteria to assess allowable states are governed by the allowable limits as described in step 5 of the methodology presented in Section 4.1. These criteria are explained next.

4.4.1 Potential snap load in slings

Snap load in slings or lift-wire is likely to occur if the hydrodynamic force surpasses the static weight of the lifted object. Since this type of load shall be to the extent possible averted during lifting operations [9], the snap load criterion is adopted in the assessment of allowable sea states.

The safe working load, SWL, can be defined as the actual static load permitted of a lifting appliance under a certain operating condition [8]. In the case of a sling, the SWL is generally expressed as the minimum breaking load, MBL, affected by a safety factor, SF, as follows:

$$SWL = \frac{MBL}{SF} \quad (4.2)$$

The MBL is also known as the ultimate structural strength [8]. The individual MBL of all slings attached to the spool is 1116kN, in addition, a SF equal to 7.0 was considered. Therefore, the SWL of the slings follows:

$$SWL_{sling} = \frac{1116\text{kN}}{7.0} = 159.43\text{kN}$$

Global dynamic load effects may be represented by means of the use of a dynamic amplification factor, DAF. This factor should be specified for comprehensive offshore lifting operations on given grounds for a dynamic analysis [1]. Therefore, the dynamic load capacity, DLC, of a sling is normally expressed as:

$$DLC_{sling} = SWL_{sling} \cdot DAF \quad (4.3)$$

In this particular case, the value established for the DAF was that previously used in the STADD analysis (DAF=2.0). Therefore,

$$DLC_{sling} = (159.43\text{kN})(2.0) = 318.86\text{kN}$$

The following criterion was defined to ensure that potential snap load would not be achieved:

$$F_{sling} < DLC_{sling}, \quad \text{thus,} \quad F_{sling} < 318.86\text{kN} \quad (4.4)$$

where F_{sling} denotes the characteristic total force (tension) in whichever sling attached to the spool.

4.4.2 Slack-wire condition of slings

Slamming and wave excitation forces can provoke slack-wire condition of a sling or lift-wire [9]. This condition may also result in snap loads, thus, slack wires should be avoided [14]. Particularly, during the lift-off phase, this condition is very likely to occur as a consequence of the re-hit of the spool against the deck of the barge.

The slack-wire condition of a sling was assumed to occur when the characteristic total force in it becomes zero (i.e. $F_{sling} = 0$). Hence, the criterion regarding slack-wire condition of slings follows:

$$F_{sling} > 0 \quad (4.5)$$

Therefore, slack-wire condition of any sling attached to the spool is avoided by fulfilling this criterion.

4.4.3 Re-hit of the spool

During an offshore lift-off operation, re-hit of the object against the supporting deck is identified as a potential critical event [31]. Here, re-hit shall mean the event in which the object hits the supporting deck after any attempt to be lifted.

Regarding re-hit, the following criterion was established:

$$F_{fender} \leq 145.2\text{kN} \quad (4.6)$$

where F_{fender} is the actual allowable force on any fender of the spool. Such force value is the maximum the spool is able to withstand without suffering from any damage. Therefore, by fulfilling this criterion, it is considered that severe re-hit does not occur during the lift-off phase.

4.4.4 Minimum clearance between the spool and the construction vessel

According to DNVGL-ST-N001 [1], a minimum 5m-clearance between the lifted object and other structures on the same vessel should be kept unless tugger lines are used. Nevertheless, this is not particularly the case since tugger lines were indeed considered for the lifting operations.

DNVGL-ST-N001 [1] also recommends that a 3m-clearance should be kept between the lifted object and the installation vessels. Therefore, 3m-clearance was defined as a criterion in the assessment of allowable sea states.

The actual clearance between the spool and the portside of the vessel was obtained from the relative motions of both bodies during the simulation processes.

Considering the right-handed coordinate system shown in Fig. 2.3, the motion of any point on the body can be obtained as follows [17]:

$$s = \eta_1 \vec{i} + \eta_2 \vec{j} + \eta_3 \vec{k} + \omega \times \mathbf{r} \quad (4.7)$$

which yields:

$$s = (\eta_1 + z\eta_5 - y\eta_6) \vec{i} + (\eta_2 - z\eta_4 + x\eta_6) \vec{j} + (\eta_3 + y\eta_4 - x\eta_5) \vec{k} \quad (4.8)$$

where,

$$\omega = \eta_4 \vec{i} + \eta_5 \vec{j} + \eta_6 \vec{k} \quad \mathbf{r} = x \vec{i} + y \vec{j} + z \vec{k}$$

In the numerical modelling in SIMA-SIMO, the following points were defined:

- Points L and R , which were added to the spool and defined as those most likely to collide with the portside of the vessel during the lifting operations (see Fig. 3.3).
- Points U and V , which were added to the vessel so representing its portside.

Motions of body-points L , R , U and V were recorded during simulation processes, and time-history series of the actual clearance between both bodies were obtained for further assessment. The minimum clearance criterion was thus checked during the whole simulation.

4.5 Presentation of results and discussion

4.5.1 Static condition analysis

The static condition analysis determines the initial conditions of a model for the subsequent dynamic analysis [29]. Static equilibrium of bodies and static forces of coupling elements can be obtained from static analysis.

Tilt of the spool

Tilt of the lifted object is a parameter that is normally monitored in lifting operations and will influence the sling loading distribution [1]. Object tilt may also cause undesirable effects such as collision with external objects and skew loads.

Based on the tilt of the spool under static condition, the correspondence between the lifting point and the actual CoF and CoG could be corroborated. Table 4.6 shows the corresponding rotational motions of the spool under static equilibrium.

Condition of the spool	Roll [°]	Pitch [°]
In the air	-0.031	0.025
Fully submerged	-1.36	1.68

Table 4.6. Tilt of the spool under static condition

Roll and pitch values of the spool while it is suspended in the air are almost zero. Therefore, one can say that there is correspondence between the lifting point (hook of the crane) and the CoG of the spool in z -direction.

When the spool is fully submerged, tilt values are slightly higher. This denotes a minor misalignment in z -direction between the lifting point and the CoF of the spool. Nevertheless, this can be neglected since these values are less than 2° , which are the maximum recommended by DNVGL-ST-N001 [1]. Effects of tilt on the sling load distribution are not normally considered when the expected maximum value is less than 2° [1].

Roll and pitch motions of the construction vessel

Table 4.7 lists the roll and pitch motion values of the construction vessel under static condition, when the spool is either suspended in the air or fully submerged. Since the spool is lifted from the crane tip, the vessel meets a moment that is reflected on an initial angle.

Condition of the spool	Roll [°]	Pitch [°]
In the air	-2.12	-0.018
Submerged	-1.49	-0.013

Table 4.7. Pitch and roll motions of the spool under static condition

According to DNVGL-RP-N201 [8], all vessels and floating objects involved in a lifting operation shall be provided with sufficient stability and reserve buoyancy. Ballasting is commonly a technique for providing stability in such a way that the vessel stays upright and prevents it from acquiring a constant lean due to asymmetrical loading [18].

The values obtained for pitch motion are directly negligible. Regarding roll values, these do not represent any operational issue during the lifting operations of interest. In addition, roll motion values are within the seakeeping criteria established by NORDFORSK [33], [18] either for light or heavy manual work vessels. Therefore, no ballasting was included in the numerical model of the vessel.

Note that, if the roll motion under static condition is adjusted, special attention should be given to the assessment of allowable sea states under the criterion minimum clearance between the spool and the portside of the vessel.

Static forces in slings, lift-wire and on fenders

Tensions in slings under static condition were already covered in Section 3.4.2. $SWL_{sling} = 159.43\text{kN}$ is not exceeded by the tension values listed in Table 3.5. The lowest tension occurs in sling $s48$, whereas the largest does in sling $s55$. Regarding the lift-wire, the resulting tension due to the static weight of the spool plus that of the crane block is 564.1kN .

With respect to the fender coupling between the spool and the deck of the barge, Table 4.8 lists their respective force value under static condition.

Fender	F_{fender} [kN]
f19	125.1
f22	110.9
f53	103.3
f55	145.2

Table 4.8. Forces on fenders under static condition

4.5.2 Allowable sea states for the lift-off of the spool from the deck of the barge

Regarding lift-off of the spool from the deck of a barge, the following criteria were established in the assessment of allowable sea states:

- Potential snap load in slings
- Re-hit of the spool

A given sea state was considered allowable provided that the aforementioned criteria were fulfilled for all the seeds evaluated. During the simulation process, the evaluation of these criteria took place from the first attempt of lift-off.

In this particular case, the seeds evaluated were those resulting from following the methodology presented in Section 4.3. The number of filtered seeds varied depending on the given combination of T_P and H_S , as well as on the Δt_{check} applied. Table 4.9 lists the allowable sea states obtained for a defined Δt_{check} . Each combination of T_P and H_S shows the respective number of filtered seeds the sea state was evaluated from.

T_P [s]	$\Delta t_{check} = 1.0s$		$\Delta t_{check} = 1.5s$		$\Delta t_{check} = 2.0s$	
	H_S [m]	No. seeds	H_S [m]	No. seeds	H_S [m]	No. seeds
4	1.3	11	1.3	3	1.9	6
5	1.2	5	1.7	5	2.1	4
6	0.9	5	1.2	1	-	0
7	0.7	2	1.2	1	-	0
8	0.7	6	-	0	-	0
9	0.9	7	1.1	4	1.3	3
10	1.2	15	1.2	8	1.3	6
11	0.8	14	1.1	12	1.1	4
12	0.8	19	1.0	12	1.1	9
13	0.8	18	1.1	13	1.2	8
14	0.8	20	1.2	13	1.2	6

Table 4.9. Allowable sea states for the lift-off of the spool from the deck of a barge based on Δt_{check}

The sea states listed in Table 4.9 are plotted in Fig. 4.3. It can be observed that the allowable sea states obtained for $\Delta t_{check} = 1.0s$ show continuity across all the values of T_P . In other words, at least one filtered seed (i.e. suitable scenario for lift-off) was found for each combination of T_P and H_S listed in Table 4.9. The values obtained for H_S when $\Delta t_{check} = 1.0s$ were in fact expected to be low in comparison with those evaluated with a larger Δt_{check} . Nevertheless, such values are significantly lower than in-practice typical values, meaning that it would be virtually impossible to carry out the lift-off operation.

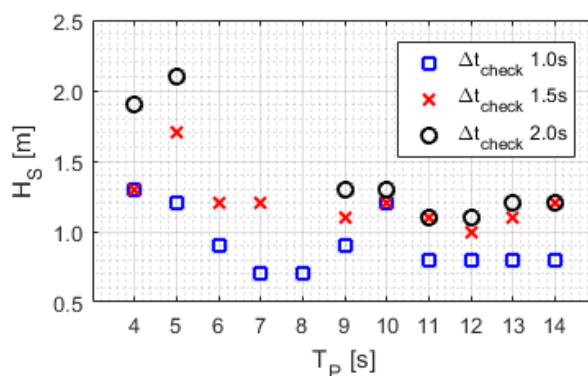


Fig. 4.3. Allowable sea states for the lift-off of the spool from the deck of a barge based on Δt_{check}

The values obtained for H_S when $\Delta t_{check} = 1.5s$ and $\Delta t_{check} = 2.0s$ suggest a better scenario for the lift-off operation. However, these values do not show continuity across all the values of T_P . Furthermore, the number of filtered seeds shows in most cases a decreasing trend for larger values of Δt_{check} , which might affect the reliability of extreme loads and responses.

Allowable sea states

The definition of the allowable sea states was suggested as a combination of those listed in Table 4.9 in such a way that:

- H_S was the closest possible to typical values for lift-off of similar structures from the deck of a barge and,
- the number of filtered seeds was as far as possible close to 10 for further estimation of extreme loads and responses.

Table 4.10 and Fig. 4.4 show the allowable sea states governing the lift-off of the spool from the deck of a barge. These are also highlighted in Table 4.9.

Sea state	1	2	3	4	5	6	7	8	9	10	11
T_P [s]	4	5	6	7	8	9	10	11	12	13	14
H_S [m]	1.9	1.7	0.9	1.2	0.7	0.9	1.2	1.1	1.1	1.2	1.2

Table 4.10. Allowable sea states for the lift-off of the spool from the deck of a barge

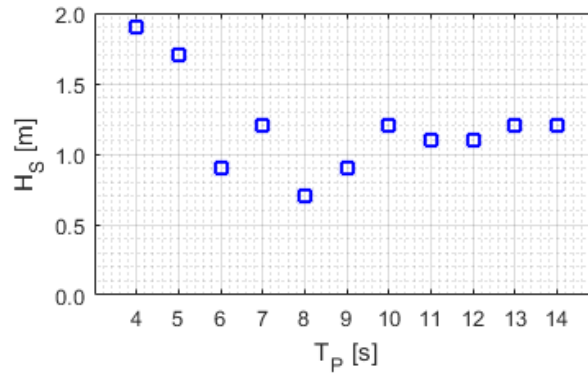


Fig. 4.4. Allowable sea states for the lift-off of the spool from the deck of a barge

In most cases, the dominating criterion in the assessment was the re-hit of the spool (at fenders *f19* and *f53*) followed by potential snap load in sling *s53*. Fig. 4.5 shows the allowable sea states obtained by applying the assessment criteria. The sea states also correspond to the Δt_{check} used during the filtering of seeds suitable for lift-off.

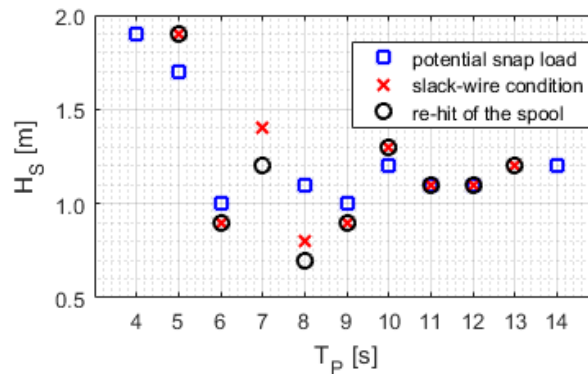


Fig. 4.5. Allowable sea states for the lift-off of the spool from the deck of a barge based on the different criteria for assessment

In Fig. 4.5, the minimum H_S is plotted when slack-wire condition occurs. It can be observed that slack-wire condition normally occurs at the same H_S limited by re-hit (e.g., $T_P = 11$ s and $H_S = 1.1$ m). This is due to re-hit of the object normally leads to slack-condition of slings. Some T_P do not show any H_S limited by potential snap load. In those cases, extreme responses of F_{sling} never surpassed the permissible limit.

Convergence study

Transient effects exist during the different phases in offshore lifting operations due to non-linearity on account of waves [34]. By running several random seeds during the analysis of operations, the response statistics is expected to converge so as to reduce the statistical uncertainty [14].

The convergence study aims at the comparison of the responses for each seed with the mean values of all filtered seeds. In addition, the accumulative averaged value is plotted for each seed number i whose calculation follows the mean value from 1 to i . In this way, the gradient of convergence can be observed [34].

Based on the methodology presented in Section 4.3, the number of filtered seeds obtained for each combination of T_P and H_S is considerably less in comparison with the initial pool of seeds (100 seeds). Such number mostly lies in the range 5 to 15 seeds. However, for the sea state no. 4 ($T_P = 7$ s and $H_S = 1.2$ m), only one filtered seed was obtained. Hence, in this particular case, statistical uncertainty is extensive.

Fig. 4.6 depicts the convergence study on the extreme responses for two random coupling elements; the maximum characteristic total force in sling $s55$, $F_{sling\ s55}$, and the minimum characteristic force in sling $s48$, $F_{sling\ s48}$. These responses correspond to the allowable sea state no. 7 ($T_P = 10$ s and $H_S = 1.2$ m) which was assessed from 15 filtered seeds. It can be seen from Fig. 4.6 that convergence of the responses occurs when reaching seed number 14. This is more noticeable for $F_{sling\ s55}$ than for $F_{sling\ s48}$.

The characteristic force on a fender (F_{fender}) cannot be used in the convergence study since its value is usually zero for all filtered seeds of an allowable sea state.

Reading of responses and limiting parameters

The responses and limiting parameters presented in this segment belong to the allowable sea state no. 8 (i.e. $T_P = 11$ s, $H_S = 1.1$ m), seed no. 8. This sea state is the same as that presented in Fig. 4.2(a), Section 4.3.

Fig. 4.7 depicts time-histories of the following limiting parameters and responses during the lift-off of the spool from the deck of a barge: roll motion of the vessel, relative motion between the hook and the deck of the barge, force on fenders, tension in slings, as well as clearance between the spool and the deck of the barge (measured to the origin the spool was modelled from).

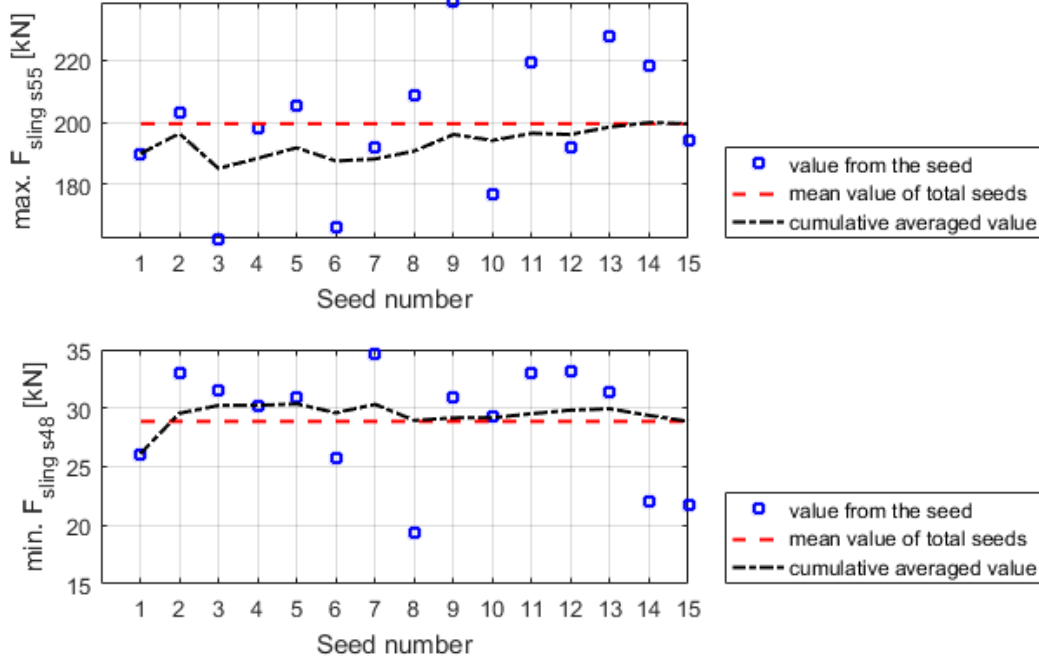


Fig. 4.6. Convergence study on extremes responses during the lift-off of the spool from the deck of a barge

Fig. 4.7 depicts the typical behaviour of responses during a successful lift-off operation. Based on the corresponding criteria, the sea state is considered allowable given that:

- the potential snap load is not reached at any moment (i.e. $F_{sling} < 318.86\text{kN}$),
- slack-wire condition is not evidenced after the slings meet positive tension for the first time (i.e. $F_{sling} > 0$ from roughly $t = 42\text{s}$ onwards) and,
- no re-hit occurs after the spool is lifted (i.e. $F_{fender} \leq 145.2\text{kN}$ from approximately $t = 42\text{s}$ onwards).

As it was mentioned in Section 4.3, the sea state has a favourable scenario for the lift-off given that the roll motion of the vessel and the relative motion between the hook and the deck of the barge show an upward trend prior to the lift-off (from approximately $t = 40\text{s}$ to $t = 42\text{s}$).

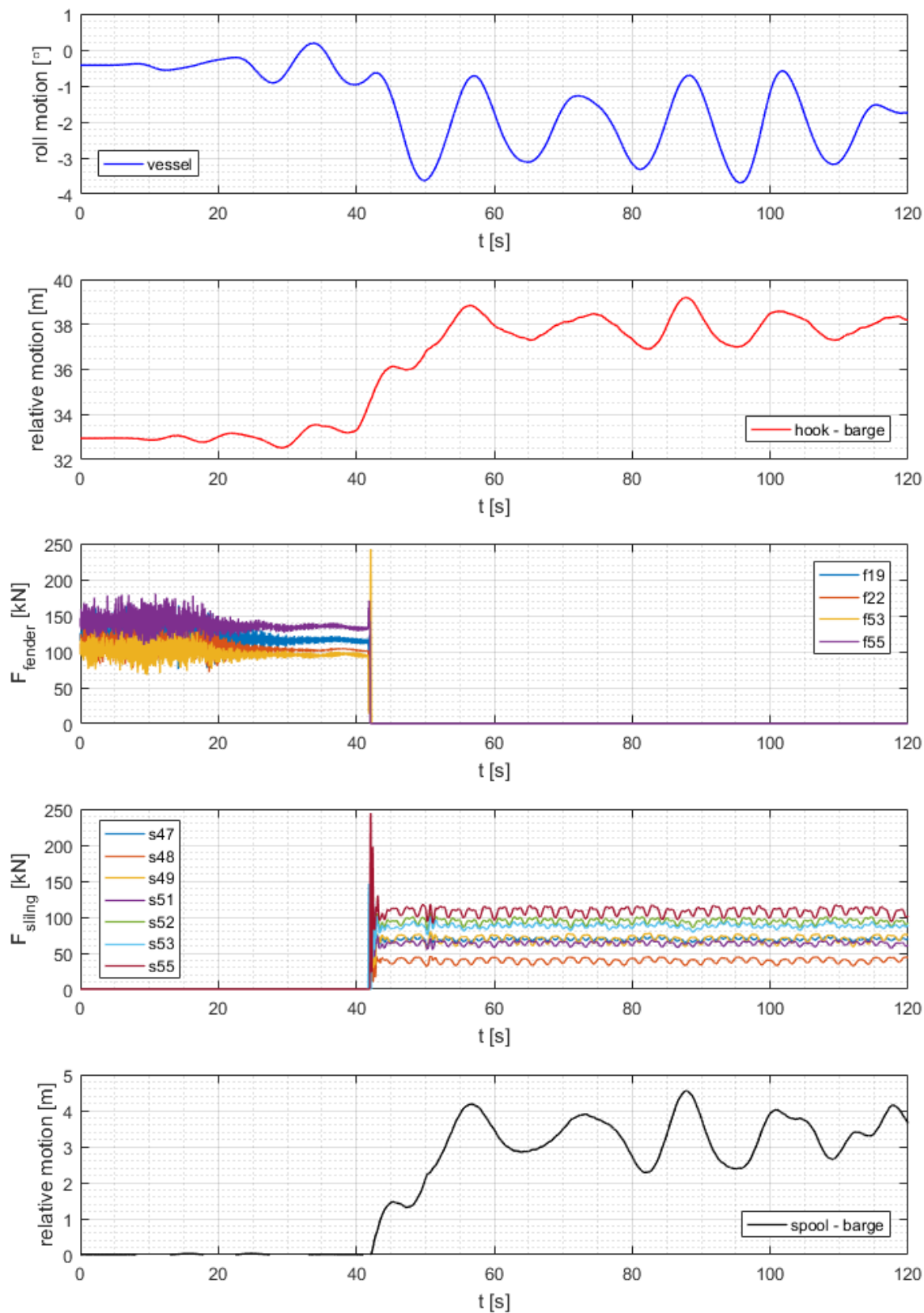


Fig. 4.7. Responses and limiting parameters of interest during the lift-off of the spool from the deck of a barge

Generally, the sequence of the events of the lift-off phase (see Table 4.1) can be observed in Fig. 4.7 as follows:

- The spool rests on the deck of the barge between the start ($t = 0$) and the lift-off (at around $t = 42$ s) where,
 - zero clearance is registered between the spool and the deck of the barge,
 - there is no positive tension met by the slings and,
 - the registered force on fenders points is that corresponding under static condition.
- Hoist (trip) of the spool occurs between approximately $t = 42$ s and $t = 50$ s where,
 - clearance between the spool and the deck of the barge progressively increases from zero until approximately 2.2m,
 - the vessel rolls noticeably towards the barge (from 0 to -4°) shortly after the lift-off occurs and,
 - positive tension is met by the slings, and force on fender points becomes zero, at the instant the lift-off occurs.
- The spool is suspended in the air (deactivation of winch at $t = 50$ s) where,
 - it remains between roughly 2.2 and 4.7m above the deck of the barge (measured at the origin the spool was modelled from),
 - tensions in slings fluctuate around their respective value met under static condition and,
 - zero force is registered on fender points.

Lastly, from Fig. 4.7 it can be observed that the roll motion of the vessel considerably influences the relative motion between the hook and the deck of the barge. To a large extent, the phase of their peaks and troughs coincide shortly after the winch is deactivated. Slight deviations of this relative motion are derived from pendulum motions of the spool and heave motions of the vessels.

Further discussion

Based on the methodology explained in Section 4.3 for the selection or filtering of suitable lift-off scenarios, the judgements below can be made.

In the same way as in Table 4.5, Table 4.11 lists the number of filtered seeds for different Δt_{check} when analysing sea states with T_P 12s. On the one hand, the cells highlighted in green denote that for such H_S , the sea state was found allowable under the given criteria. On the other hand, the cells highlighted in red denote that the corresponding sea state was found not allowable for the lift-off phase.

It can be observed that, for a given H_S , the longer Δt_{check} , the less number of filtered seeds filtered, however, the higher probability of finding the sea state allowable. This is due to roll motion of the vessel opposite to the barge takes longer, which normally leads to an increasing relative motion between the deck of the barge and the hook right before the lift-off occurs. Furthermore, a longer Δt_{check} affords the necessary time to lift the spool at a certain height before the vessel rolls back to the barge, thus, the likelihood of having re-hit is reduced.

H_S [m]	Δt_{check} [s]		
	1.0	1.5	2.0
0.6	15	4	0
0.7	17	7	2
0.8	19	10	5
0.9	20	10	5
1.0	20	12	7
1.1	22	17	9
1.2	22	17	11
1.3	22	17	11

Table 4.11. Filtered seeds suitable for lift-off from a barge (analysis of sea states with T_P 12s and results)

This time looking at the sensitivity for a given Δt_{check} , the higher the H_S becomes, the more number of filtered seeds is obtained, however, the lower probability of finding the sea state allowable. Firstly, a larger number of filtered seeds emerges on account of the steepness of the roll motion of the vessel when having higher H_S . Secondly, higher-fluctuating heave motion of floating vessels may occur so fast that the spool cannot reach enough height above the deck of the barge before re-hit occurs.

4.5.3 Allowable sea states for the lowering of the spool through the wave zone

The following criteria were established in the assessment of allowable sea states for the lowering of the spool through the wave zone:

- Potential snap load in slings
- Slack-wire condition of slings
- Minimum clearance between the spool and the portside of the construction vessel

A given sea state is catalogued as allowable on the condition that all the criteria above are fulfilled for all the seeds evaluated (50 seeds). Different from the lift-off of the spool from the deck of a barge, the aforementioned criteria were evaluated continuously for the total duration of the time-domain simulation for the lowering phase.

Allowable sea states

Table 4.12 and Fig. 4.8 show the allowable sea states governing the lowering of the spool through the wave zone.

Sea state	1	2	3	4	5	6	7	8	9	10	11
T_P [s]	4	5	6	7	8	9	10	11	12	13	14
H_S [m]	2.4	2.4	2.3	2.0	1.8	1.9	1.7	1.6	1.7	1.8	1.4

Table 4.12. Allowable sea states for the lowering of the spool through the wave zone

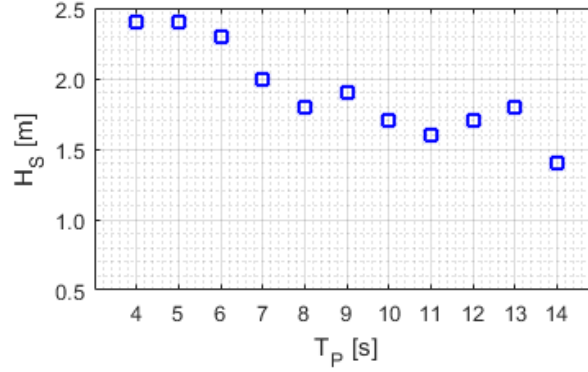


Fig. 4.8. Allowable sea states for the lowering of the spool through the wave zone

In most cases, the dominating criterion during the assessment was the slack-wire condition in slings $s48$, $s49$ and $s47$ (in that order of influence) followed by the minimum clearance between the spool and the portside of the vessel measured at point R .

Fig. 4.9 shows the allowable sea states based on the different criteria. Note that some T_P do not show any H_S delimited by the criteria potential snap load nor minimum clearance between the spool and the portside of the vessel. This is due to their extreme response never surpassed the corresponding permissible limit.

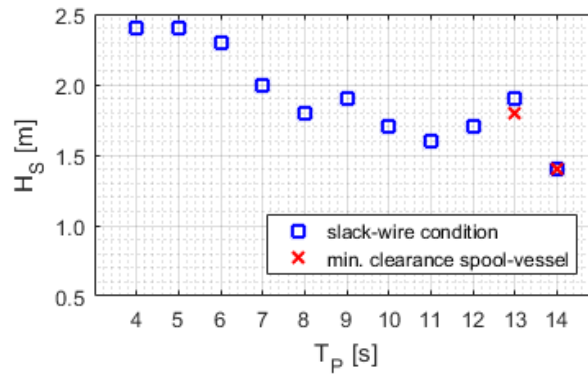


Fig. 4.9. Allowable sea states for the lowering of the spool through the wave zone based on the different criteria for assessment

Convergence study

The lowering phase did not require a filtering process of seeds like that conducted for the lift-off phase presented in Section 4.3, hence, the total number for random seeds simulated was 50 for each combination of T_P and H_S .

Fig. 4.10 depicts the convergence study on the extreme responses of the following limiting parameters: minimum characteristic total force in sling $s48$ ($F_{sling\ s48}$), as well as the minimum clearance between the spool and the portside of the vessel (with respect to points L and R). The values shown correspond to the allowable sea state no. 3 (i.e. $T_P = 6s$ and $H_S = 2.3m$).

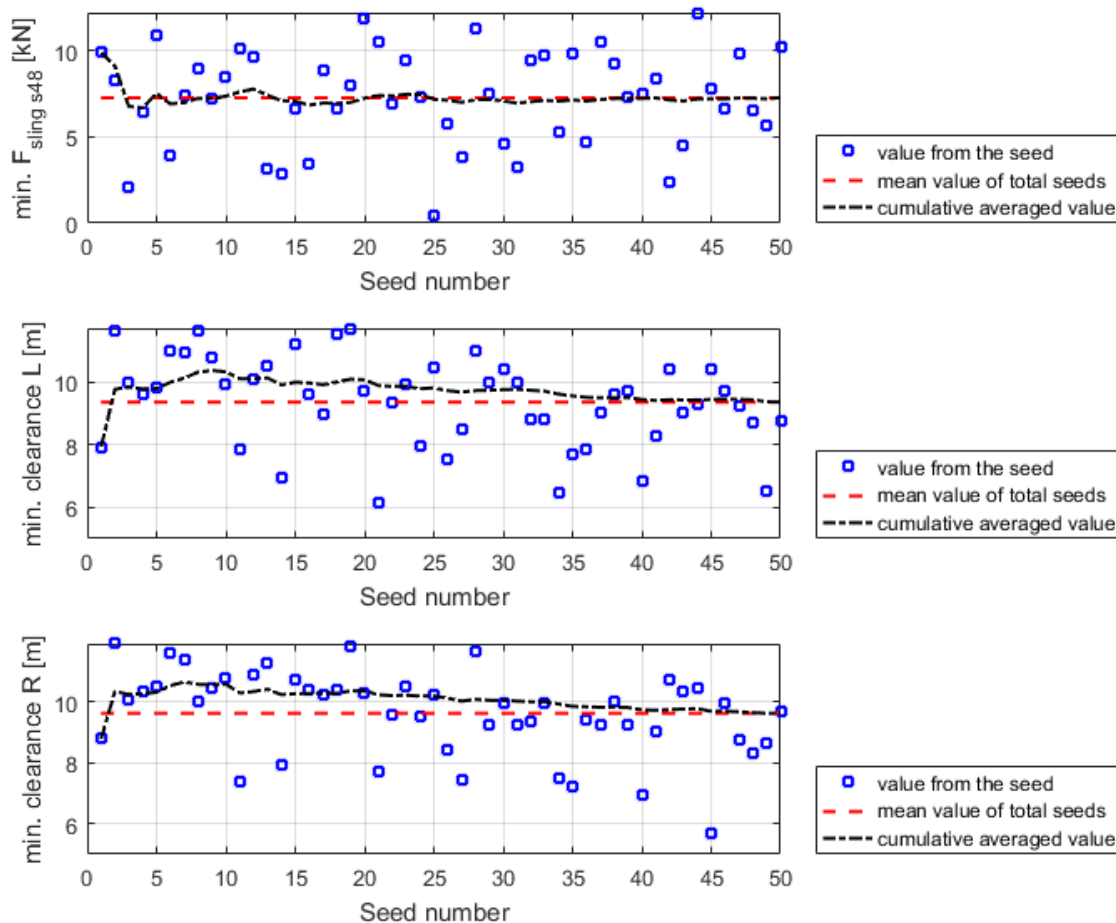


Fig. 4.10. Convergence study on extremes responses during the lowering of the spool through the wave zone

In the case of the minimum characteristic total force in sling $s48$ ($F_{sling\ s48}$), around 25 seeds were enough to obtain convergence of the results. However, regarding the minimum clearance between the spool and the vessel (points L and R), it takes a larger number of seeds to achieve convergence, which is around 40 seeds. Therefore, a total of 50 seeds was sufficient to obtain convergent results, meaning that statistical uncertainty is reduced.

Reading of responses and limiting parameters

The responses and limiting parameters presented in this segment belong to seed no. 22 of the allowable sea state no. 3 (i.e. $T_P = 6$ s and $H_S = 2.3$ m). On average, for the three limiting parameters covered in the convergence study above (see Fig. 4.10), seed no. 22 has the closest responses to the corresponding mean values.

Fig. 4.11 depicts time-histories of the following limiting parameters and responses during the lowering of the spool: tension in slings, clearance between of the spool (points L and R) and the portside of the vessel, as well as the displacement of the spool in z -direction (i.e. heave motion) with respect to global coordinate system.

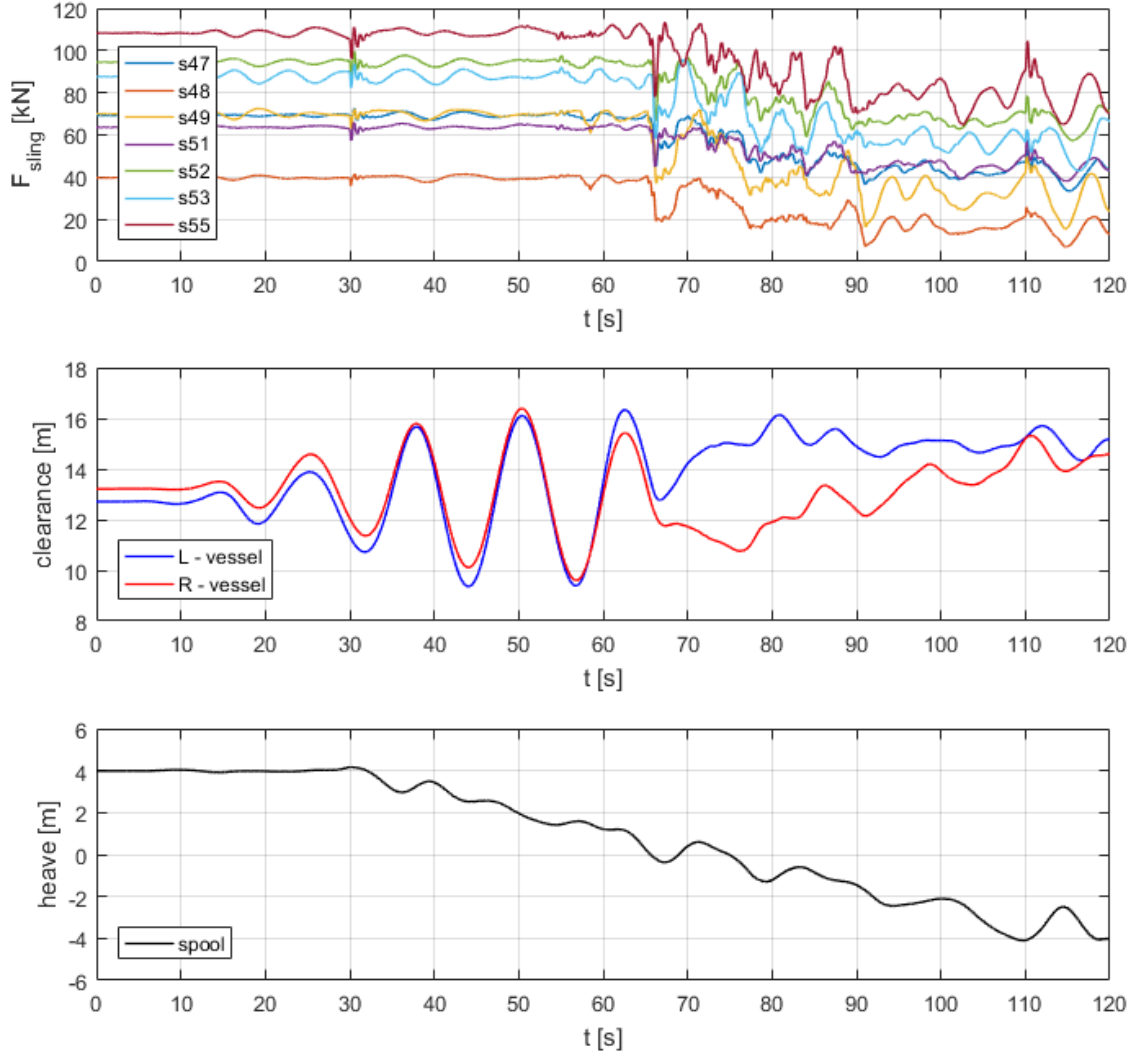


Fig. 4.11. Responses and limiting parameters of interest during the lowering of the spool through the wave zone

On the whole, the lowest and largest tensions are met by slings $s48$ and $s55$, respectively. This is due to the fact that a trend exists for the slings to follow the same load distribution as in static condition (see Table 3.5). Note that under static condition, sling $s48$ meets a tension 23.9kN smaller than the second least loaded sling (i.e. $s51$).

On the one hand, sling $s48$, followed by $s49$ and $s47$, was the driver throughout the assessment of allowable sea states under the criterion slack-condition of slings. For instance, this phenomenon can be seen in Fig. 4.11, where the three slings with the lowest tension values registered are $s48$, $s49$ and $s47$ (occurring at approximately $t = 115$ s in that order of influence).

On the second hand, sling $s55$ cannot be considered the driver under the criterion potential snap load in slings since their dynamic load capacity $DLC_{sling} = 318.86$ kN was never reached. In fact, this criterion was fulfilled by all the combinations of T_P and H_S subjected to analysis.

Table 4.13 lists the minimum and maximum tensions registered across all seeds of the allowable sea states for the lowering of the spool. Note that these never met, nor surpassed, the corresponding allowable limits (i.e. $0 < F_{sling} < DLC_{sling}$).

Sea state	F_{sling} [kN]	
	Minimum	Maximum
1	1.08	140.40
2	0.58	130.37
3	0.45	127.14
4	0.03	119.28
5	0.86	118.73
6	0.27	120.82
7	0.98	121.50
8	0.37	124.10
9	0.28	124.46
10	1.63	123.79
11	0.45	118.12

Table 4.13. Minimum and maximum tensions in slings during the lowering of the spool through wave zone

Lastly, the sequence of actions of the lowering phase (Table 4.3) observed in Fig. 4.11 are summarized as follows:

- The activation of the winch is represented by the small disturbance of the tension in slings at $t = 30$ s.
- It can be deduced that the spool crosses the actual wave zone from approximately $t = 65$ s to $t = 102$ s since there is a relatively large and arbitrary fluctuation of the tension in slings.
- The spool seems to be fully submerged shortly before $t = 110$ s. The fluctuation of tensions in slings, as well as of the clearance between points L and R , has its amplitude reduced (e.g., the latter eventually converge to approximately 15m).
- Finally, progressive displacement of the spool in negative z -direction is not registered after $t = 110$ s, at which a small disturbance in the tension of slings is registered due to the winch deactivation.

Further discussion

With regard to the clearance between the spool and the portside of the vessel, this response is dominated in most cases by the sway motion of the spool due to its pendulum motions rather than yaw motion.

Fig. 4.12 shows the comparison between sway motion of the spool and the variation of clearance between the spool and the portside of the vessel with respect to points L and R . The latter was calculated by subtracting the initial value of clearance from the corresponding time-history series for each point. Furthermore, this response may be assumed as the sway motion of points L and R on the spool.

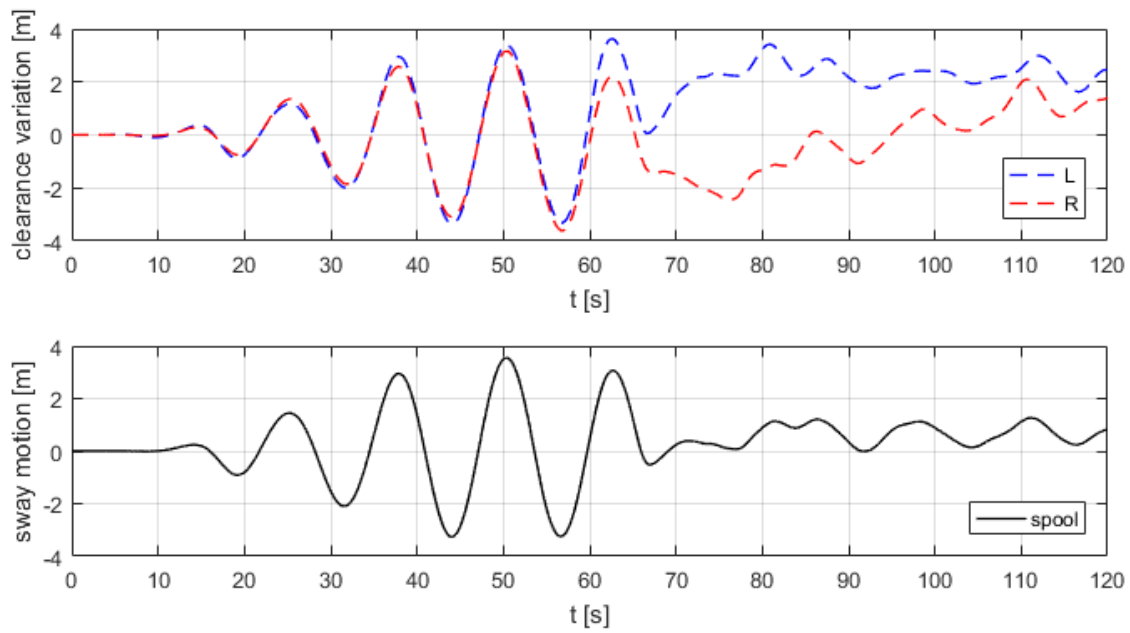


Fig. 4.12. Comparison between sway motion of the spool and variation of clearance between the spool and the vessel

It can be observed that both time-history series present a similar behaviour in terms of phase and amplitude before the spool starts to cross the wave zone (i.e. at approximately $t = 65$ s). Hence, the influence of yaw motion of the spool is virtually negligible. With the aim of simulating the use of tugger lines, yaw stiffness was added to the numerical model of the spool which accounts for its minor yaw motion.

Chapter 5

Operability analysis

5.1 General

According to DNVGL-ST-N001 [1], the planning of marine operations shall lead to safe and sound practice. During the planning phase, methodical procedures to complete marine operations are normally devised from data of the offshore location and the equipment [4]. Moreover, all the assumptions made during this phase shall be fulfilled when executing marine operations [1].

Operability of marine operations plays an important role during the planning phase since it provides relevant information about the feasibility of the operations within an operating season, selection of vessels and logistics. The analysis of the operability of marine operations is normally based on the operational limits involved, which are required to be assessed for potential critical activities that may lead to critical events [4].

It is recommended that the operability of marine operations is assessed from weather window analysis where relevant features of each activity are included (e.g. sequence, duration, and continuity). In this work, weather window analysis was conducted by following one of the methodologies suggested by Guachamin Acero et al. [4].

Unlike considering the operability as a representation of the available time for executing an operation in a given reference period [4], this work assesses the operability of a marine operation based on the period of time required for it to be completed.

This chapter presents the operability analysis conducted for two installation methods, which were devised for the installation of the spool. The main objective of the operability analysis is to determine which of the methods, for the installation of a given number of spools, is the most effective option in terms of time to go with.

The analysis consisted of two statistical analyses, whose outcomes are presented across the months within the operating season and the number of spools to be installed. In addition, a sensitivity study on the navigation time of the vessel is included.

5.1.1 Planning of marine operations

The following concepts defined by DNVGL-ST-N001 [1] are of interest for the planning of marine operations.

- T_R is the operation reference period which defines the duration of marine operations and follows:

$$T_R = T_{POP} + T_C \quad (5.1)$$

- T_{POP} is the planned operation period which shall be specified from a detailed schedule of the operation
- T_C is the estimated maximum contingency time, which shall address:
 - General uncertainty in the T_{POP}
 - Idle time during the operation
 - Additional time demanded for possible measures to complete the operation

According to DNVGL-ST-N001 [1], marine operations with T_R and T_{POP} less than 96h and 72h, respectively, are considered weather restricted operations. The execution of this type of operations shall take place within a workable weather window as shown in Fig. 5.1.

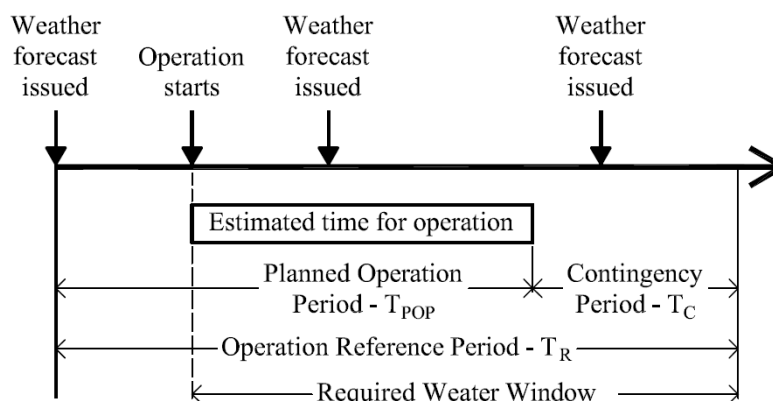


Fig. 5.1. Operation periods [1]

A workable weather window (WOWW) can be defined as a span where continuous allowable sea states occur and whose duration is long enough to complete a marine operation. These windows are used during the planning phase of marine operations for the estimation of the operability, as well as in the execution phase for supporting decision-making processes [4].

Contribution of different sources of uncertainty normally exists during the planning and execution of lifting operations. For instance, during the latter, update of weather forecast of the offshore location is required to identify weather windows. Since the identification process involves forecasted wave parameters (T_P and H_S), uncertainty shall therefore be considered. This can be done by affecting the permissive limits of the limiting parameters with a reduction factor [4].

For instance, DNVGL-ST-N001 [1] suggests the inclusion of an α -factor allowing for weather forecasting inaccuracies. The definition of forecasted operational criteria, OP_{WF} , is suggested in such a way that,

$$OP_{WF} = \alpha \times OP_{LIM} \quad (5.2)$$

where OP_{LIM} is the operational limiting criteria (i.e. operational limits). The use of α -factor shall ensure that the probability of exceeding OP_{LIM} by more than 50% is less than 10^{-4} [1].

In this work, OP_{LIM} can be directly linked to the wave spectral parameters H_S and T_P used during the identification of WOWWs. Furthermore, since T_P is a relevant parameter to the behaviour of floating vessels, this shall also be included [4]. Regarding H_S , the forecasted operational criterion (H_{Sop}) applicable to installation methods can be defined as follows:

$$H_{Sop} = \alpha \times H_S \quad (5.3)$$

Sources of uncertainty are not covered in this work, nevertheless, these will be required for further reliability analysis of the lifting operations.

Too low weather restricted design environmental condition may provoke critical waiting on weather delays [1]. This might be the case of the allowable sea states obtained for the lift-off of the spool for the deck of the barge. In that case, DNVGL-ST-N001 [1] recommends that an overall operability analysis should endorse the selection of the design environmental condition.

5.1.2 Metocean condition

The metocean condition is a relevant parameter for the installation of subsea structures and its effects on project costs and schedule are normally higher for deepwater developments [3]. Although the installation of the spool(s) was not planned to take place in deepwater fields, an offshore site was chosen where its metocean data was representative for the intended location.

The main features of the site chosen are listed in Table 5.1. This site (no. 14) from Li et al. [35] was considered as representative of the North Sea for this operability analysis.

Site no.	Area	Name	Water depth [m]	Distance to shore [km]	Average wave power density [kW/m]	50-year H_S [m]	Mean value of T_P [s]
14	North Sea	Norway 5	202	30	46.43	10.96	11.06

Table 5.1. General information and statistics of the offshore site chosen for metocean condition

The wave data used for the operability analysis were sampled hourly and generated from a hindcast model from 2001 to 2010. Its 10-year scatter diagram of H_S and T_P is given in Table A.1.

In this way, the environmental conditions used for the operability analysis are documented by reliable statistical data as recommended by DNVGL-ST-N001 [1].

5.2 Methodology to conduct the operability analysis

The identification of WOWWs was carried by following one of the methodologies suggested by Guachamin Acero et al. [4], which consists in comparing hindcast wave data and the allowable sea states of the activities established by the installation methods (see Fig. 5.2). Consequentially, its outcome allowed for conducting the operability analysis of two installation methods for the installation of a given number of spools. This analysis is based on the overall installation time (OIT), that is the lapse of time required for their installation when starting at a given instant t_0 within the operating season.

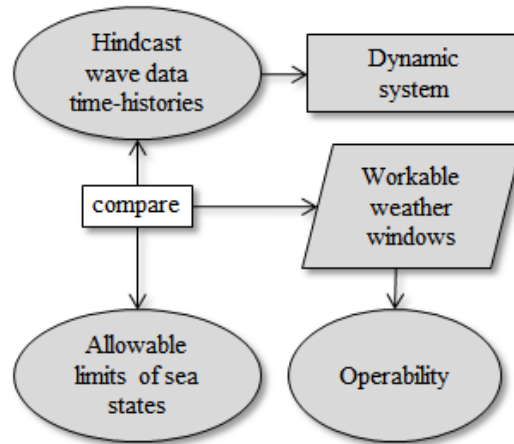


Fig. 5.2. Methodology for weather window analysis during the planning of marine operations [4, p. 312]

The operating season to initiate operations offshore was assumed from June 01st 00:00h to August 31st 23:00. Performing the operations during the whole year is not possible since it becomes risky due to the instability and harshness of environmental conditions. That being said, the operations become risky Nevertheless, for the purpose of conducting the operability analysis, marine operations were not limited to finish by August 31st 23:00.

Regarding the two installation methods, the following stages were included:

- load-out of the spool onshore
- transportation to the offshore site
- installation of the required number of spools
- sailing of the vessel back to harbour

5.2.1 Methods for installation of the spool

Based on a given number N of spools planned to be serially installed, two installation methods were defined for the operability analysis.

Installation method 1 (IM1) Includes one single construction vessel. Both the transportation and the installation of the spools are carried out by the vessel. Thus, the number of trips back and forth between the harbour and the offshore site is the same as N .

Installation method 2 (IM2) Includes one construction vessel and at least one transportation barge. The transportation and installation of the first spool is carried out by the vessel. For the second or remaining spools, their transportation is carried out by one or more barges while the vessel is positioned at the offshore site to continue the installation.

The purpose of defining IM2 was to reduce costs by avoiding trips of the vessel going back and forth between the harbour and the offshore site when various spools are required to be installed. The rate of a construction vessel is normally more expensive than that of a transportation barge. That being said, the main objective of the operability analysis is to determine which of the methods, for the installation of a given number of spools, is the most effective option in terms of installation time to go with. In other words, the 'break-even spool' for the two installation methods can be found from conducting the operability analysis.

The marine operations established by IM1 and IM2 can be considered weather restricted up to a certain number of spools planned to be installed. For the former, the installation of 8 spools results in $T_R=96\text{h}$, whereas for the latter, the installation of 10 spools does in $T_R=57\text{h}$.

Installation method 1 (IM1)

Table 5.2 lists the set of activities established by IM1 with their respective duration and allowable sea states. Note that this set was defined for the installation of one single spool. Therefore, if additional spools are planned to be installed, the complete set needs to be repeated $N-1$ more times.

Activity		T_R	Allowable sea states
No.	Description	[h]	
1	Load-out and transportation	4	$H_S=3\text{m}$ for all T_P
2	Preparation, lift process and deployment	2	those in Fig. 4.8
3	ROV survey	3	$H_S=3\text{m}$ for all T_P
4	Sailing of the vessel back to harbour	3	$H_S=3\text{m}$ for all T_P

Table 5.2. Activities established by IM1

Activity no. 1 gathers all the required sub-activities to accomplish the load-out and transportation of the spool. Its duration or operation reference period, T_R , was calculated based on 1.5h for load-out time plus 2.5h for transportation time. The latter was estimated based on an averaged speed of the vessel equal to 11 knots. The allowable sea states for this activity were assumed $H_S = 3\text{m}$ for all T_P .

Activity no. 2 considers all the necessary sub-activities from the preparation of the spool until the retrieval of the rigging assembly. The T_R of this activity was assumed 2h.

DNVGL-RP-N103 [9] points out that, for an object transported on a crane vessel, the lift-off is a simple operation since the relative motion between the crane tip and the deck of the vessel is virtually negligible. That being said, the allowable sea states applicable to the lift-off of the spool from the deck of the vessel were not considered the same as those when it is lifted-off from the deck of the barge.

The allowable sea states required for lowering an object down to sea bed, as well as for its positioning and landing, are less critical than those for its lowering through the wave zone. For instance, the construction vessel is provided with a AHC system, which allows for lowering a load down to seabed in a controlled way [3]. Due to all of the above, activity no. 2 is ruled by the allowable sea states found for lowering of the spool through the wave zone (Section 4.5.3).

Regarding activities no. 3 and 4, no interaction between the vessel and the spool occurs. The allowable sea states limiting these activities were assumed the same as those of activity no. 1. The T_R for both activities was assumed 3h each.

Fig. 5.3 shows the allowable sea states for the different activities established by IM1.

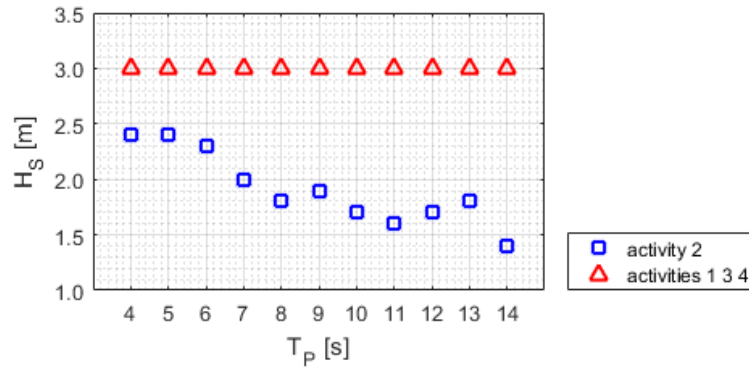


Fig. 5.3. Allowable sea states governing the activities established by IM1

Finally, the planned overall installation time (OIT_{plan}) of this installation method is the summation of all the T_R listed in Table 5.2. Hence, 12h is the planned total installation time for one single spool. For N spools, the OIT_{plan} for IM1 can be obtained as follows:

$$OIT_{IM1plan} = N \times 12h \quad (5.4)$$

Installation method 2 (IM2)

Table 5.3 lists the set of activities established by IM2 for N number of spools. Note that this set involves the installation of at least two spools (i.e. $N \geq 2$). The first spool is transported on-board the vessel, whereas the other(s) are transported by barge(s).

Given that transportation barges are supporting the transportation and installation of $N-1$ spools, the activities involving the lift-off from their deck are limited by the corresponding allowable sea states (Section 4.5.2).

Fig. 5.4 shows the allowable sea states for the different activities established by IM2.

The load-out and transportation of a spool on a barge were given $T_R=1h$ and $3h$, respectively (i.e. total $T_R=4h$). The allowable sea states for the transportation were assumed to be $H_S=3m$ for all T_P . That being said, these activities are carried out while the deployment of the previous spool and its ROV survey take place. Therefore, waiting on weather for the vessel is not expected due to barge-activity.

Spool	No.	Description	Activity	T_R [h]	Allowable sea states	Activity of the barge(s)
	1	Load-out and transportation onto the vessel		4	$H_S=3m$ for all T_P	
1	2	Preparation, lift process and deployment		2	those in Table 4.12	Load-out and transportation of spool 2 on the first barge ($T_R=4h$)
	3	ROV survey		3	$H_S=3m$ for all T_P	
2	4	Preparation and lift-off from the first barge		1	those in Table 4.10	First barge holds on the offshore site during the lift-off of spool 2
	5	Lowering and deployment		1	those in Table 4.12	Load-out and transportation of spool 3 on the next barge ($T_R=4h$)
	6	ROV survey		3	$H_S=3m$ for all T_P	First barge sails back to harbour ($T_R=3h$)
	∴	∴		∴	∴	∴
N	4	Preparation and lift-off from the last barge		1	those in Table 4.10	Last barge holds on the offshore site during the lift-off of spool N
	5	Lowering and deployment		1	those in Table 4.12	
	6	ROV survey		3	$H_S=3m$ for all T_P	Last barge sails back to harbour ($T_R=3h$)
	7	Sailing of the vessel back to harbour		3	$H_S=3m$ for all T_P	

Table 5.3. Activities established by IM2

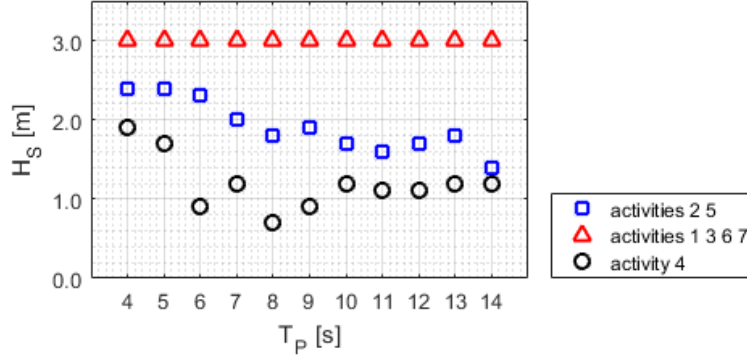


Fig. 5.4. Allowable sea states governing the activities established by IM2

Nevertheless, it should be pointed out that the allowable sea states for the activity involving the lift-off from the barge (i.e. activity 4) are far lower than those for activities 2 and 5 that also belong to the deployment of the spool. The difference varies between 0.2 and 1.4m across the range of T_P . This will probably entail long waiting time, and thus, a longer OIT.

For installation method IM2, the OIT_{plan} for N number of spools is calculated as follows:

$$OIT_{IM2plan} = T_{R \text{ activities 1 to 3}} + (N - 1) \times T_{R \text{ activities 4 to 6}} + T_{R \text{ activity 7}}$$

$$OIT_{IM2plan} = 12\text{hr} + (N - 1)5\text{hr} \quad \text{where } N \geq 2 \quad (5.5)$$

5.2.2 Comparative study on the operability between installation methods

A weather window analysis of the two installation methods was conducted from the hindcast wave data presented in Section 5.1.2. Furthermore, comparison of the methods in terms of overall installation time was carried out by means of statistical analyses.

Weather window analysis

Fig. 5.5 depicts the methodology suggested by Guachamin Acero et al. [4] for weather window analysis. Furthermore, Fig. 5.5 shows how the overall installation time (OIT) is calculated in this work by taking as an example the installation of one spool by using IM1 (Table 5.2).

WOWWs can be obtained from time-history series of wave data (T_P , H_S), see Fig. 5.5(a). For every time step, and based on the calculated allowable sea states, the allowable H_{S_i} for each activity is obtained from using the corresponding T_{P_i} (see Fig. 5.5(b)). The WOWW of each activity is then obtained by comparing the time-history series of hindcast H_S and the allowable H_S for the corresponding T_P (see Fig. 5.5(c)) [4].

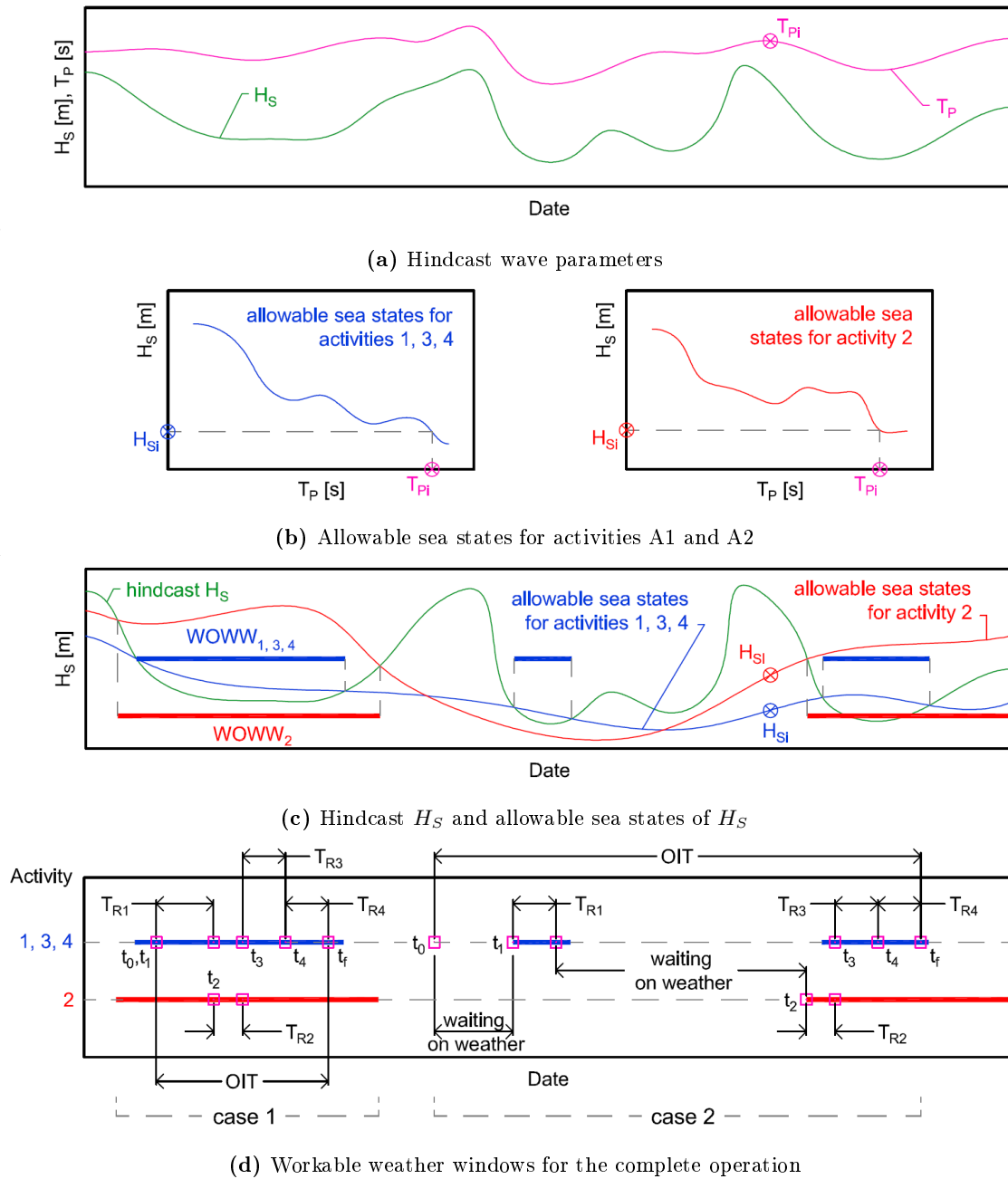


Fig. 5.5. Methodology for estimating the OIT and WOWWs

The point t_0 was defined as the instant OIT is calculated from, see Fig. 5.5(d). Next, all the activities required are put in sequence along their respective WOWWs and based on their operation reference period T_R . The instant t_0 does not necessarily coincides with t_1 , which is the starting point of activity no. 1 (t_2 is the starting point of activity no. 2, so on and so fort). In case 1, t_0 and t_1 do coincide and there is no waiting on weather since there is no interruption between the activities. However, in case 2, t_0 and t_1 do not coincide, thus, waiting on weather exists between these points. The point t_f is the instant the last activity finishes (i.e. activity no. 4). Finally, the actual OIT of the installation method is calculated from the difference between t_f and t_0 .

Note that waiting on weather also occurs in case 2 between activities no. 1 and 2, given that the WOWWs of both activities are not simultaneous nor continuous.

Statistical analysis no. 1

The statistical analysis no. 1 was conducted,

- based on 10-years data
- for a given number of spools, $N \leq 10$
- for both installation methods and,
- starting at any instant (hour) t_i within the operating season.

One common way of characterising data samples is by estimating their mean [22]. Suggest that for a variable X , an ordered data sample of size n exists:

$$\{x_1 \leq x_2 \leq \dots \leq x_k \leq \dots \leq x_n\}$$

where k is the number of observations less or equal to x_k . Their mean is therefore estimated as follows:

$$\bar{x} = \frac{1}{n} \sum_{j=1}^n x_j \quad (5.6)$$

In this particular case,

- n is the number of years available in the hindcast data (i.e. 10 years),
- x_j is the OIT in year j and,
- \bar{x} is the mean over n years

In this work, \bar{x} is denoted as the averaged overall installation time (OIT_{mean}). In other words, the statistical analysis no.1 allows for estimating how long the installation of a given number of spools will take if operations start at a given instant t_i (based on the arithmetic mean of OITs obtained for the same instant t_i over 10 years).

The computation can be extended to a given period. For instance, in order to estimate the expected OIT_{mean} if operations commence within a given month of the operating season.

This statistical analysis also allows for comparing the two installations methods based on the parameter OIT_{mean} .

Statistical analysis no. 2

The statistical analysis no. 2 was conducted in order to obtain the estimates P10, P50 and P90 based on the use of the empirical distribution function.

The empirical distribution function follows [22]:

$$\hat{F}_X(x_k) = \frac{k}{m+1} \quad (5.7)$$

In this particular case,

- m is the number of possible starting points in a month (i.e. 7200 for June, and 7440 for July and August)

The majority of results focus on P50 in the comparative study. P50 is a statistical confidence level for an estimate when probabilistic Monte Carlo methods are used [36]. Moreover, P50 indicates how data is distributed in a sample. For instance, when using a probability of exceedance curve, the P50 of X in the distribution means that 50% of the observations will exceed the value of X [37]. In this study, the notation for the P50 of the overall installation time is OIT_{P50} .

5.2.3 Sensitivity of the installation methods to the navigation time of the construction vessel

With the aim of including flexibility to the operability analysis, a sensitivity study was conducted to observe how sensitive the installation methods are to the navigation time of the vessel.

In the case of IM2, one can say that the navigation time of the barge(s) is also affected. However, it was considered that the necessary number of barges may commute simultaneously to supply the vessel in a timely manner and no waiting time will occur due to barge activity. Table 5.4 lists the activities affected by the navigation time of the vessel and their T_R for the suggested sensitivity cases.

Activity description	T_R [hr]	
	Case 1	Case 2
Load-out and transportation onto the vessel	11	21
Sailing of the vessel back to harbour	10	20

Table 5.4. Sensitivity cases to the navigation time of the construction vessel

5.3 Results and discussion

5.3.1 Base case

The base case for operability analysis and discussion of results is that defined by Tables 5.2 and 5.3 regardless of the number of spools to be installed.

Statistical analysis no. 1

Fig. 5.6 shows the comparison of the averaged overall installation time over 10 years, OIT_{mean} , between the installation methods IM1 and IM2 obtained for the following scenarios: the installation of 2 (minimum to compare the two methods), 6 and 10 spools.

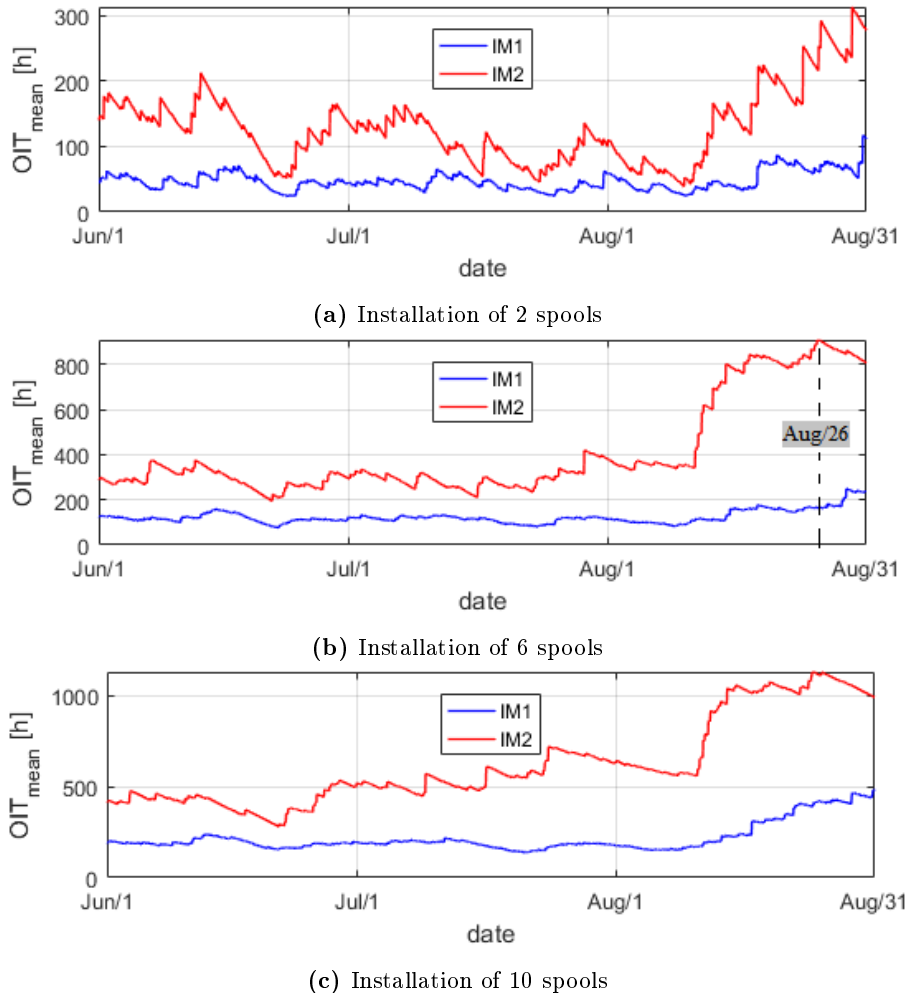


Fig. 5.6. Comparison of OIT_{mean} between IM1 and IM2 along the operating season

On the whole, IM2 presents a longer OIT_{mean} than IM1 following the length of the operating season. OIT_{mean} has a notable increase when the installation of spools starts within roughly the last three weeks of August. Furthermore, the difference between the two installation methods becomes larger.

The behaviour of OIT_{mean} explained above is directly attributed to the harshness of the weather based on the hindcast data (see Section 5.1.2). For instance, if the installation of 6 spools was planned to start on 26 Aug 01:00, the expected OIT_{mean} by following IM2 would result in 908h (38d, which is the maximum), whereas by following IM1 it would result in 164h (7d). From Eqs. (5.4) and (5.5), the planned overall installation time (OIT_{plan}) for the installation of 6 spools is 72 and 37h by following IM1 and IM2, respectively. In this vein, IM2 does not show any advantage over IM1 in terms of installation time and August is not a recommended season to start operations.

Fig. 5.7 shows the comparison of OIT_{mean} between IM1 and IM2 for a certain number of spools when their installation is planned to start in either June, July or August. OIT_{mean} for a given month was estimated as the mean of the sample, whose size is the possible number of start points in such month (i.e. the total number of hours in the month).

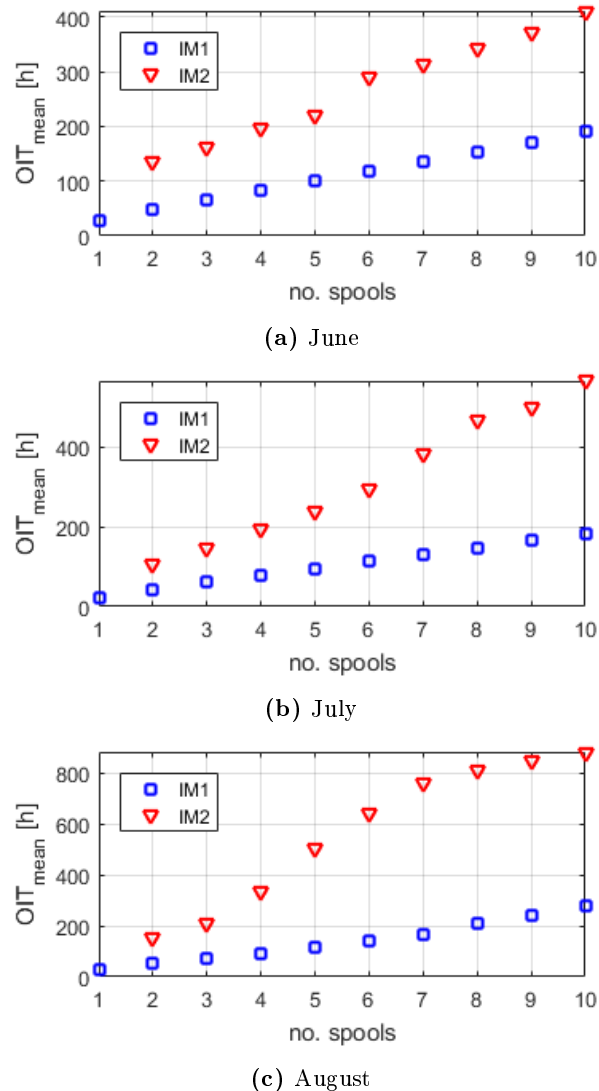


Fig. 5.7. Comparison of OIT_{mean} : by month

The difference of OIT_{mean} between the two installation methods is increasingly noticeable as the number of spools also increases. IM2 is still found to have longer OIT_{mean} regardless of the number of spools. This outcome derives from the major two differences between the installation methods which are:

- Navigation time of the vessel going back and forth between the harbour and the offshore location when following IM1. These extra trips are avoided when following IM2.
- The allowable sea states governing the activity involving the lift-off of the spool.

The most influencing factor on the outcome is that the allowable sea states governing the lift-off of the spool in IM2 are far lower than in IM1.

IM1 requires that the vessel makes a number of trips back and forth between the harbour and the offshore site that is equal to the number of spools to be installed. Having said that, one might expect that IM2 shows an advantage over IM1 from a certain number of spools onwards. However, based on Figs. 5.6 and 5.7, this does not occur. Fundamentally, due to the fact that the allowable sea states governing the lift-off of the spool in IM2 are far lower than in IM1. Therefore, IM2 is expected to have a longer overall installation.

Figs. 5.8(a) and 5.8(b) offer another option for comparing OIT_{mean} when starting in a given month by following either IM1 or IM2, respectively. From these figures, one can say that both June and July, followed by August is the order of months OIT_{mean} goes from representing a more convenient to a less convenient operative outlook. Figs. 5.8(a) and 5.8(b) also show the planned OIT_{mean} corresponding to the installation method and the number of spools to be installed.

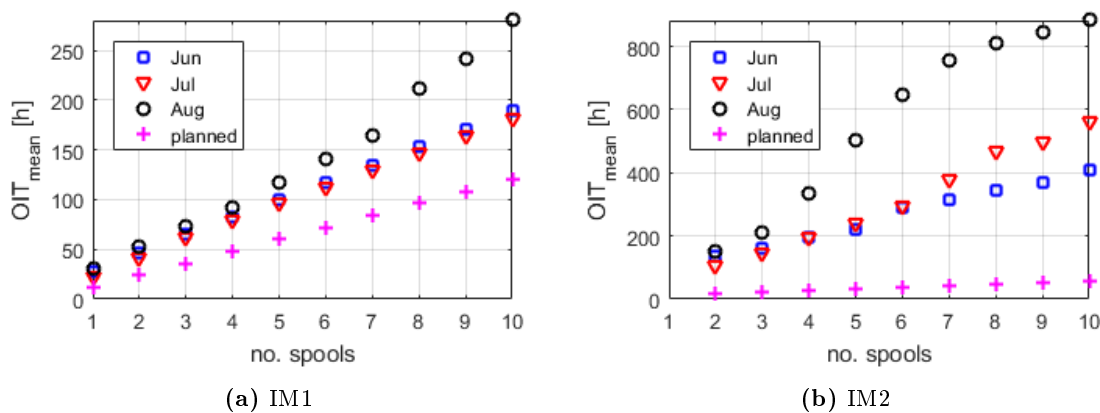


Fig. 5.8. Comparison of OIT_{mean} : by method of installation

Statistical analysis no. 2

With the purpose of obtaining the estimates P10, P50 and P90, the empirical distribution function of the overall installation time (OIT) is plotted for a given number of spools. Fig. 5.9 shows the empirical distribution of OIT for 2 spools when their installation is planned to start at any instant in June, July or August by following either IM1 or IM2.

With reference to Fig. 5.9, P10 results in the planned OIT established by IM1 and IM2 (i.e. 24 and 17h, respectively). Regarding P50, OIT varies between 24 and 27h for IM1, whereas for IM2 it lies in the range 75 to 91h. In the case of P90, the difference becomes more remarkable, mainly, when using IM2. P90 for IM1 lies in the range 88 to 109hr, whereas for IM2 the lowest occurs in July (246h), followed by June (342h) and the longest does in August (411h).

Fig. 5.10 shows the comparison of the estimate P50 (OIT_{P50}) between IM1 and IM2 for a certain number of spools when their installation starts either in June, July or August. Likewise in Fig. 5.7, the difference between IM1 and IM2 is increasingly noticeable as the number of spools also rises. On the whole, IM2 presents larger values P50 than IM1.

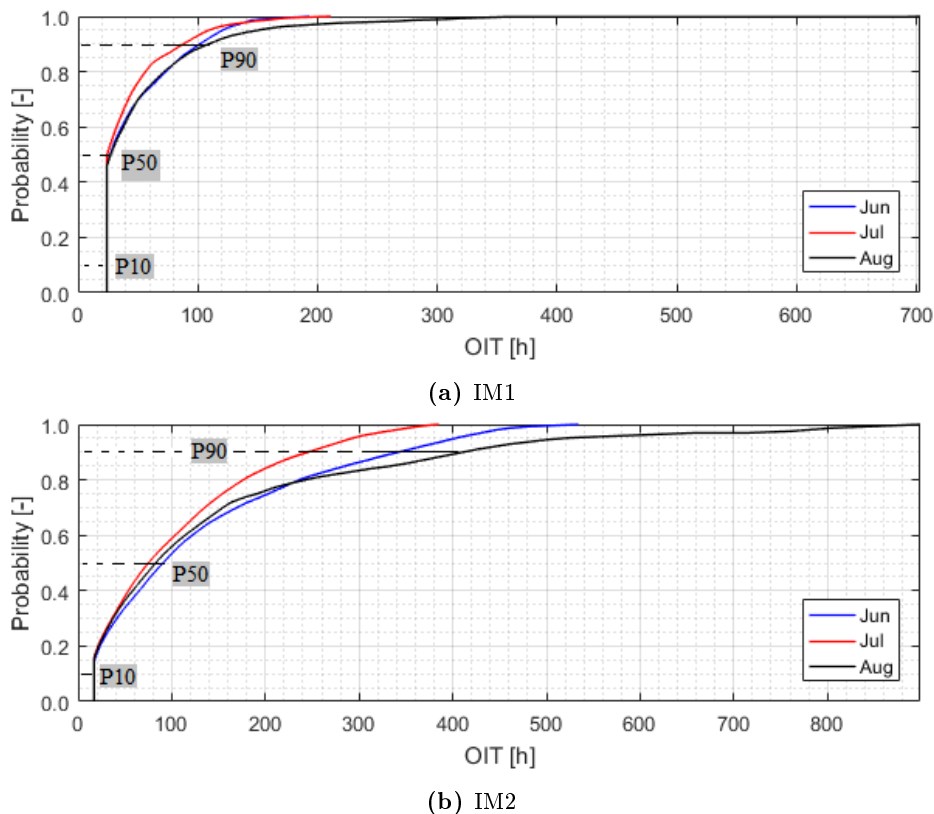


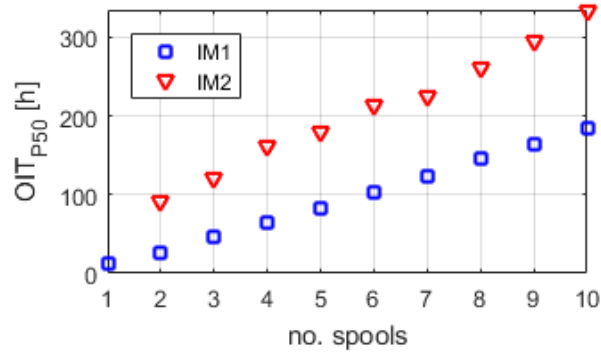
Fig. 5.9. Empirical distribution function of OIT when installing 2 spools

Guachamin Acero et al. [4] suggests that the operability of a complete marine operation can be estimated as the ratio between the available and maximum possible number of WOWWs in the total period of analysis. Nevertheless, in this work, a new term is added for evaluation of the methods in terms of installation time; the *feasibility* refers to the ratio between the planned overall installation time (OIT_{plan}) and the estimate P50 (OIT_{P50}), therefore,

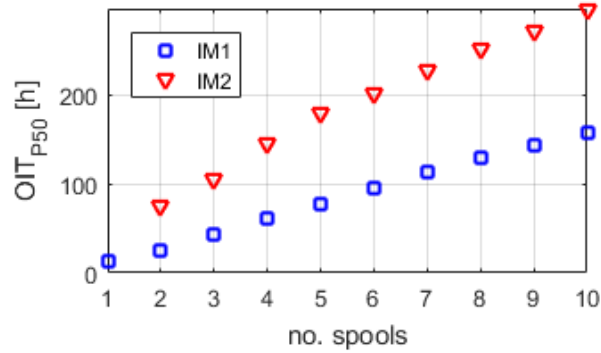
$$feasibility = \frac{OIT_{plan}}{OIT_{P50}} \quad (5.8)$$

In this way, the feasibility of the marine operation is considered as the chance, in terms of time, of successfully completing the installation program. Note that the marine operation is established by an installation method and a given number of spools planned to be installed. Therefore, the feasibility of the marine operation can be also referred to these parameters.

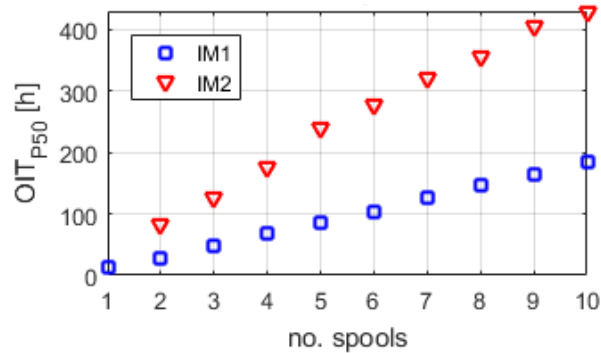
Fig. 5.11 shows the feasibility of IM1 and IM2 for every month within the operating season and for a given number of spools. The feasibility of IM1 is as a whole rather larger than that of IM2. The feasibility of IM1 lies in the range 64.7 to 100%, whereas that of IM2 does in the range 13.3 to 22.7% at most. The feasibility of both installation methods shows a downward trend as the number of spools increases. This is due to fact that the more number of spools, the more likely to happen waiting on weather is, mainly, if operations start in August.



(a) June

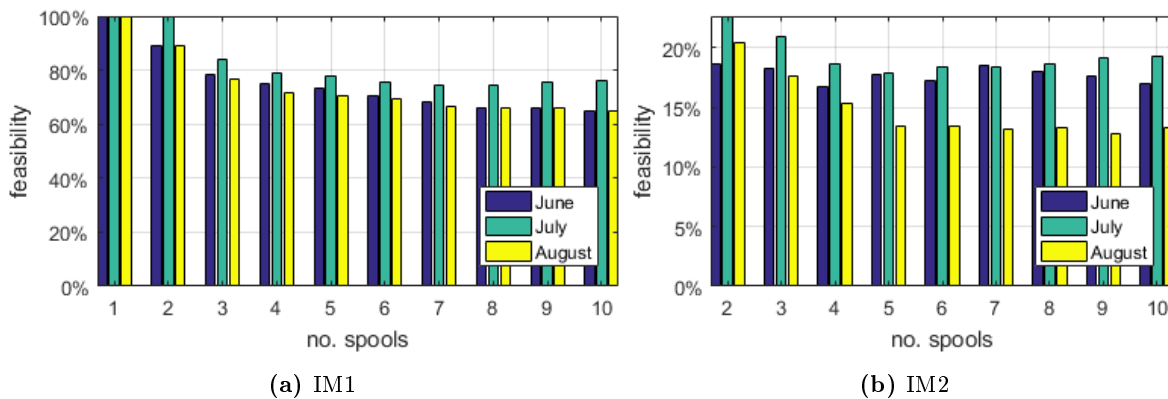


(b) July



(c) August

Fig. 5.10. Comparison of the estimate P50 between IM1 and IM2: by month



(a) IM1

(b) IM2

Fig. 5.11. Feasibility of the installation methods based on the estimate P50

Across all the results for the estimates P10, P50 and P90, August is definitively the least appropriate month to initiate operations. Regarding P50, July suggests the best scenario to start operations. This appraisal is based on the analyses conducted for the installation of up to 10 spools.

Based on the outcomes from conducting the two statistical analysis, it can be said that low allowable sea states governing one single activity may virtually make a marine operation unfeasible.

5.3.2 Sensitivity of the installation methods to the navigation time of the construction vessel

By increasing the navigation time of the vessel, the OIT_{mean} and the values of the estimates P10, P50 and P90 also increase.

Fig. 5.12 depicts the comparison of P50 values (OIT_{P50}) between IM1 and IM2 for the sensitivity cases no. 1 and 2, respectively. When approaching to a certain number of spools, the trend of both installation methods intersect each other at roughly a certain number of spools to be installed. Therefore, IM2 becomes an interesting option over IM1 after such number of spools. This is more prominent for the sensitivity case no. 2 since the navigation time of the vessel is longer for the corresponding activities than for case no. 1.

In this vein, for sensitivity case no. 2, IM2 becomes an interesting option over IM1 from 3 spools when starting in either June or July, or else, from 5 spools starting in August. In the sensitivity case no. 1, one can say that IM2 becomes an interesting option over IM1 when installing from 7 and 9 spools starting in June and July, respectively. In August, IM2 is not a convenient option to go with.

Based on the analysis above, it can be suggested that the navigation time of the construction vessel may become decisive in determining whether transportation barges should be integrated in order to reduce the overall installation time.

Although IM2 offers a better option in terms of installation time from a certain number of spools onwards, a further economic analysis is highly advisable. IM2 still calls for renting transportation barges and their number is likely to increase as the navigation time of the vessel also does.

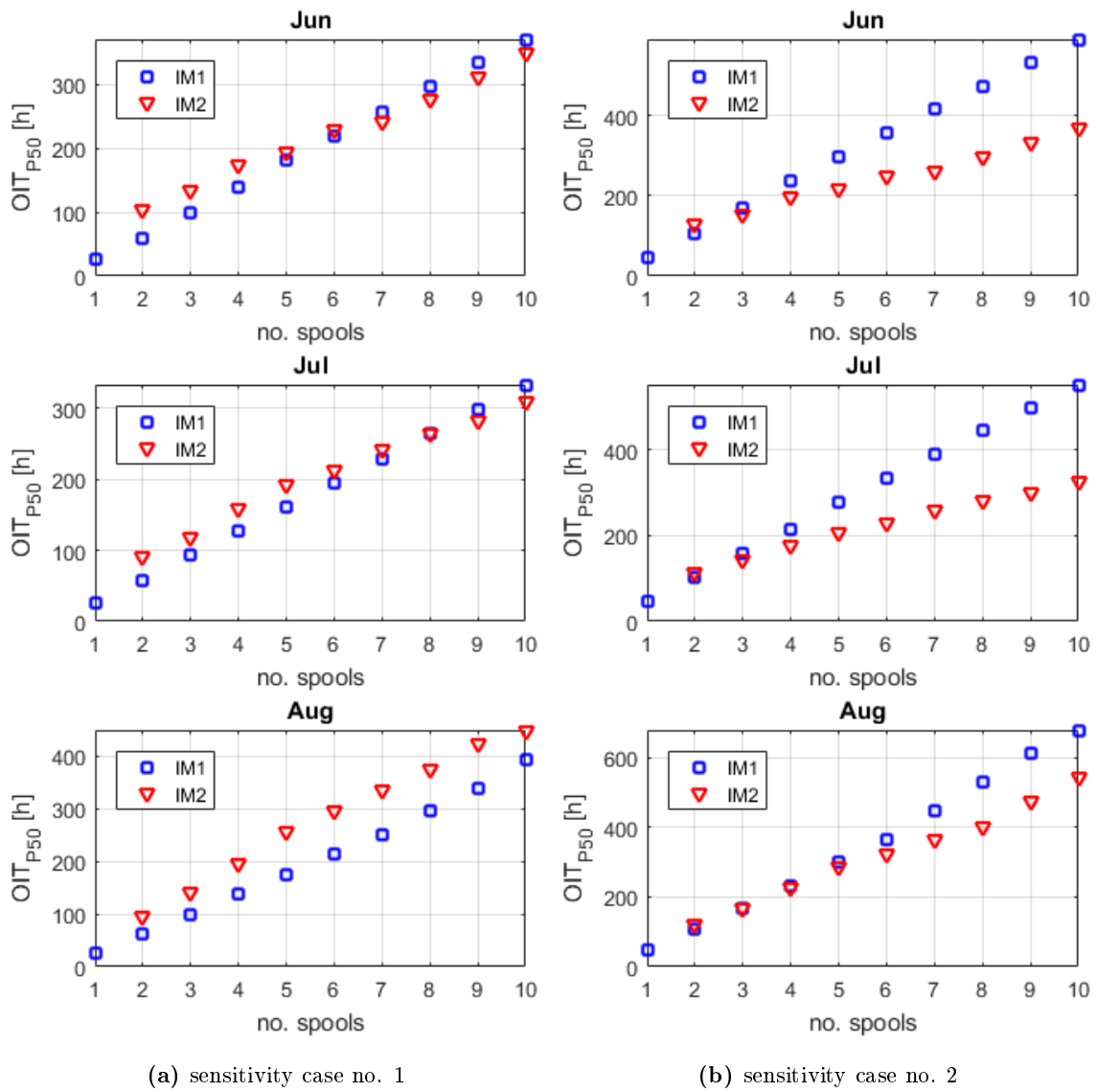


Fig. 5.12. Comparison of the estimate P50 for sensitivity cases no. 1 and no. 2

Chapter 6

Conclusions and recommendations for future work

This thesis studied two particular operations (phases) within the subsea lift process of a spool; the lift-off of the spool from the deck of a transportation barge, and its lowering through the wave zone. Firstly, the numerical models of the lifting system for each phase were developed. This process included the hydrodynamic analysis of the floating vessels. Consequently, the allowable sea states for each lifting operation were obtained based on dynamic analyses and by means of time-domain simulations. Lastly, an operability analysis of two installation methods was conducted.

The conclusions and the recommendations for future work are presented in this chapter.

6.1 Conclusions

The lifting systems are primarily composed by the subsea spool, the construction vessel and the transportation barge. The latter is only required for studying the lift-off phase. The numerical modelling and dynamic analyses were demarcated, to a large extent, by recommended practices and guidelines given in DNV-GL standards.

The numerical modelling of the lifting systems was carried out in the environment SIMA-SIMO. In broad terms, this process included the modelling of the lift-wire, the seven slings attached to the spool and the positioning system of the floating vessels. Furthermore, the lift-off phase required the numerical modelling of four fenders accounting for the supports between the spool and the deck of the barge. The spool is characterised as a slender structure. Its hydrodynamics was studied upon the Morison's load formula (i.e. hydrodynamics coefficients were estimated). Depth-dependent scaling of hydrodynamic coefficients was carried out in order to estimate the slamming loads on the spool when crossing the wave zone.

Based on the outcome from the static condition analysis, it was found that the tilt values of the spool obtained were smaller than 2° when it is either suspended in the air or fully submerged.

Therefore, there is a good correspondence between the connecting point to the crane hook and both the CoG and CoF of the spool in z -direction. Concerning the construction vessel, no ballast was considered for any lift phase. However, the pitch and roll values still lie in the seakeeping criteria range established by NORDFORSK [33]. With regard to the slings, their resultant force under static condition did not exceed their SWL.

A methodology to select seeds that present a suitable scenario for the lift-off of the spool from the barge deck was suggested. As a result, the number of filtered seeds was found to be rather small in comparison with that of the initial pool of seeds. However, the filtered seeds show a favourable condition for the lift-off. The relative motion between the hook and the deck of the barge shows an upward trend during the lift-off span-zone, and therefore, no (immediate) re-hit occurs shortly after the lift-off does.

The criteria defined for the assessment of allowable sea states for the lift-off phase were; potential snap load in slings and re-hit of the spool against the deck of the barge. The dominating criterion in the assessment was the re-hit of the spool. For some of the allowable sea states obtained, the number of filtered seeds obtained is small. Hence, in those cases it is not possible to prove that the response statistics converge, nor the statistical uncertainty is reduced either. The roll motion of the vessel considerably influenced the relative motion between the crane hook (i.e. the crane tip) and the deck of the barge.

The criteria in the assessment of allowable sea states for the lowering phase were; potential snap load in slings, slack-wire condition of slings, as well as minimum clearance between the spool and the portside of the vessel. The dominating criterion was the slack-wire condition in slings followed by minimum clearance between the two bodies. DLC_{sling} was never reached. The convergence study demonstrated that a total of 50 seeds was sufficient to obtain convergent results. Tension in slings along time-histories virtually followed the same trend as in the load distribution under static condition. The clearance between the spool and the vessel was significantly influenced by the sway motion of the former due to pendulum motions.

Fig. 6.1 shows the allowable sea states obtained for the lift-off phase and the lowering phase. In relation to H_S , the states obtained for the lift-off phase are far lower than those for the lowering phase. The difference varies between 0.2m and 1.4m across the range of T_P .

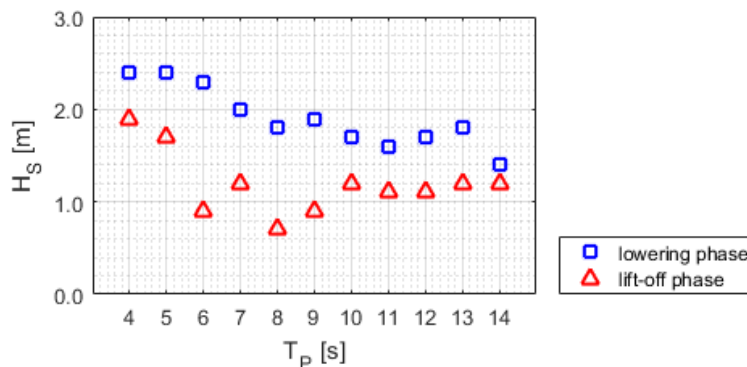


Fig. 6.1. Comparison of allowable sea states: lift-off phase vs. lowering phase

With regard to the operability analysis, two methods (IM1 and IM2) were devised for the installation of a given number of spools starting within the operating season (June 1st to August 31st). The operability analysis aimed at determining which of the methods, for the installation of a given number of spools, is the most effective option in terms of overall installation time (OIT). The entire subsea lift process of the spool in IM1 is governed by the allowable sea states obtained for the lowering phase, whereas in IM2, the lift-off occurs from the deck of a transportation barge and thus the corresponding allowable sea states apply. The weather window analysis was based on the OIT. From the results, it can be concluded that IM2 entails longer averaged overall installation time (OIT_{mean}) and its difference with respect to IM1 is increasingly noticeable as the number of spools increases. In regard to OIT_{mean} , June and July offer a more convenient operative outlook than August. Concerning the estimate P50 (OIT_{P50}), IM2 presents larger values than IM1. Their difference is increasingly noticeable as the number of spools rises.

The term *feasibility* was included and defined as the ratio between the plain OIT (i.e. no downtime) to OIT_{P50} . On the whole, the feasibility of IM1 is far larger than that of IM2. For IM1, the feasibility lies in the range 64.7 to 100%, whereas for IP2 it does in the range 13.3 to 22.7% at most. The feasibility of both installation methods shows a downward trend as the number of spools increases. Across all the results for the estimates P10, P50 and P90, August is definitively the least appropriate month to initiate operations. Regarding OIT_{P50} , July accounts for the best scenario to start operations.

IM1 requires that the vessel makes a number of trips back and forth between the harbour and the offshore site that is equal to the number of spools to be installed. Having said that, it was expected that IM2 would show advantage over IM1 from a certain number of spools onwards. This conjecture never occurred, fundamentally, due to the fact that the allowable sea states governing the lift-off of the spool in IM2 are far lower than in IM1. On the whole, in comparison with IM2, IM1 represents a better operative option in terms of OIT. Furthermore, IM1 is highly likely to lead to lower installation costs (i.e. lower capital expenditure) since no transportation barges are required either.

Concerning the sensitivity study on the navigation time of the vessel, the results show that the trend lines of OIT_{P50} in IM1 and IM2 intersect each other at a certain number of spools to be installed. This is more prominent for the sensitivity case no. 2, where the navigation time of the vessel is longer than for the case no. 1. That being said, in sensitivity case no. 2, IM2 becomes an interesting option over IM1 from 3 spools when starting in either June or July, or else, from 5 spools starting in August. In the sensitivity case no. 1, one can say that IM2 becomes an interesting option over IM1 when installing from 7 and 9 spools, and operations start in June and July, respectively. In August, IM2 is not a convenient option to go with. The outcome suggests that the navigation time of the construction vessel may become decisive in determining whether transportation barges should be integrated in order to reduce the overall installation time.

6.2 Recommendations for future work

Due to the lengthy OIT_{mean} and OIT_{P50} found for IM2, the most advisable aspect to focus on is the improvement of the allowable sea states that govern the lift-off of the spool from the deck of the transportation barge. The corresponding recommendations are presented next:

- *Inclusion of shielding effects from the construction vessel:* By including shielding effects from the vessel, it may be possible to reduce extreme responses while working in close proximity with a barge at adequate vessel heading angles [38]. Besides the fact that a more realistic approach would be integrated, responses such as heave motion of the barge may show smaller variation or amplitude. Thus, a more favourable context for the lift-off might be achieved. The lowest values of H_S correspond to T_P 6s, 8s and 9s (see Fig. 6.1), that which can be classified as short waves. It should be mentioned that shielding has a stronger effect in short waves than in long waves [38].
- *Modelling of collapsible or retractable supports for the spool on the deck of the barge:* One of the practices during the lift-off of spool in the Wheatstone Project was the use of collapsible supports specifically designed to ensure a smooth lift [10]. SIMA-SIMO does not give the option of modelling fender couplings of such nature. By including collapsible or retractable supports in the numerical modelling and analysis of the lift-off phase, an improvement in the allowable sea states might be achieved. Note that the most dominating criterion during the assessment of the allowable sea states for the lift-off phase was the re-hit of the spool against the deck of the barge.
- *Sensitivity analysis on the hoisting speed and the maximum run acceleration for winch:* Bai and Bai [3] suggest that determining the minimum hoisting speed is the main purpose during the analysis of the lift-off of a subsea manifold from a barge deck. A sensitivity study on the hoisting speed is highly advisable in order to optimize the allowable sea states for the lift-off phase. It should be noted that higher hoisting speed will lower the probability of having re-hit. However, it may increase the characteristic snap load in a wire coupling [9].

As discussed in Section 4.5.3 regarding the lowering phase, the clearance between the spool and the vessel was significantly influenced by the sway motion of the former due to pendulum motions. Therefore, if the crane tip is relocated closer to the vessel (i.e. shorter lift radius), the minimum clearance between these bodies might become the dominating criterion during the assessment of the allowable sea states. Concerning the use of tugger lines, the development of adequate wire couplings in SIMA-SIMO will probably control the horizontal motion of the lifted object in a better way. A similar approach is suggested by DNVGL-RP-N103 [9], where the modelling of guide wires as constraints or horizontal springs in the equations of motion for the lifted object is recommended.

With regard to the results obtained for the sensitivity case no. 2 (see Section 5.3.2), although it is true that IM2 offers a better option in terms of operability from a certain number of spools onwards, further economic analysis is also advisable. IM2 still calls for renting transportation barges and their number is likely to increase as the navigation time of the vessel also does.

Bibliography

- [1] DNV·GL, *Standard: Marine operations and marine warranty*, DNVGL-ST-N001, June 2016.
- [2] L. Li, Z. Gao, and T. Moan, “Response analysis of a nonstationary lowering operation for an offshore wind turbine monopile substructure,” *Journal of Offshore Mechanics and Arctic Engineering*, vol. 137, p. 051902, 2015.
- [3] Y. Bai and Q. Bai, *Subsea engineering handbook*. Gulf Professional Publishing, 2010.
- [4] W. Guachamin Acero, L. Li, Z. Gao, and T. Moan, “Methodology for assessment of the operational limits and operability of marine operations,” *Ocean Engineering*, vol. 125, pp. 308–327, 2016.
- [5] L. Li, Z. Gao, and T. Moan, “Operability analysis of monopile lowering operation using different numerical approaches,” in *International Journal of Offshore and Polar Engineering*, vol. 26, no. 2, Jun. 2016, pp. 88–99.
- [6] N. Standard, *Petroleum and natural gas industries, Design and operation of subsea production systems, Part 1: General requirements and recommendations (ISO 13628-1:2005)*, NS-EN ISO 13628-1, March 2006.
- [7] FMC Technologies, “Subsea production systems,” available: <http://www.fmctechnologies.com/>, accessed on: Jun. 24, 2018.
- [8] DNV·GL, *Recommended practice: Lifting appliances used in subsea operations*, DNVGL-RP-N201, June 2017.
- [9] DNV·GL, *Recommended practice: Modelling and analysis of marine operations*, DNVGL-RP-N103, July 2017.
- [10] D. Cosson, M. Rowe, W. Koolhof *et al.*, “Wheatstone subsea installation - Challenges associated with large numbers of subsea heavy lifts and spools offshore Australia,” in *Offshore Technology Conference Asia*. Kuala Lumpur, Malaysia: Offshore Technology Conference, Mar. 20–23 2018.
- [11] K. Aarset, A. Sarkar, D. Karunakaran *et al.*, “Lessons learnt from lifting operations and towing of heavy structures in North Sea,” in *Offshore Technology Conference*. Houston,

- Texas, USA: OTC 21680, May 2–5 2011.
- [12] DNV·GL, *Recommended practice: Risk management in marine and subsea operations*, DNVGL-RP-N101, June 2017.
- [13] DNV·GL, *Offshore standard: Design of offshore steel structures, general - LRFD method*, DNVGL-OS-C101, July 2017.
- [14] L. Li, “Dynamic analysis of the installation of monopiles for offshore wind turbines,” Ph.D. thesis, Dept. Marine Technol., NTNU, Trondheim, 2016.
- [15] M. Wu, “Numerical analysis of docking operation between service vessels and offshore wind turbines,” *Ocean Engineering*, vol. 91, pp. 379–388, 2014.
- [16] H. Yang, C. G. Koh, Y. M. Low, X. Zhang, A. Hussain, and P. F. B. Adaikalaraj, “Probabilistic operability analysis of drilling riser by metamodel methodology,” in *Proceedings of the Twenty-seventh International Ocean and Polar Engineering Conference*. San Francisco, CA, USA: International Society of Offshore and Polar Engineers, Jun. 25–30 2017.
- [17] O. M. Faltinsen, *Sea loads on ships and offshore structures*. Cambridge University Press, 1990.
- [18] O. T. Gudmestad, *Marine technology and operations: theory & practice*. WIT Press, 2015.
- [19] J. M. J. Journée and W. W. Massie, *Offshore hydrodynamics*, 1st ed., Delft University of Technology, Jan. 2001.
- [20] DNV GL - Software, “WADAM, Sesam User Manual,” Mar. 2017.
- [21] S. M. G. Andersen, “motion control during offshore lift operations,” M.S. thesis, Dept. Marine Technol., NTNU, Trondheim, 2017, available: <http://hdl.handle.net/11250/2455240>.
- [22] S. Haver, *Metoccean modelling and prediction of extremes*, (draft) 1st ed., Haver & havet, University of Stavanger, NTNU, Stavanger, May 2017.
- [23] A. Naess and T. Moan, *Stochastic dynamics of marine structures*. Cambridge University Press, 2013.
- [24] DNV·GL, *Recommended practice: Environmental conditions and environmental loads*, DNVGL-RP-C205, Aug. 2017.
- [25] J. R. Morison, M. P. O’Brien, J. W. Johnson, and S. A. Schaaf, “The force exerted by surface waves on piles,” *Petroleum Trans., AIME 1950*, vol. 189, pp. 149–157, 1950.
- [26] M. C. Eames, “Steady state theory of towing cables,” *Trans. of the Royal Inst. of Naval Architects*, vol. 10, 1968.

- [27] DNV GL - Software, "Sesam, Feature Description," April 2018.
- [28] J. R. Chaplin and Y. Ikeda, "Viscous forces on offshore structures and their effects on the motion of floating bodies," in *Proceedings of the Ninth International Offshore and Polar Engineering Conference*. Brest, France: International Society of Offshore and Polar Engineers, May 30 – Jun. 4 1999.
- [29] MARINTEK, "SIMO 4.8.7 User Guide," Jan. 2017.
- [30] MARINTEK, "SIMO 4.8.7 Theory Manual," Jan. 2017.
- [31] H. Zhu, L. Li, and M. C. Ong, "Study of lifting operation of a tripod foundation for offshore wind turbine," *IOP Conf. Series: Materials Science and Engineering*, vol. 276, p. 012012, 2017, doi:10.1088/1757-899X/276/1/012012, [Online].
- [32] R. C. Dorf, *The engineering handbook*, 2nd ed. CRC Press, 2005.
- [33] NORDFORSK, "Criteria for merchant ships, criteria for amongst others, vertical and transverse accelerations, roll, slamming and deck wetness," MARINTEK, Trondheim, Norway, ISB 87-982637-1-4, 1987.
- [34] L. Li, Z. Gao, and T. Moan, "Numerical simulations for installation of offshore wind turbine monopiles using floating vessels," in *Proceedings of the ASME 32th International Conference on Ocean, Offshore and Arctic Engineering*. Nantes, France: ASME, Jun. 9–14 2013.
- [35] L. Li, Z. Gao, and T. Moan, "Joint distribution of environmental condition at five european offshore sites for design of combined wind and wave energy devices," *Journal of Offshore Mechanics and Arctic Engineering*, vol. 137, p. 031901, 2015.
- [36] Cooper Energy, "P50 (and P90, Mean, Expected and P10)," available: <http://www.cooperenergy.com.au>, accessed on: Jun. 24, 2018.
- [37] V. Borges, "Terminology Explained: P10, P50 and P90," 2016, available: <https://blogs.dnvgl.com/software/2016/12/p10-p50-and-p90/>, accessed on: Jun. 28, 2018.
- [38] L. Li, Z. Gao, T. Moan, and H. Ormberg, "Analysis of lifting operation of a monopile for an offshore wind turbine considering vessel shielding effects," *Marine Structures*, vol. 39, pp. 287–314, 2014.

Appendix A

Hindcast wave data

H_S [m]	T_P [s]								Sum
	2	4	6	8	10	12	14	16	
0.5	16	40	96	190	289	70	10	3	714
1.0	599	697	870	1094	1433	1741	927	377	7738
1.5	1565	2207	820	2345	2009	1720	1367	984	15017
2.0	1934	2543	3023	2489	2070	1328	969	692	15048
2.5	1612	2143	2676	2320	1798	1044	621	278	12492
3.0	1143	1536	2009	1913	1531	876	465	180	9653
3.5	706	934	1325	1305	1124	859	556	316	7125
4.0	355	679	783	851	833	744	480	270	4995
4.5	292	458	630	528	645	574	443	190	3760
5.0	303	364	498	478	510	360	232	158	2903
5.5	233	316	363	300	301	177	97	43	1830
6.0	122	173	238	214	156	126	97	47	1173
6.5	62	79	142	128	116	113	75	36	751
7.0	57	76	88	84	74	58	35	20	492
8.0	67	88	152	111	127	87	34	29	695
9.0	26	30	23	16	11	1	0	0	107
10.0	22	42	45	13	14	18	1	0	155
Sum	9114	12405	15781	14379	13041	9896	6409	3623	84648

Table A.1. 10-year scatter diagram of H_S and T_P of the offshore site chosen for metocean condition [35]